MINISTERUL EDUCAȚIEI ȘI CERCETĂRII

ANALELE UNIVERSITĂȚII
"DUNĂREA DE JOS" DIN GALAȚI

Fascicula IX

FACULTATEA DE
METALURGIE ȘI ȘTIINȚA MATERIALELOR

ANUL XXIII (XXVIII), mai 2005, nr.1

MINISTRY OF EDUCATION AND RESEARCH

THE ANNALS OF
"DUNAREA DE JOS" UNIVERSITY OF GALATI

Fascicle IX

FACULTY OF
METALLURGY AND MATERIALS SCIENCE

YEAR XXIII (XXVIII), May 2005, no.1

Table of Content

THE PROPERTIES OF HARDENED LEAD

Florentina POTECASU, Octavian POTECASU, Elena DRUGESCU

"Dunarea de Jos"University of Galati,
e-mail: **fpotec@ugal.ro**

ABSTRACT

Lead hardened through oxide scattering is investigated as raw materials for the fabrication of the support gratings of lead accumulators in order to increase their life service. For the preparation of lead powder hardened through oxide scattering we used air jet pulverisation, a technique specific to powder metallurgy. Two research approaches are presented in the paper: one in which the oxide was introduced through oxidised lead powder, and the other in which additional lead oxide was introduced. Oxide dispersion into metallic matrix was achieved by pronounced deformation through extrusion of the powder. During extrusion, the particles are compelled to pass through the mould calibration zone and consequently they are considerably deformed. As an effect of this deformation, the particles of fragile oxide which cover the lead powder particles are crashed and carried away to the material flowing through the matrix longitudinally on the extruded semi-product. The content of oxide introduced in matrix by the oxidised lead powder depends on the powder particle size. This paper presents the effect of the powder particle size and oxide phase dispersion in the metallic matrix on the mechanical, chemical and electrical properties of the extruded semi-products. The semi-products made from lead powder belonging to the grain size class of < 40 µm and oxide particles allowance have the highest mechanical resistance and the best corrosion behaviour. Using controlled oxidised lead powder better extruded semi-products are obtained in terms of mechanical resistance, corrosion behaviour and electrical conductivity as compared with lead and Pb-Sb alloy. A higher electrical conductivity represents an important advantage especially for the starting accumulators where the voltage fall should be as low as possible.

KEYWORDS: mechanical resistance, lead accumulators, oxide dispersion

1. Introduction

Lead hardened through oxide scattering is investigated as raw materials for the fabrication of the support gratings of lead accumulators in order to increase their life service [1-2].

Two research approaches in order to obtain hardened materials by oxide phase dispersed in Pb metallic products were discussed previously [3-5]. In the first variant partially (superficial) oxidised Pb metallic powder has been used. In the second approach fine lead oxide particles $PbO \cdot Pb_2O_3$ were added to the partially oxidised powder mixture belonging to the finest grain size class (< 40 m). Oxide scattering into the metallic matrix was achieved by deforming the compressed product through extrusion. During extrusion, the particles are compelled to pass through the matrix calibration zone and consequently they are considerably deformed. As an effect of this deformation, the films of fragile oxide which cover the lead powder particles are crashed and carried away by the material that flows through the mould, thus being obtained a fine and uniform dispersion along the length of the extruded samples. Due to the material flowing under the three-dimensional compression, oxide-free surfaces are created, which facilitate the lead atom diffusion among particles, thus achieving sintering and therefore material consolidation. As a blank assay, were used lead and Pb – 8 % Sb alloy, which were extruded under the same conditions as the powder compressed samples.

This paper presents the effect of the oxide phases dispersion in the Pb metallic matrix on the mechanical resistance, creep strength and electrical resistivity of the lead hardened by oxide dispersion as compared to the properties of lead and Pb-Sb alloy.

1.Experimental conditions

In parallel, eight series of materials have been prepared and investigated in terms of mechanical and electrical properties:
– series I: cast and extruded lead;
– series II: cast and extruded Pb - 8% Sb alloy;

– series III: extruded superficially oxidised lead powder of (56 –71) μm grain size;
– series IV: extruded superficially oxidised lead powder of (40 –56) μm grain size;
series V: extruded superficially oxidised lead powder of < 40 μm grain size.
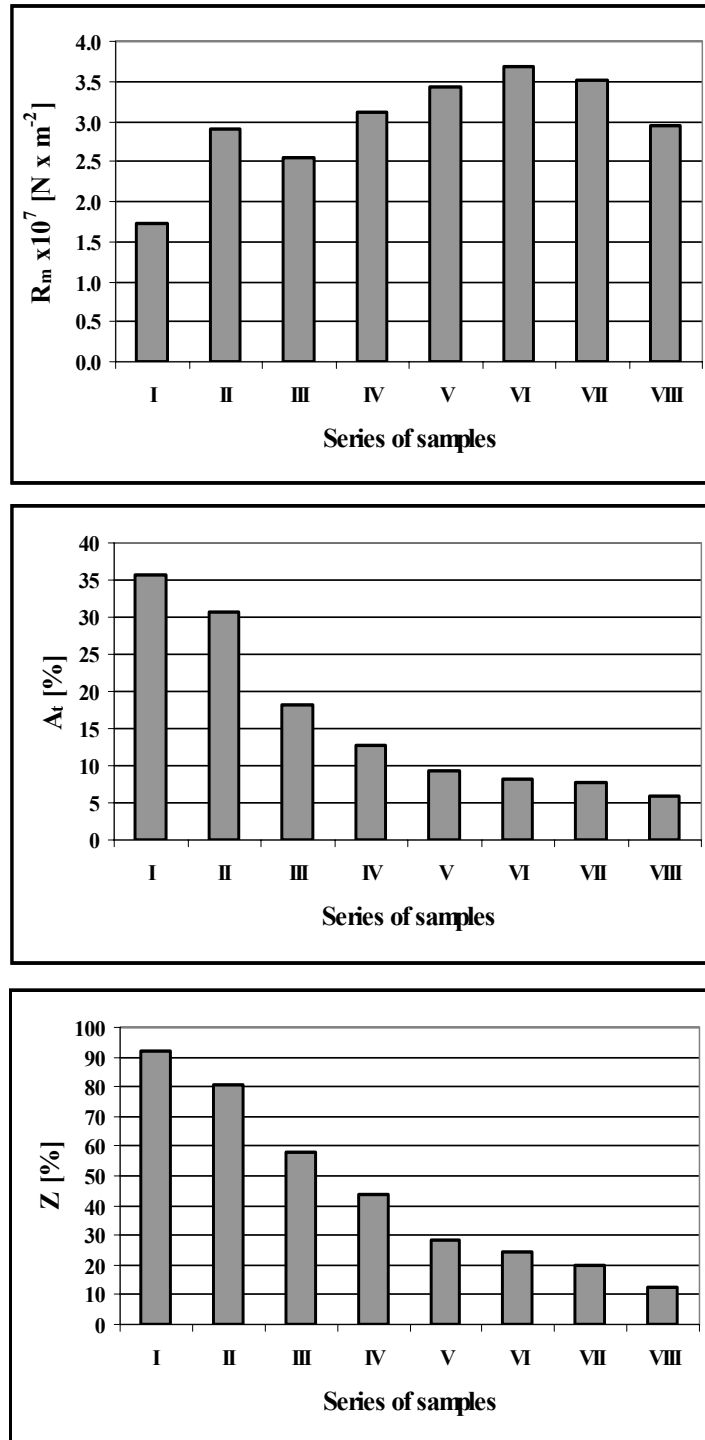
Figure 1. The mechanical characteristics determined
at tensile test for the 8 studied series of samples.

− series VI: extruded superficially oxidised lead powder of grain size < 40 μm, adding 0.5 % Pb_3O_4

− series VII: extruded superficially oxidised lead powder of grain size < 40 μm, adding 1 % Pb_3O_4

− Series VIII: extruded superficially oxidised lead powder of grain size < 40 μm, adding 2 % Pb_3O_4.

The superficially oxidised powder was obtained by the authors by air-atomization, in an installation with horizontal jet. Compressed samples were achieved in a steel die pressing with the diameter of 20 mm, using the oxidised powder and the mixture of oxidised powder with powder of $PbO·Pb_2O_3$. In order to achieve the oxide-dispersion in the lead matrix, the compressed samples were extruded, thus obtaining the final samples, semi-products (wires), with diameters of 8, 6 and 4 mm and a length greater than 300 mm.

For comparison, lead samples of technical cleanliness and of Pb - 8% Sb alloy, used for acid lead accumulators, having a diameter of 20 mm, were cast. The cast samples were obtained through extrusion under the same conditions as the compressed ones from powders.

In each series under investigation, samples taken from the extruded semi-products having the deformation degree of $\varepsilon_1 = 6.25$, $\varepsilon_2 = 11$, $\varepsilon_3 = 25$ were used. The degree of deformation "ε" was calculated with respect to the initial section before deformation and the final section of the extruded semi-products ($\varepsilon = S_0 / S_f$). The paper presents only the results concerning the samples having the highest deformation degree through extrusion: the assays with the diameter of 4 mm, where the ratio between the initial section and the extruded section equals to 25.
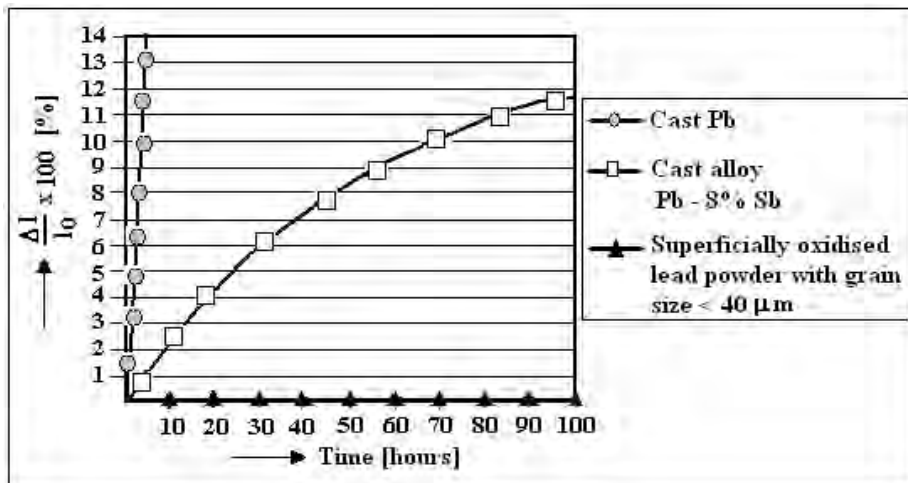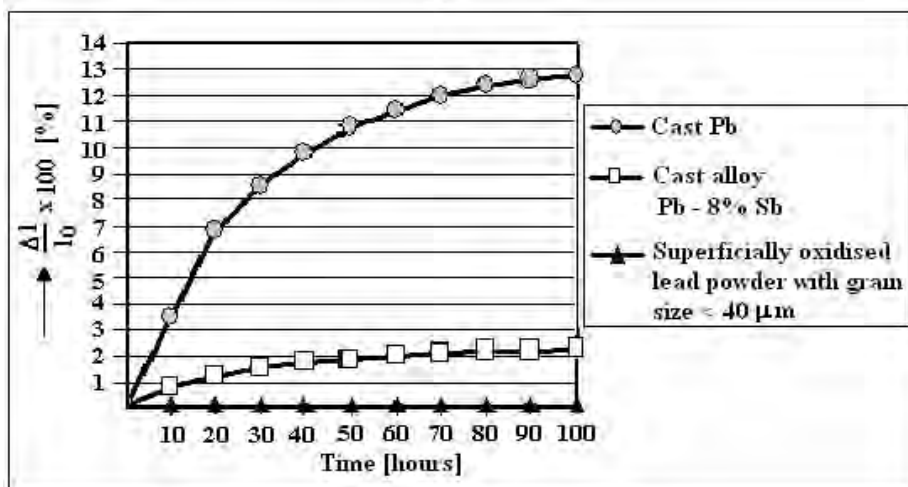
Figure 2. The creep behaviour of the materials made by extrusion and strained at:
$\sigma_1 = 0.5x10^7$ Pa (a) and $\sigma_2 = 1x10^7$ Pa (b)

2.Experimental Results

3.1 Mechanical Properties of Hardened Samples

The effect of the following parameters on the mechanical properties was investigated:

- powder particle size (1st variant of research - series III, IV, V);
- amount of particles pre-introduced into the lead oxide (2nd variant - series VI, VII, VIII).

The following determinations were made: tensile strength (R_m), percentage total elongation at fracture (A_t), percentage reduction of area (Z). The results are presented in the figure 1.

Based on these results, the following remarks can be pointed out:

1. The tensile strength of the partially oxidised lead powder samples of different grain size (series III, IV, V) is higher than that of the blank assays made from cast lead (series I).
2. As the powder grain size is being refined (series III, IV, V) there is an increase in the number of fine particles of oxide dispersed in the lead matrix; consequently, there is a considerable increase in the mechanical resistance, while the rigidity gets much improved (this is necessary for the gratings used as support in the lead accumulators) as compared to the materials in the series I and II;

3. The addition of oxide particles to the finest powder in small quantities, below 2 % Pb_3O_4 (series VI, VII) leads to a higher mechanical resistance and a greater rigidity of the deformed materials;
4. Increasing the mass percentage of particles from 0.5 % to 1 % (series VI-VII), decreases slightly the tensile strength; this trend is more pronounced when the mass percentage is increased to 2% (series VIII);
5. Addition of oxide to the finest powder (< 40 μm) should be made in small amounts (mass percentage below 2%) to prevent the decrease in the mechanical characteristics (R_m, A_t, Z).

3.2 Creep Behaviour of Hardened Samples

The creep behaviour of the samples was evaluated for two constant tensile loads at the temperature of 20°C. The results are presented in figure 2.

One can notice a much better behaviour of the hardened samples by oxide dispersion as compared to the blank assays of Pb or Pb – 8 % Sb.

The high creep resistance is accounted for by the presence in the lead matrix of fine oxide particles crashed by deformation; these particles act as inhibitors and therefore cause a delay in the growth of the new recrystallised grains.

.
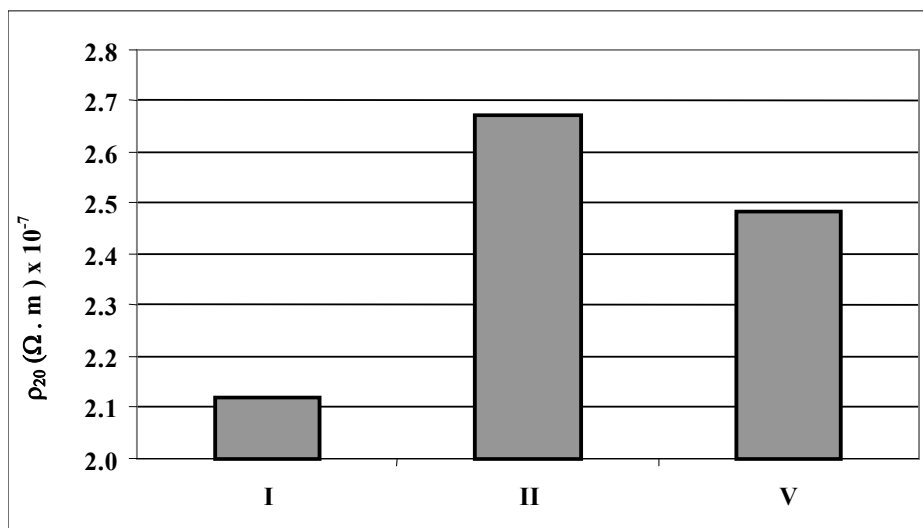
Figure 3. The electrical resistivity of the semi-products obtained by extrusion.

3.3 Electrical Resistivity of Hardened Samples

The measurements to determine the electrical resistivities were carried out by the fall voltage method on the samples being run by a calibrated current of 10 A at the temperature of 20°C. The figure 3 presents the electrical resistivity of the blank assays and for the samples from the V series, hardened by oxide dispersion. One can notice that both the Pb-Sb alloy and the hardened lead by oxide dispersion present a higher resistivity compared to the lead with technical cleanliness.

4.Conclusions

The results of the research show that the oxide dispersion in the lead matrix leads to a significant improvement of the creep strength and to an increase close to 20 % of the mechanical resistance, as compared to the Pb – 8 % Sb alloy, and close to 100 %, as compared to the lead with technical cleanliness. That recommends the lead hardened by oxide dispersion for producing the support gratings for acid accumulators with lead used for cars, as they are particularly subjected to creep, because of the high density of the lead combined with a low mechanical resistance.

By determining the electrical resistivity, it was shown that using the lead hardened through oxide dispersion, instead of the Pb – 8 % Sb alloy, does not lead to the increase of the internal electrical resistance of the accumulator and it keeps the conversion capacity of the high current strength needed for car-starters.

References

[1].T.W. Clyne, P.J. Withers: *An Introduction to metal matrix Composites* (Cambridge University Press, London, 1993).

[2].F. L. Matthews and R.D.R. Rawhings: *Composite Materials: Engineering and Science,* (Published by Chapman and Hall, London SE18HN, Oxford ISBN 0412559609(HB), 1994).

[3].O. Potecasu, F. Potecasu, E. Drugescu, P. Alexandru: Proceedings of the European Conference Junior - Euromat, 26-30 Aug. 1996 (Deutsche Gesellschaft für Materialkunde e.V., Lausanne, Switzerland 1996), p. 156.

[4].F. Potecasu, O. Potecasu, E. Drugescu, P. Alexandru: Proceeding of the 40th International Seminar on Modelling and Optimisation of Composites MOC'40, Odessa, April 2001 (IAE - International Academy of Engineering, ISBN 966-549-565-8, Odessa, Ukraine 2001), p. 172.

[5].O. Potecaşu, F. Potecaşu, E. Drugescu, P. Alexandru: Proceedings of The Fourth International Congress Science and Engineering, Universitatea Tehnică "Gheorghe Asachi", Jassy 2002 (Bulletin of the Polytechnic Institute of Jassy 18-20 April 2002, volume XLVIII-LII, Nr 3-4, The Technical University, ISSN 1453-1690, Jassy, Romania), p. 9

NANOSTRUCTURED SiC-Ni COMPOSITE COATINGS OBTAINED BY ELECTRODEPOSITION – A TRIBOCORROSION STUDY

Lidia BENEA[1], Viorel IORDACHE[2],
François WENGER[2], Pierre PONTHIAUX[2]

[1]Dunarea de Jos University, GALATI, Romania
[2]Ecole Centrale Paris, Laboratoire LGPM, France
e-mail: Lidia.Benea@ugal.ro

ABSTRACT

The tribocorrosion properties of SiC (20nm) - Ni nanostructured coatings have been studied in pin on disc tribocorrosimeter connected with an electrochemical cell. The objectives of our study in principal is to fully understanding the tribocorrosion process kinetic and mechanism of modified surfaces by co-depositing nano silicon carbide particles with nickel. The samples with coating on a top of a cylinder were installed in a cell, containing the electrolyte and electrodes, and mounted on a pin-on-disc tribometer, with the working surface of the specimen facing upwards. The counterbody (pin) was a corrundum cylinder (7 mm in diameter), mounted vertically on a rotating head, above the specimen. The lower spherical end (radius = 100 mm) of the pin, was then applied against the composite surface (disc) with an adjustable normal force. When rotation was applied, the end of the pin draws a circular wear track (16 mm in diameter) on the working composite surface. Continuous friction tests were carried out. Different friction forces were applied during 10000 tours with a rotation speed of counterbody from 30 to 120 tours/min. Some features of these tests reproduce the wear conditions of composite coatings in real conditions. K_2SO_4 0.5M was used as corrosive and passivating electrolyte for tribocorrosion tests.

KEYWORDS: composite, coatings, dispersed particles, tribocorrosion, wear.

1.Introduction

In industry, e.g. automotive applications, there is always the risk of material touching each other under sliding conditions. In many cases, these industrial components, e.g. bearings, pumps, rolling mill bearings, are required to operate in aqueous environments (corrosive media) in which water is either deliberately introduced as a coolant or present as a working fluid. The combined action of wear and corrosion, named tribocorrosion, often results in a significant increase in the total material loss. Thus, there are required materials having the desired corrosion, friction, and wear properties. Accordingly, many efforts have been made to develop suitable materials to aqueous environment. Composite coatings obtained by metal co-deposition of various dispersed phases during electrocrystallisation have been given special attention in recent years [1-10]. Ni-based alloys, which are in general designed for uses at high temperature, possess some extraordinary characteristics such as excellent mechanical properties, good thermal stability, chemical inertness,

and high wear resistance. The Ni-based composites are successfully used due to their capability of having self-lubricating property in a wide temperature range, for instance, the turbine engines used in aviation and electric industries, the radiator sealing systems of the automobile engines, and the mechanical devices in the atomic reactors [1-3]. However, few are reported on their friction and wear properties as well as wear mechanism in water environment [3,11]. In particular, during recent years, Ni-SiC composites have been widely investigated and successfully commercialized in the automotive and aerospace industry as a result of their improved mechanical and tribological properties. The metal-matrix composites are materials in which the properties of a metallic host material are modified with addition of a second phase (ceramics) by electrodeposition process. The second phase can be hard oxide (Al_2O_3, TiO_2, SiO_2) or carbides particles (SiC, WC), or diamond, or solid lubricant (PTFE, graphite or MoS_2), or even liquid containing microcapsules [4]. Most composite coatings contain micron-sized particles. The major challenges with the codeposition of second phase particles are the

achievement of a high level of codeposition and avoiding the agglomeration of particles suspended in the electrolytes. The aim of this work is to investigate the influence of nano-sized SiC particles dispersed in the Ni matrix on the tribocorrosion behavior of Ni-SiC nanostructured coatings in aqueous environment.

2. Experimental

2.1. Preparation of nano SiC - Ni composite coatings

Nickel silicon carbide co-depositions were made in common nickel plating electrolytes (sulfate and chloride). The electrolyte was prepared from p.a. chemicals and distilled water, which provided the required purity for the potentiodynamic investigations and characterizations of the coatings obtained. Pure dispersed nano sized silicon carbide at different concentrations ($50 gL^{-1}$) was suspended in the electrolysis bath. The average particle size was 20 nm. Thickness of composite deposits were obtained at 50 µm and were verified by measuring the weight before and after deposition and also by light microscopy on cross section. The particles were kept in suspension by mechanical or magnetic stirring at a rotation rate at 200 r.p.m. A saturated calomel electrode was used as reference electrode (SCE) in order to determine the influence of the dispersed phase on nickel electrodeposition.

2.2. Structural and chemical analyses

Nano SiC (20nm) amount in the composite coating by surface and cross section analysis was performed with X-ray disperse energy system (EDX). Nano SiC content in the coating was obtained at 8.99 as weight % or calculated at ~25 as volume %.

2.3. Wear - corrosion studies

For electrochemical measurements (open-circuit potential, potentiodynamic polarization) a three-electrode set-up was used, with the sample as working electrode, a circular platinum gauze as counter electrode and a "Hg/Hg_2SO_4/saturated K_2SO_4 solution" as reference electrode (SSE=+670mV/NHE), see Fig. 1. The electrodes were connected to a PAR273A potentiostat controlled through a computer by using Corrware 2.2 (Scribner) software.

The tribocorrosion properties have been studied in the following conditions:

Solution: 0.5M K_2SO_4.
Normal Force: 10N – 15N.
Rotation Speed: 30-120 tours/min.

The samples were then installed in a cell, containing the electrolyte and electrodes, and mounted on a pin-on-disc tribometer, with the working surface of the specimen facing upwards.
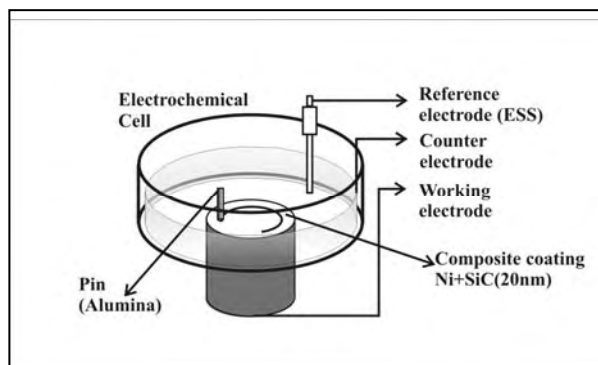
Fig. 1. *Schematic set-up for electrochemical measurements on a working electrode as Ni-SiC composite coating (WE).*

The counterbody (pin) was a corrundum cylinder (7 mm in diameter), mounted vertically on a rotating head, above the specimen. The lower spherical end (radius = 100 mm) of the pin, was then applied against the composite surface (disc) with an adjustable normal force. When rotation was applied, the end of the pin draws a circular wear track (16 mm in diameter) on the working composite surface (Fig. 1).

3. Results and discussion

3.1. Open circuit potential measurements

This method gives information on the electrochemical state of a material, for example active or passive state. However, open circuit potential measurements provide limited information on the kinetics of surface reactions.
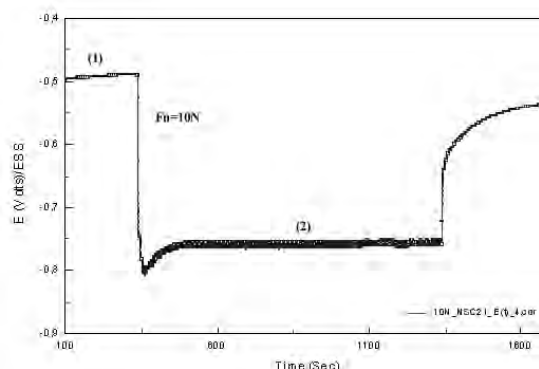
Fig. 2. *Variation of the open circuit potential of Ni-SiC nanostructured coating immersed in 0.5 M K_2SO_4 before(area 1), and during sliding tests (area 2)*

3.2. Polarization diagrams

The open circuit potential recorded during uni-directional pin-on-disk sliding tests in which the disk is the material under investigation, is a mixed potential reflecting the combined state of the unworn disk material and the material in the wear track [12,13,14]. An example of the evolution of the open circuit potential before and during sliding is shown in Figure 2.

The polarization curves of Ni-SiC nanostructured composite coatings in 0.5 M K_2SO_4 were recorded under continuous friction (applied load 10N and 15N; 120 rpm), and without applied friction, by direct potentiodynamic scan from the hydrogen evolution potential domain up to the beginning of transpassive dissolution domain. These curves are presented in Figure 3.
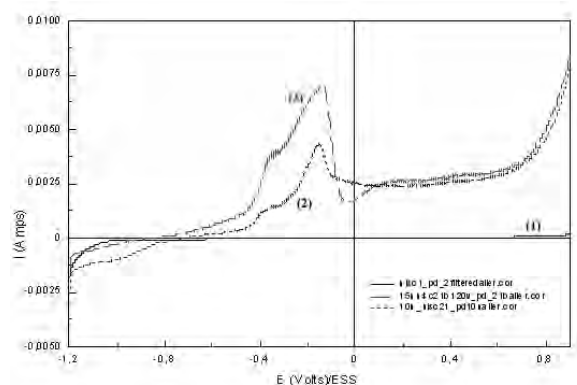
Fig. 3. *Potentiodynamic polarization curves of Ni-SiC nanostructured composite coating immersed in 0.5 M K_2SO_4 recorded by direct potential scan at 0.1 V per minute. Black Curve(1): no friction applied; Blue Curve (2): continuous friction (10 N; 120 rpm);Red Curve(3): Continuous friction (15N, 120 rpm).*

When friction is applied (red and blue curves), the shape of the polarization diagram changes: hydrogen evolution on composite surface is not modified, but an anodic current appears in the potential range from [-0.8 ; -0.0] V/SSE, indicating a dissolution of the coating.

A first approach for interpreting the polarization curves under friction can be developed on the following considerations, based on a concept of "*active wear track*".

The measured current, I can be considered as the sum of two partial currents I_t and I_p ($I=I_t+I_p$). I_t is the current originated from the wear track areas where the passive film is destroyed and metal is active, and I_p the current linked to the surface not subjected to friction and that remains in passive state.

3.3. Current evolution during sliding at different potentials

The current during sliding change from cathodic (without sliding) to an anodic one, and slow variation versus applied load. In Figure 4 it is shown the evolution of current during sliding (Red diagram at 15 N applied force, black diagram at 10 N applied force) at imposed potential of E=-0.710V/ESS.
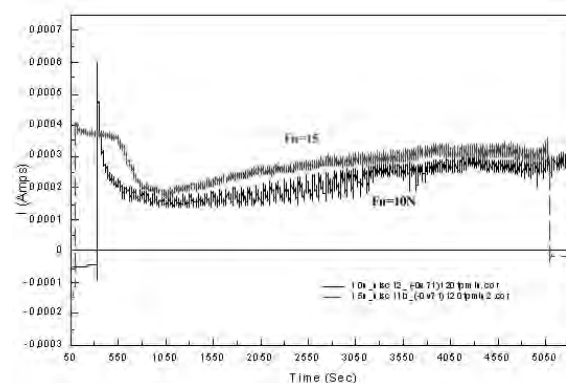
Fig. 4. *Current evolution diagrams under sliding for Ni-SiC nanostructured composite coating immersed in 0.5 M K_2SO_4 recorded under sliding: Red Curve (1): continuous friction (15 N; 120 rpm); Black Curve (2): Continuous friction (10N, 120 rpm).*

3.4. Microtopographic survey of the worn surface

Local wear in the wear track was also measured. It was deduced from surveys of the wear track recorded with an optical high resolution microtopograph, with a lateral resolution of 1 µm and a vertical resolution of 30 nm: the volume of the wear track was measured and the corresponding weight loss was calculated. On Figures 5 and 6 are presented a 3D surface and a profile measured after intermittent sliding test on Ni-SiC nanostructured composite coating, with 15N sliding force and 120 rpm, after 10000 cycles.
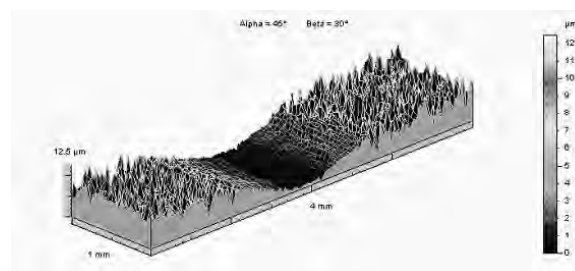
Fig. 5. *3D microtopograph image of wear track area aftercontinuous sliding of Ni-SiC nanostructured composite coating (Fn=15N, 120 rpm, 10 000 cycles)*
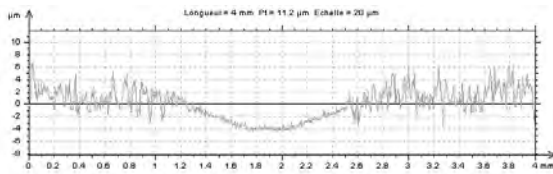
Fig. 6. *2D microtopograph profile of wear track area after continuous sliding of Ni-SiC nanostructured composite coating (Fn=15N, 120 rpm, 10 000 cycles)*

Surface roughness parameters in the middle of the scar (mean value) are: R_a= 0,96 μm; R_t= 5.63μm compared with the non rubbed surface with a R_a= 1.65 μm and R_t=12.4 μm. The introduction of a harder reinforcing phase in the ductile matrix by a certain volume fraction can reduce ductility of the matrix material in the contact region and wear of the matrix can be reduced as a result. The results have to be more worked to have the real conclusions.

Scar surface profiles of pure Ni coating showed higher debris and higher roughness parameters [15]. The experimental data have to be more worked in order to have the conclusion and comparaison with others published data.

3.5. SEM surface morphology after continuous friction

After triboccorosion tests the surface of samples was analysed by SEM and EDS systems. On Figs 7-10 there are the SEM images (at different magnifications) of unrubbed surface (near area along the track) and wear track after continuous friction tests with a normal force of 15 N and 120 tours/min, after 10000 tours of friction.
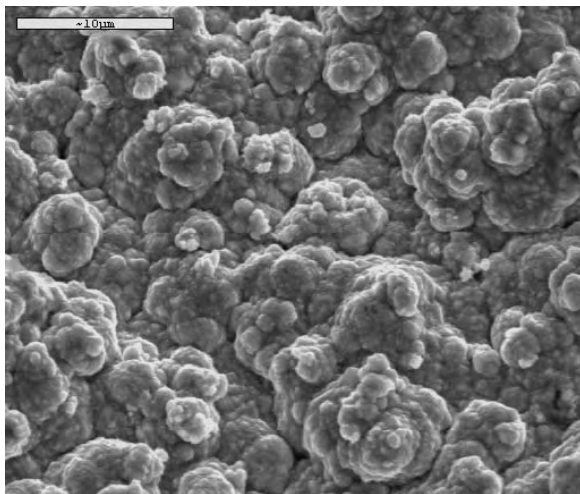
Fig. 7. *SEM image of nanostructured SiC-Ni coating on un- rubbed surface*

On the unrubbed nano structured composite surface (Fig. 7) we observe the nodular disturbed growth of layer with high roughness. The general overview of track area is presented on Fig. 8. The details of wear track are presented on Figs. 9 and 10.

The mechanical damage of the sample surfaces induces an activation of the metal structure, which is well described by the corrosion potential. However the trend with time shows a further increase in the corrosion potential towards more noble values. The equilibrium between the mechanical damage and the electrochemical processes at the metal surface needs some time to be reached.
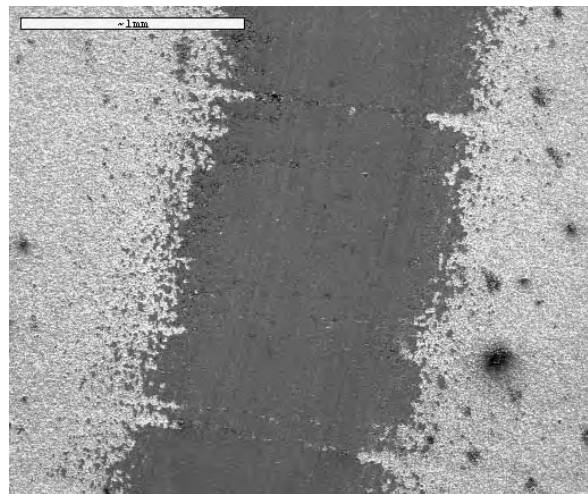
Fig. 8. *SEM image of Wear track after continuous friction test with a normal force of 15 N and 120 tours/min, 10000 tours of friction*
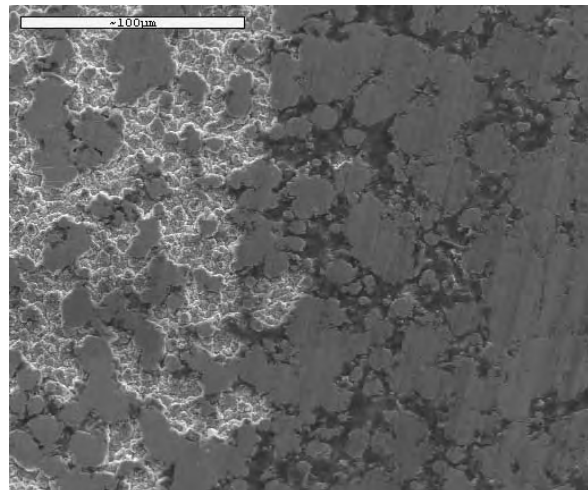
Fig. 9. *SEM image of Wear track details after continuous friction test with a normal force of 15 N and 120 tours/min, 10000 tours of friction.*
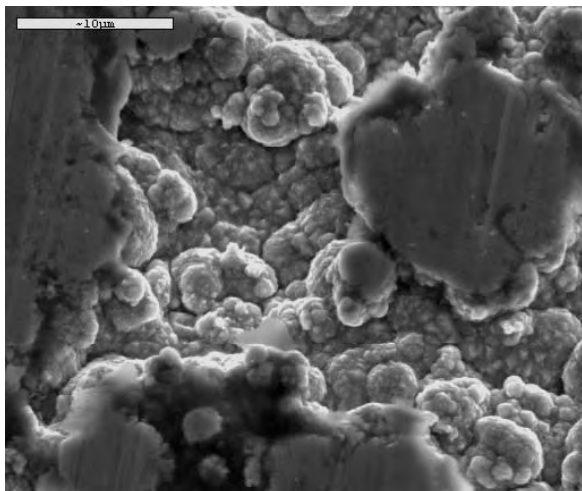
Fig. 10. *SEM image of near area along the track (15 N and 120 tours/min, 10000 tours of friction)*

At the beginning, the mechanical wear induces a rapid deterioration of the protective surface layers, which causes a drastic decrease of the corrosion potential.

4. Conclusions

The tribocorrosion behaviour of nanosized dispersed SiC - Ni-ZrO$_2$ composite coatings in a pin on disk sliding system in 0.5 M K$_2$SO$_4$ solution was investigated combined with *in-situ* electrochemical (potential and polarization diagrams) measurements and *ex-situ* SEM –EDS and microtopographic surveys.

This overview points out the capabilities of electrochemical methods like open circuit potential measurements, polarization curves measurements, for the *in situ* investigation of materials used under tribocorrosive conditions in sliding contacts. They can provide not only essential information on the surface conditions of composite surface in sliding contacts, but also on the kinetics of reactions that control the corrosion component in the material loss during tribocorrosion tests.

Aspects of the tribocorrosion mechanism that can be clarified in this way are the nature of electrochemical reactions, the formation of protective passive surface films, the interactions between electrochemical reactions and friction. Information can also be gained on kinetics such as corrosion rate, rate of depassivation by mechanical action in the contact area, and rate of repassivation.

Nickel – nano silicon carbide composite coating is affected by a tribocorrosion process when subjected to friction in 0.5 M K$_2$SO$_4$. This tribocorrosion process involves mechanical destruction of the passive film on the contact areas by friction, and subsequent restoration of the film (repassivation) when friction stops.

The surface morphology of composite layers are different compared with pure nickel coating. The surface structure is disturbed by dispersed particles. The crystal growth of nickel matrix result in a preferentially random than, in an oriented one.

Acknowledgements

References

[1]. **N. Guglielmi**, *J. Electrochem. Soc*. **8**, 119 (1972) 1009-1012.

[2]. **L. BENEA, P. L. BONORA, A. BORELLO, S. MARTELLI, F. WENGER , P. PONTHIAUX, J. GALLAND**; *J. Electrochem. Soc.*., **148** (7) C461-C465 (2001)

[3]. **BENEA L., BONORA P.L., BORELLO A., MARTELLI S.**; *Materials and Corrosion,* **53**, 23-29 (2002)

[4]. **L. Benea, P. L. Bonora, F. WENGER, P. PONTHIAUX, J. GALLAND**; "Processing and Properties of Electrodeposited Composite Coatings: Results and Perspectives", *KEY NOTE Lecture, CD-ROM Proceeding:* 15TH International Corrosion Congress -Frontiers in Corrosion Science and Technology, Granada, Spania, 22-27 Septembrie 2002

[5]. **L. Benea**, *Composite Electrodeposition -Theory and Practice*, Ed: PORTO FRANCO, Romania, ISBN 973 557 490 X, (1998).

[6] **S. W. Watson**; *J. Electrochem Soc*., 140, 2235 (1993).

[7]. **G. Maurin** and **A. Lavanant**; *J. Appl. Electrochem*., 25, 1113-1121 (1995)

[8]. **J. Fransaer**, J. P. Celis and J.R.Roos; *J. Electrochem. Soc*., 139, 413-425 (1992).

[9]. **J. Fransaer**, J. P. Celis and J. R. Roos; *Metal Finishing*, 91, 97-100 (1993).

[10]. **L. Benea** and **G. Carac**, *Metallurgy and New Materials Researches* V No 2, 1-19(1997).

[11]. **K. H. Hou, M.D. Ger, L.M. Wang, S.T. Ke**, *Wear* 253 [(2002) 994-1003

[12]. **R. Oltra**, in "Wear-Corrosion Interactions in Liquid Media" edited by A. A. Sagües and E. I. Meletis, Minerals, Metals and Materials Soc. (1991) 3.

[13]. **Garcia, D. Drees and J.P. Celis,** Wear, 249, p.452-460 (2001).

[14]. **L. Benea, P. Ponthiaux, F. Wenger, J. Galland, D. Hertz, J. Y. Malo**; *Wear, Special Issue Wear Modelling,*256 (2004) Issues 9-10, p. 948-953.

[15]. **L. BENEA, P. L. BONORA, A. BORELLO, S. MARTELLI;** *Wear,* 249, Issue 10-11, Nov-2001, p. 995-1003.

A RESEARCHES FOR THE DETERMINATION OF THE ATC Si10Mg ALLOY FATIGUE LIFE, FUNCTION OF DIFFERENT APPLIED THERMAL TREATMENT CYCLES

Adrian DIMA[1], Alina Adriana MINEA[1], Iulia-Margareta DIMA[2]

[1] Technical University "Gh. Asachi", Iassy;
[2] Tutora School, Iassy
e-mail: aminea@tuiasi.ro

ABSTRACT

The experimental researches which were made, emphasized the opportunity of applying heat treatment cycles, in order to increase fatigue life of ATC Si 10 Mg alloy. The increase of minimum fatigue resistance is approximately 2,5 when complex heat treatment cycles apply.

KEYWORDS: aluminum alloys, heat treatment cycles, fatigue resistance.

1. Introduction

The aluminum alloys which are suited to plastic deformation processing are much more often studied from the view point of their physico-mechanical and structural properties, on account of their usage in machine elements building.

The casting alloys, especially the complex silico-aluminium-magnesium ones, are used nowadays more and more at the casting of parts which are subjected to variable stresses; this fact leads to the necessity of studying the alloy behavior at fatigue.

1. Experimental

The approach to the experimental researches carried out to establish the fatigue behavior of the discussed alloy, namely the ATC Si 10 Mg one, was meant to determine the fatigue life variation of the casting state- and thermal treated alloy, after different thermal treatment cycles imposed by the research.

The used experimental research methodology is as follows:
i) The determination of the chemical composition of the studied alloy.
ii) The obtaining of NPL-434 Amsler test bars, necessary for studying both the fatigue strength and the fatigue life (constant bending cycle).
iii) The adaptation and the testing of various complex thermal treatment cycles which are in accordance both with the 201/2 - 7 STAS specifications and with the ternary equilibrium diagram of the studied alloy.

iv) The determination of the Wohler fatigue strength curves of the discussed alloy, both in a costing and in a case-hardened and 160°C artificial aged state, time of exposure 7 hours, the purpose is to study the influence of the thermal treatments on the fatigue strength.

As part of the experimental researches, the variation curves have been drawn:

$$\sigma_{-1} = f(\lg N) \qquad (1)$$

Where: σ_{-1}- the fatigue bending strength for the symmetrical alternating cycle (daN/mm^2); N — number of loading cycles.

v) The determination of the fatigue life curves till the failure of the test bars occurs; the fatigue life curves are experimentally determined for all the complex experimental thermal treatments cycles, and are of the type

$$gN=f(t). \qquad (2)$$

Where: N- number of loading cycles till failure; t-time of exposure at constant temperature for artificial aging, hours.

From the specialized literature for plastically deforming hard aluminum alloys, one can see that tolerable strength at alternating stresses ranges from 2 to 2.7 daN/mm^2.

For light non-ferrous alloys, the strength at alterating stresses can be approximated as being:

$$\tau_{-1} = (0.25...0.5)R \qquad (3)$$

As it is known, the metal fatigue strength can be influenced by various factors which may be divided in three major groups.

1. Constructive factors (shape of the work, assembly type, machining accuracy, etc.).

2. Technological factors (material, surface quality, machining, accuracy etc.).

3. Working conditions (type of loading, the asymmetry degree of the cycle, short time overloading Ann-under loading, shocks, loading frequency, working temperature, corrosive action of the working medium).

To determine the fatigue strength, the corrosion strength under stress, and the corrosion durability under constant mechanical stress, only the test bars whose spreading field of both the maximum roughness values and of the ovality of the profiled section is in accordance with the STAS specifications, have been selected.

To carry out this research, the test bars cast in chills under gravimetrical pressure (in conditions similar to the production process) have been used; these test bars have been made in a single melting operation and are responding to the 201/1-71 STAS specifications (Table 1) from the view point of the chemical composition.

Table 1

Alloy mark		Chemical composition %				
		Cu	Si	Mg	Mn	Al
ATC Si 10 Mg	STAS	−0.1	9 … 11	0.15 … 0.4	0.2 … 0.6	6 res
	obtained (819 melting operation)	−0.1	10.6 … 10.72	0.2 … 0.3	0.25	res
Impurities						
		Fə	Zn	Pb	Ni	
STAS		0.7	0.1	0.005	0.1	
obtained (819 melting operation)		0.47 … 0.52	—	—	—	
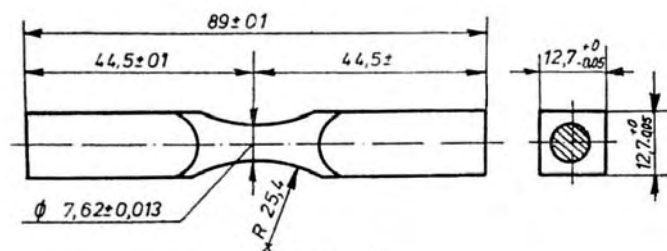
Fig. 1

To study the fatigue life and the fatigue strength variation, some Amsler test bars have been manufactured (Fig. 1.); these test bars have been milled off, machined with profiled tools and finished with coated abrasives fastened on a profiled support. The thermal treatment cycles taken into consideration during experiments (Fig. 2) have been chosen function both of the ternary equilibrium diagram of the studied alloy and of the 201/2-71 STAS specifications. During tests, the so-called "placing in solution" has been used, at the same heating temperature as the same temperatures (520°C) as indicated by standards; the times of exposure temperatures for the artificial aging thermal treatment have been increased (27 cycles of thermal treatments). The high time of exposure is justified

considering that as cast parts the precipitates are much more rough then as the plastically deforming alloys; this fact leads to the necessity of a longer time

of exposure at the temperature of, "placing in solution" for their dissolution.
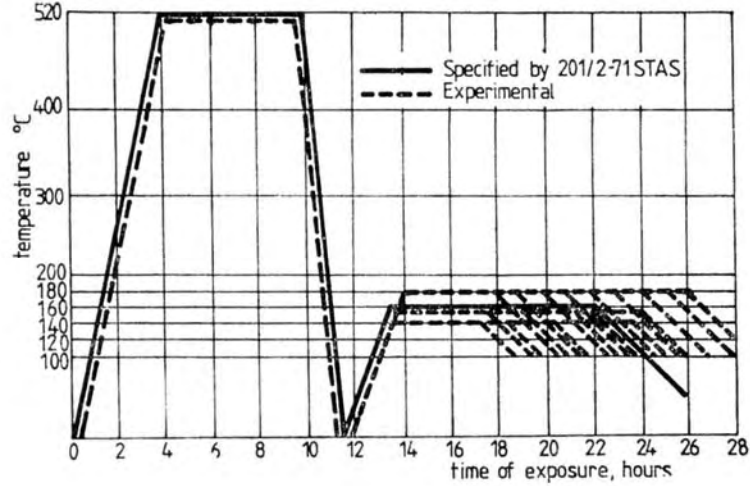
Fig. 2

The hardening thermal treatment has been done immediately after the "placing in solution" in hot water at 80...90°C, a medium which supported an optimal rate of coaling (140°...160°C/s) and, at the same time avoided the coming out of the deformations produced under the action of the hardening thermal stresses.

The constant keeping of the temperature of "placing in solution" of the alloys has been adapted after preliminary experiments of the cycles of thermal

treatment indicated in 201/2—71 STAS; as the result of these tests, the optimal values for the mechanical properties in the case of the adaptation of a "placing in solution" at 520°C, for 6 hours, have been obtained.

The whole set of the test bars necessary for experiments have been measured by the methodology of determining both the roughness R_{max} and the ovality Q_r.
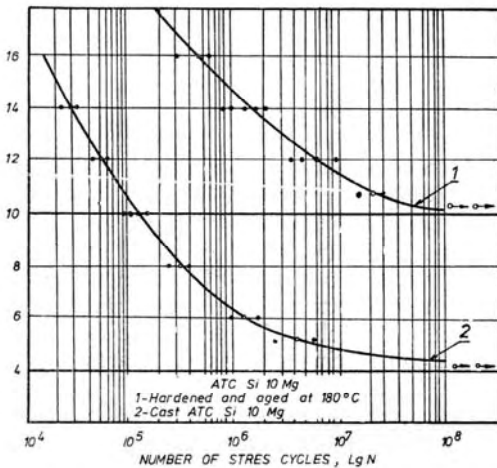
Fig 3
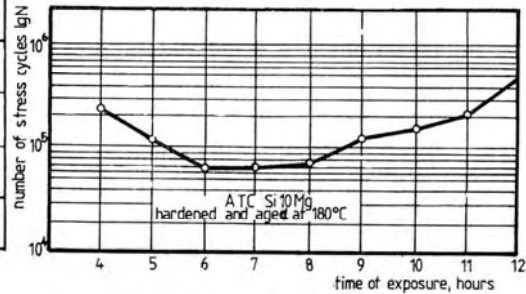
Fig. 4

To determine the Wohler fatigue curves at variable cyclical alternating symmetrical bending loadings, the classic working methodology has been used, by taking a number of 14... 16 samples for each plotted curve. To determine the fatigue strength of the

discussed alloy, the number of bending cycles has been reduced to 10^8 cycles.

During the experiments, we have plotted the Wohler-type diagrams for the cast alloy and for the

ATC Si 10 Mg alloy hardened and aged at 180°C, time of exposure 10 hours, with a complete cycle of thermal treatment; the maximal static-mechanical characteristics have been obtained (Fig. 3).

By the comparative study of the obtained diagrams, it has been noticed that by applying the complete thermal treatment cycle, the fatigue strength of the alloy σ_{-1} is increased from 4 daN/mm^2 to 10 daN/mm^2, this is a phenomenon which justifies in excess the necessity of employing thermal treatments to this type of alloys.

For determining the fatigue life variation of the alloy, the semi-logarithmic variation curves of durability up to failure, at a constant strain loading (14 daN/mm^2) for the whole range of thermal treatment cycles tested on the alloy (Fig. 4) have been drawn.

2. Conclusions

From the study of the durability variation curves, function both of temperature and time of exposure during the thermal treatment of artificial aging, it results the following principal aspects.

1. The durability has, for every exposure temperature, a minimal value for reduced times of exposure (6 hours), a fact which is explained by the loss of coherence with the solid solution of the distinct structural phase of the type ; this change leads to the annulling of coherence with the solid solution.

2. The cycles of complex thermal treatment which contain artificial aging at 180°C lead to maximum values of durability.

3. All the cycles of complex thermal treatment lead to durability values considerably higher then the durability of the cast state alloy.

As a conclusion, the experimental determination carried out in this study, pointed out the fact that the application of cycles of complete thermal treatment structural hardening leads, in totality, to an increase both of the fatigue strength and of the durability at a constant strain loading of the studied alloy.

The hardening thermal treatment is, therefore, a very efficient method of increasing the mechanical characteristics of the Romanian-made aluminum alloys.

References

[1]. Speidel M.O., *Conference on Fundamental Aspects of Stress Corrosion Cracking*, State University, Columbus, Ohio State, 11—15, 1967.

[2]. Nadasan S., *Oboseala metalelor*. Ed. tehn., Buc, 1962.

[3]. Dima Ad., *Contributii la studiul micsorarii efectelor coroziunii sub sarcina asupra aliajelor de aluminiu românesti, prin actiunea unui ciclu de tratament termic adecvat*, Teza de doctorat, Institutul Politehnic din Iasi, 1980.

ESTIMATION OF THE METALLURGICAL INDUSTRY IMPACT ON THE ENVIRONMENT

Aurel CIUREA, Marian BORDEI

"Dunarea de Jos" University of Galati
e-mail: **ciurea.aurel@ugal.ro**

ABSTRACT

Objectively, the ecosystem in its development and working implies the accumulations on of some nonconcordances. Summing these disfunctions without taking into consideration their attenuation, may lead to producing, achieving of the risk, with various intensities.

The evaluations of the impact on the environment represents an instrument that is used to help and improve the process of taking decisions.

KEYWORDS: environment, impact, metallurgical industry

1. Introduction

The economical activity is strongly related to the environment by what is called materials balance. According to the law of thermodinamic, the law of mass and energy conservation, the raw material, the energy consumed for its processing, which were taken from the ambient environment, must appear elsewhere and under other kind as part of the economical system.

In other words: $\sum i = \sum e$ where: i is the imputs and e reprezent the outputs.

Practically, processing the raw materials and the materials must have results as both finite products and also wastes witch can be solid, gaseous or liquid. These wastes, depending on their toxicity may affect more or less the environment.

The problem that must be taken into consideration nowadays and in future is to find the technological solutions, the most adequate ones to reduce the polluting emission.

The industry with its various branches represents the main source of the environment pollution.

The metallurgical industry both because of the kind of raw materials and of the enormous quantities used, and by the complexity of its technological process, is one of the main artificial pollution sources of the environment with gaseous and powders containing heavy metals. That is why an important preoccupation in this sector must be the exact determination of the metallurgy contribution to the general pollution of the environment and consequently the continuous improvement of the pollution control installations.

2. The evaluation of the impact on the environment

In the functioning and developing of the ecosystem there is a certain capacity of tolerance, limited by a threshold. At the overfulfilment of this threshold, the ecosystem enters in a fragile state, which through some lack of balance it generates negative phenomena with severe consequences in its functioning or existence.

Considering its feature, metallurgy represents a risk, in consequences a possible danger of appearing a situation when the development of an action to be submitted to a perturbation or even its breaking off.

Objectivelly, the ecosystem in its development and functioning implies the accumulation of a particular structure. Summing all these malfunctions without taking them into consideration or their attenuation may lead strictly to the risk, with various intensities: accident, break, disaster.

The evaluation of the impact on the environment represents an instrument which is used to help and improve the process of decision taking. The aim of an EIM (Evaluation of the Impact on the Environment) is to determine the potential effects of a suggested development project regarding the environment, society, health.

Although there are some definitions of EIM, neither of them is generally accepted. The definition after Clark (1989) seems to be the more comprising and direct: "*The evolution of the impact on the environment is a procedure to encourage the decision responsibles (managers) to take into account the*

possible effects of investments development regarding the environment quality and raw materials productivity and an instrument for collecting and assembling data which are considered necessary by the planners in order to achieve development projects, more durable and favourable for the environment. Usually the EIM is applied in view to sustain the policy towards a more rational and durable use of the resources for the economical development".

As part of the European Union which aims to a political, economical integration and stability the environment policy came into operation in 1973.

UE established two main principles to which all the environment policy measures must subordinate.

First Principle: "The pollution source must pay for the control costs of the emissions and for the antipollution measures"

Second Principle: "Better prevent than cure" (Williams, 1998).

The implementation of the European instructions regarding the effects evaluation on the environment is a logical measure, in accordance with the second principle.

In March 1985, The Environment Council of the European Community approved the NORM 85/337/EEC, which was officially put into use on 27 June 1985. This is known also as "EIM NORM". The aim of this NORM "regarding the evolution of some public and private project effects on the environment" is immense. This takes into consideration both the direct effects and the indirect ones of a project on the following factors:

-popullation, flora, fauna;

-soil, water, air, climate and landscape;

-interactions among the factors mentioned at the previous points;

-the material possessions and the cultural heritage.

The environment impact must be analyzed from a triple perspectives.

-the opportunity cost of the natural ressources use, which influences the economical value of the environment foods.

-the modification of the self-adjustment capacity of the environment.

-the modification of the human welfare.

From a graphical point of view, the environment impact may be shown as in fig.1.
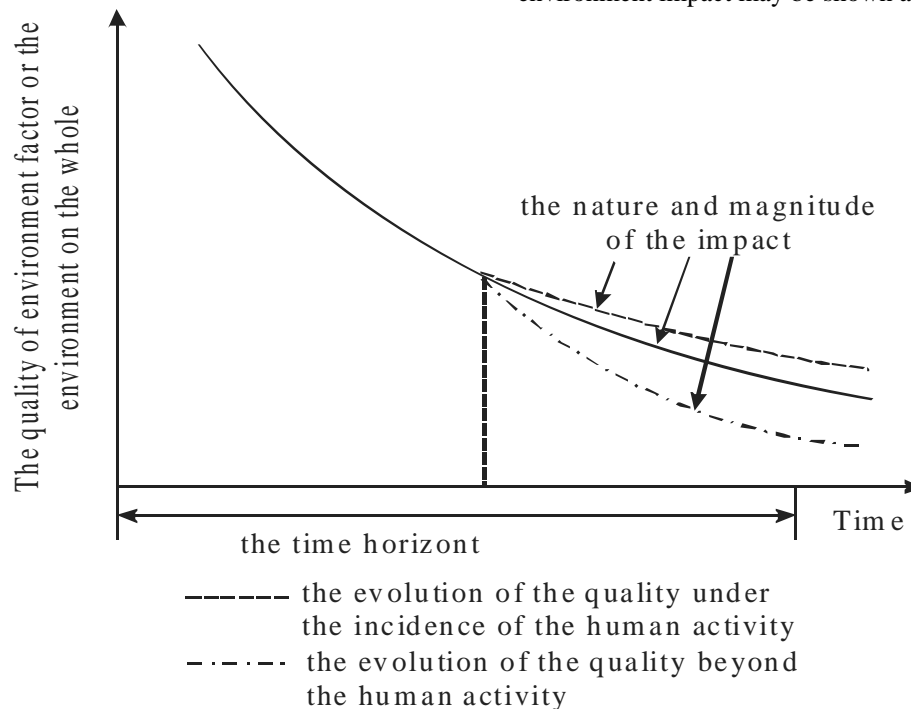
Fig.1. *The platting of the environment impact concept.*

The perception of the impact on the environment is according to the adopted criterion namely:

a). According to the may of appearance:

-direct impact

-indirect impact

-cumulative impact

-synergic impact

b). According to the duration:

-permanent impact

-temporary impact

c). According to the effect kind:

-positive impact

-negative impact

d). According to the sphere of extent and importance:

    -global impact

    -residual impact

    -main impact

    -secondary impact.

Although there are different norms for drawing up EIM we may identify some main stages for the fulfillment of the process. These stages, diagramed in fig.2, they are main because the process will not function if they are not taken into account.

Analyse of the suggested project
↓
Defining the field of activity
↓
Preparing the final form of CIM
↓
Public verifying and participating
↓
Preparing the final form for CIM
↓
Final checking
↓
Decision taking
↓
Evolution and monitoring
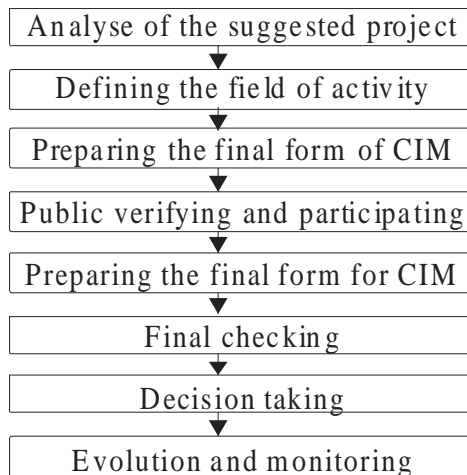
Fig.2. *The main stages of EIM,*
where CIM-communication environment impact.

A complete description of all possible impacts of a project suggested would represent a enormous task and also, one very inefficient because there is a significant number of minor impacts as importance. From this reason, EIM aims mainly at the important impacts on the environment.

An important role in this respect has the identification, which must be achieved in at least two stages:

a). at designing, stage when it must and may apply "The second principle of the prevention"

b). in exploitation, stage in which it is strictly determined the way in which the project responds to the imposed theme and measures are established to rectify the eventually deficiencies.

The American norms define the identification as a "early and open process, aiming at identifying the significant aspects connected to the suggested activity.

One of the identification targets is that of informing and implying all the agencies and persons that are interested or affected by the suggested project.

Another target is that of identifying the aspects that must be minutely analyzed, the same those which not being sufficiently important, will be ignored".

Stage b) does not have connection with the permanent monitoring of the projected and worked objective and refers to stage of putting into function and has in view to correct the negative effects that can appear from the projection and working stages.

In parralel with the identification of the risks it is necessary their cuantification and the measures in order to prevent. In this respect, we will mark with 1

10 the risks alongside with the impact rise. (1 being the minimum risk accepted according to the environment norms) and with -10 -1 the imposed measures (adding that 0 risk does not exist and in this respect, the suggested valuable measures, summed up with the risk, cannot lead to 0 risk).

For the evolution of the environment impact (EIM) we suggest the following diagram, shown in table 1.

This presents the following advantages:

    -identifies risks;

    -visualize the measures of reducing the risks and their effects;

    -creates the basis for an efficient monitoring.

Table 1. *Diagram evolution environment impact where: E-estimated; R-achieved.*

Activity	Affected structure	Effect (1 → 10)		Measure	Effect (-10 → -1)		Total	
		E	R		E	R	E	R
1 .	water							
	air							
	soil							
. n	water							
	air							
	soil							

3. Conclusions

The past faults due mainly to the idea of an rapid, economic growth at any rate, even without taking into account the effects produced an the environment had frequently to ecological damages, very difficult to be remedied.

The destruction of the environment is considered by many people as a price to be paid in order to obtain a high standard of living.

The question that may be asked nowadays is: how can the preoccupations from the environment protection domain be integrated in the economical rise wanted by everybody? In this respect, EIM cumulated with the adequate measures represent an important step.

References

[1]. Radu, C., Stanciu, R. – *Management industrial*, Ed. Bren, Bucuresti, 1998.
[2]. Vadineanu A. – *Dezvoltarea durabila-teorie si practica,* Ed. Un iversitatii Bucuresti, 1999.

ASPECTS REGARDING
THE ATMOSPHERE POLLUTION MONITORING

**Lucica BALINT, Minodora RÎPĂ, Petre NIŢĂ,
Simion BALINT,Tamara RADU, Simona LEBĂDĂ**

"Dunarea de Jos" University of Galati
e-mail: lucia.balint@ugal.ro

ABSTRACT

This paper presents information regarding the variation of aerosols concentration in a central area in Galati city. For a period of time of 2 years and 5 months, there have been done correlations between aerosols concentrations with grading classes and the dominant wind directions (E-W, N-NW~S-SE, S~N, N~NE~S-SW).

The results of the measurements are particular for only a point in time, being influenced by random variables (traffic intensity, temperature, pressure, wind speed, humidity etc.).

Keywords**:** aerosol, pollution, particulate matter, air quality.

1.Introduction

Air pollution in urban areas represents a major issue related to public health and environment protection. The development of an air quality management system is therefore an objective of utmost importance for the local public authorities.

Air pollution is one of the side effects of human activity and has a negative impact on public health. The structural changes that took place in the industrialized society, characterized by intense industrial polluting processes and services, determined an increase of the pollution level.

The strategy for improving and/or preserving the air quality involves the following steps:

- Collecting information and data concerning the origin and the concentrations of the urban pollutants, as well as their harmful effects on the environment (emissions measurements and epidemiologic data specific for urban air pollution);

- Collecting information on the causes that generate air pollution by assessing the polluting emissions (inventorying the air pollution sources)

- Adopting administrative, economic and technical control measures of air pollution in order to decrease and/or eliminate urban air pollution and its effects.

As a result of the three steps mentioned above, the main goals of Air Quality Monitoring System in urban areas are:

o assessment of air pollution sources;

o air quality measurements;

o evaluation of the transport, diffusion and transformation processes of pollutants in the urban atmosphere;

o forecasting the evolution trends of air quality, related to the emission/imission standards, as well as the effects on public health and specific environmental elements of urban areas.

1.2. Air monitoring in urban areas

The Air Quality Monitoring System in Urban Areas (AQMSUA) is a part of the Air quality management system that ensures the knowledge and the objective aggregation of information concerning air quality, useful in order to plan the environment quality, as well as to build the control loop intended to achieve the objectives of these planning.

The main goal of the Air Quality Monitoring System in urban areas is to assist the decision makers in:

- air quality planning;

- monitoring the environment quality;

- verifying (by using the monitoring data) the level of compliance with the environmental standards and regulated conditions, for each potentially polluting company;

- applying the measures for preventing, rehabilitating and controlling the air quality, in order to comply with the planned objectives.

1.3. Atmospheric pollutants

Airborne particulate matter represents a complex mixture of organic and inorganic substances. Mass and composition in urban environments tend to be divided into two principal groups: coarse particles and fine particles. The barrier between these two fractions of particles usually lies between 1 μm and 2.5 μm. However, the limit between coarse and fine particles is sometimes fixed by convention at 2.5 μm in aerodynamic diameter (aerodynamic diameter that is the size of a unit density sphere with the same aerodynamic characteristics) for measurement purposes.

The smaller particles contain the secondarily formed aerosols (gas-to-particle conversion), combustion particles and recondensed organic and metal vapours. The larger particles usually contain earth crust materials and fugitive dust from roads and industries. The fine fraction contains most of the acidity (hydrogen ion) and mutagenic activity of particulate matter, although in fog some coarse acid droplets are also present. Whereas most of the mass is usually in the fine mode (particles between 100 nm and 2.5 μm), the largest number of particles is found in the very small sizes, less than 100 nm.
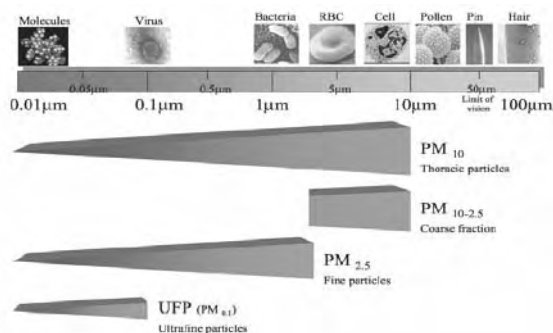
Fig. 1. *Particulate mateer classification [16].*

As anticipated from the relationship of particle volume with mass, these so-called ultrafine particles often contribute only a few percents to the mass, at the same time contributing to over 90% of the numbers. Particulate air pollution is a mixture of solid, liquid or solid and liquid particles suspended in the air. These suspended particles vary in size, composition and origin. It is convenient to classify particles by their aerodynamic properties because: (a) these properties govern the transport and removal of particles from the air; (b) they also govern their deposition within the respiratory system and (c) they are associated with the chemical composition and sources of particles.

These properties are conveniently summarized by the aerodynamic diameter. Particles are sampled and described on the basis of their aerodynamic diameter, usually called simply the particle size. The size of suspended particles in the atmosphere varies over four orders of magnitude, from a few nanometres to tens of micrometres. The largest particles, called the coarse fraction (or mode), are mechanically produced by the break-up of larger solid particles. The smallest particles, less than 0.1 μm, are formed by nucleation, that is, condensation of low-vapour-pressure substances formed by high-temperature vaporization or by chemical reactions in the atmosphere to form new particles (nuclei). Particles in this nucleation range or mode grow by coagulation (the combination of two or more particles to form a larger particle), or by condensation (the condensation of gas or vapour molecules on the surface of existing particles).

Therefore the efficiency of both coagulation and condensation decreases as particle size increases, which effectively produces an upper limit such that particles do not grow by these processes beyond approximately 1 μm. Thus particles tend to "accumulate" between 0.1 and 1 μm, the so-called accumulation range. Sub micrometre-sized particles can be produced by the condensation of metals or organic compounds that are vaporized in high-temperature combustion processes. They can also be produced by condensation of gases that have been converted in atmospheric reactions to low vapour-pressure substances.

The particles produced by the intermediate reactions of gases in the atmosphere are called secondary particles. Secondary sulphate and nitrate particles are usually the dominant component of fine particles. Combustion of fossil fuels such as coal, oil and petrol can produce coarse particles from the release of non-combustible materials, i.e. fly ash, fine particles from the condensation of materials vaporized during combustion, and secondary particles through the atmospheric reactions of sulphurxides and nitrogen oxides initially released as gases. Because of its complexity and the importance of particle size in determining exposure and human dose, numerous terms are used to describe particulate matter.

Some are derived from and defined by sampling and/or analytic methods, e.g. "suspended particulate matter", "total suspended particulates", "black smoke". Others refer more to the site of deposition in the respiratory tract, e.g. "inhalable particles", which pass into the upper airways (nose and mouth), and "thoracic particles", which deposit within the lower respiratory tract, and "respirable particles", which penetrate to the gas-exchange region of the lungs. Other terms, such as "PM10", have both physiological and sampling connotations [16].

According to the international and national legislation, particulate matter (PM) is defined in the following manner (EPA: 1997; Council Directive 1999/30/EC of 22 April 1999 relating to limit values

for sulphur dioxide, nitrogen dioxide and oxides of nitrogen, particulate matter and lead in ambient air, Romanian OMAPM No. 592/25.06.2002 (OJ No 765/21.10.2004)).
 - PM$_{10}$ - particles which pass a 50% inlet cut-off at the aerodynamic diameter of 10 μm;
 - PM$_{2.5}$ - particles which pass a 50% inlet cut-off at the aerodynamic diameter of 2.5 μm.

1.4. Limits of atmosphere pollutants emission

In the industrialized countries, the emission standardization has been used in the policy of environment protection together with air quality standards that limit pollutant concentrations that may be allowed to the atmosphere in a certain period.

Table 1. *Particulate Matter in the Atmosphere*

Total Suspended Particulate mass TSP < 35 μm	35 to 10 μm, mostly natural Dust, sea salt, pollen, …
Inhalable Aerosols PM10 < 10 μm	10 to 2.5 μm, largely natural Dust, sea spray, some nitrates
Fine Aerosols PM2.5 < 2.5 μm	2.5 to 0.25 μm, mostly man made Fine dust, nitrates, sulfates,organics, smoke
Very fine aerosols, < 0.25 μm,	0.25 to circa 0.01 μm, Almost entirely man made;
Ultra fine aerosols, < 0.10 μm	high temperature combustion, heavy organics, soot, metals

1.5. Aerosols' action on the human body

The particulate matter parameters of potential interest for public health are: size, surface area, number, acidity, metals, elemental and organic carbon, mass, size , distribution, ions, bioaerosols.

The respiratory system is most frequently affected by the atmospheric aerosols. Size of particles is directly linked to their potential for causing health problems. Small particles less than 10μm pose the greater problems, because they can get deep into the lungs, and some may even get into the bloodstream. Larger particles are of less concern, although they can irritate eyes, nose, and throat.

People with heart or lung diseases, older adults, and children are considered at greater risk from particles than other people, especialy when they are physically active.
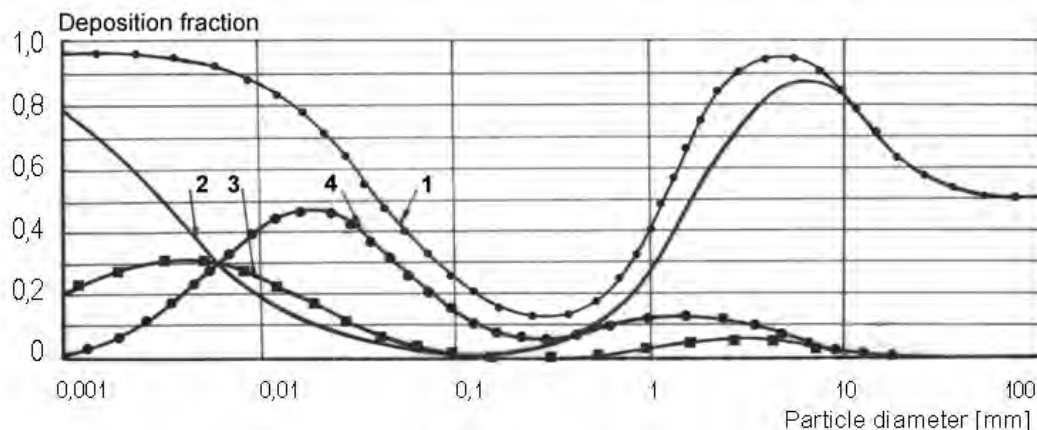
Fig. 2. *Probability of deposition in various parts of the lung, relative to particle size: 1. Total deposition; 2. head airways; 3. tracheobronchial region; 4. alveolar deposition (pulmonary region) ([15], ICRP[1]-1975).*

---

[1] International Commission on Radiological Protection

According to P. E. Marrow's diagram (fig. 2) one could observes that aerosols with particle diameter in the size range 0,1 – 10,0 μm get into the pulmonary alveoli, considered the most sensitive part of the respiratory system.

The harmful action of this particulate matter depends on the retained quantity.

2. Experimental results

The air quality has been monitored from November 2002 to April 2005 by "Environmental Engineering" Laboratory of the Faculty of Metallurgy and Materials' Sciences, University "Dunărea de Jos" of Galati.

The monitoring activity led to finding and accumulating information and data on the atmospheric aerosols charge in the neighbourhood of Domneasca and Basarabiei crossing street (fig. 3) [3, 4, 5].

In this area, due to the extremely intense traffic and the depletion of the natural arboreous curtain, from both sides of the street, supplementary pollutants were added to the pollutants occurring from industrial plant emissions.

Fig. 3. *The localization of the area of experimental researches, on the Galaţi city map and the most frecvently wind directions: 1- E~W, 2 - N-NW~S-SE, 3 - S-N, 4 - N-NE~S-SW.*

The instrument used for measurements is a particle counter that can measure up to 750 000 particles in a dm^3 of air from the environment, based on the following diameter size ranges (Table 2), that were also used on the following plots.

Table 2. *Diameter size ranges*

a	b	c	d	e	f	g	h	i	j	k
0,4-0,5 [μm]	0,5-0,6 [μm]	0,6-0,7 [μm]	0,7-0,8 [μm]	0,8-0,9 [μm]	0,9-1 [μm]	1-1,5 [μm]	1,5-2 [μm]	2-4 [μm]	4-7 [μm]	7-10 [μm]

The research period was between April 2002 and May 2005. Figures 4 and 5 presents examples of the particulate matter analysis, for two days, in the research period.

Figures 7 – 20 presents the particles' concentration, analysed for a specific particle diameter size range.

a	b	c	d	e	f	g	h	i	j	k
192000	60000	78000	7200	6000	1800	11100	1800	2100	0	0
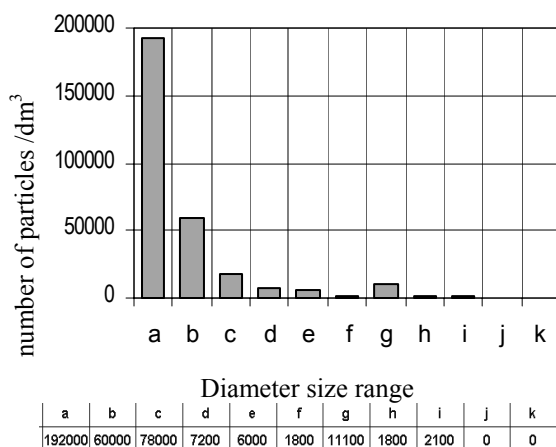
Fig. 4. *Particulate matter analysis on 18.03.02*

a	b	c	d	e	f	g	h	i	j	k
90000	25000	20000	24000	18000	21500	1000	1500	2900	50	0
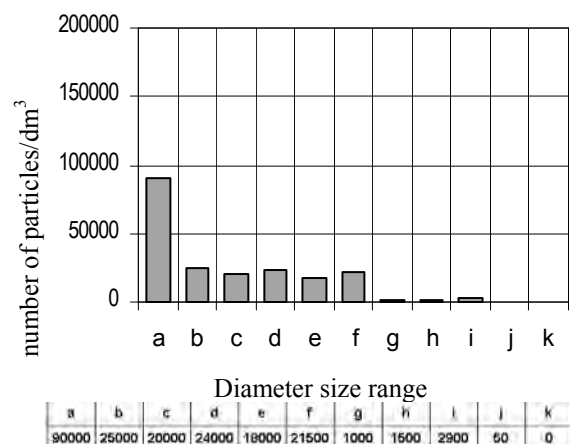
Fig. 5. *Particulate matter analysis on 8.03.05*

Figure	Date	Temperature [^{0}C]	Humidity [%]	Visibility [km]	Wind direction
4	18.03.02	9	97	10	N-NE
5	8.03.05	-1	52	6	N-NV
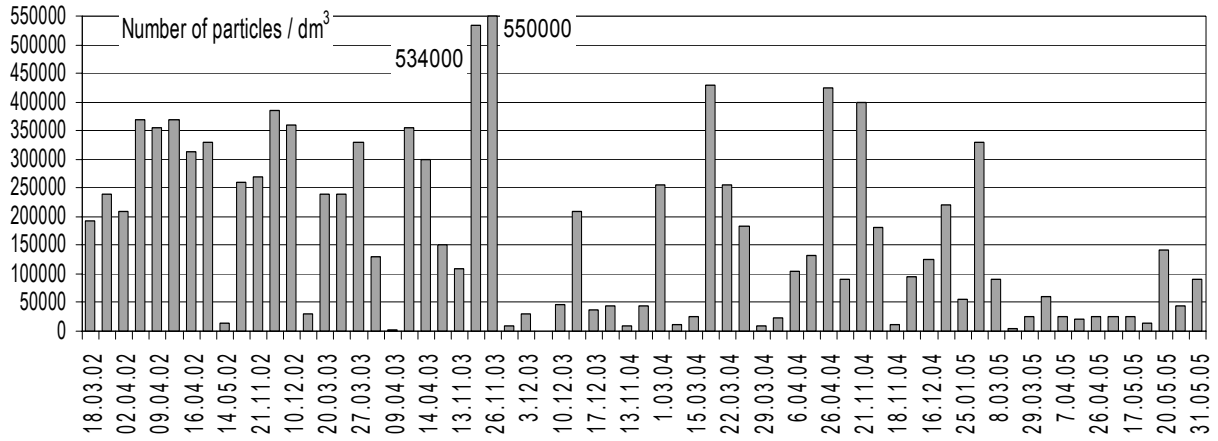
Fig.6. *Particles' concentration (diameter size range 0,4 – 0,5 μm)*
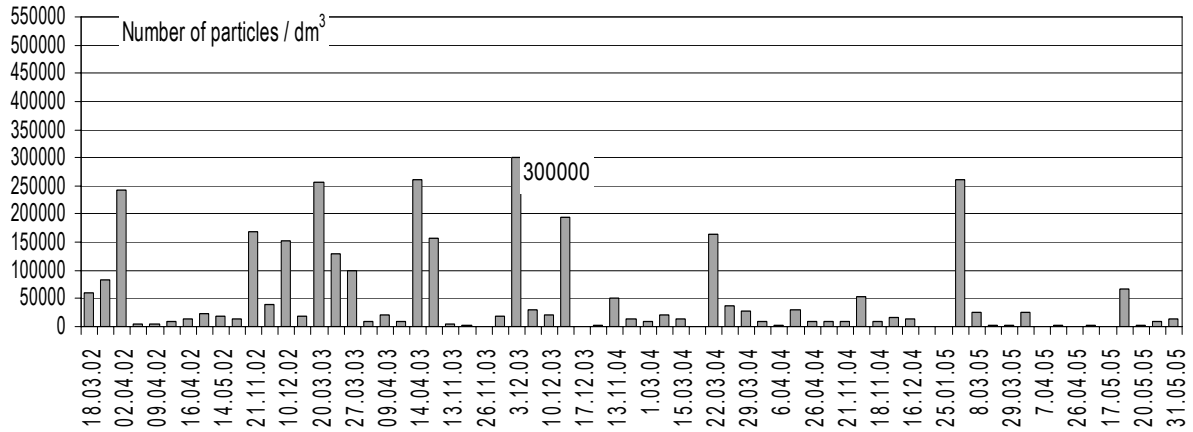
Fig.7. *Particles' concentration (diameter size range 0,5 – 0,6 μm)*
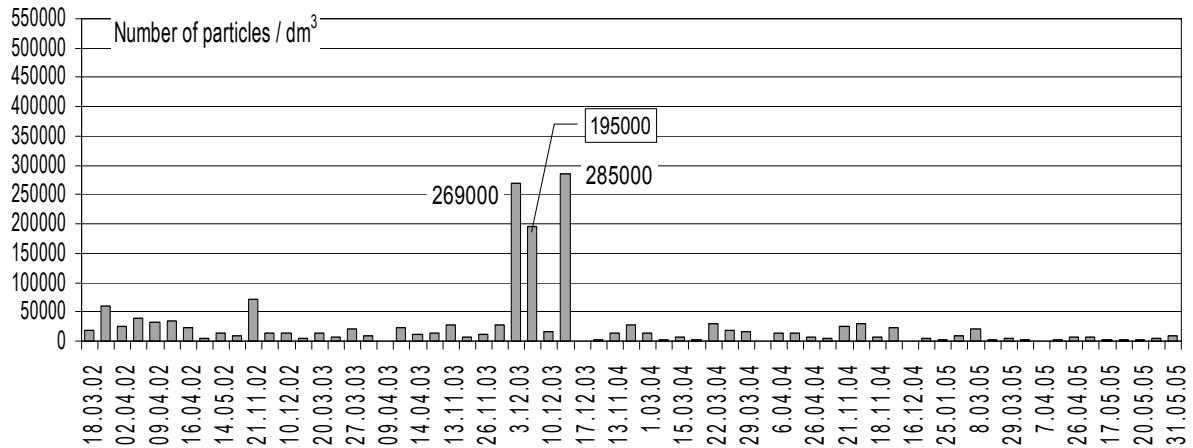
Fig.8. *Particles' concentration (diameter size range 0,6 – 0,7 μm)*
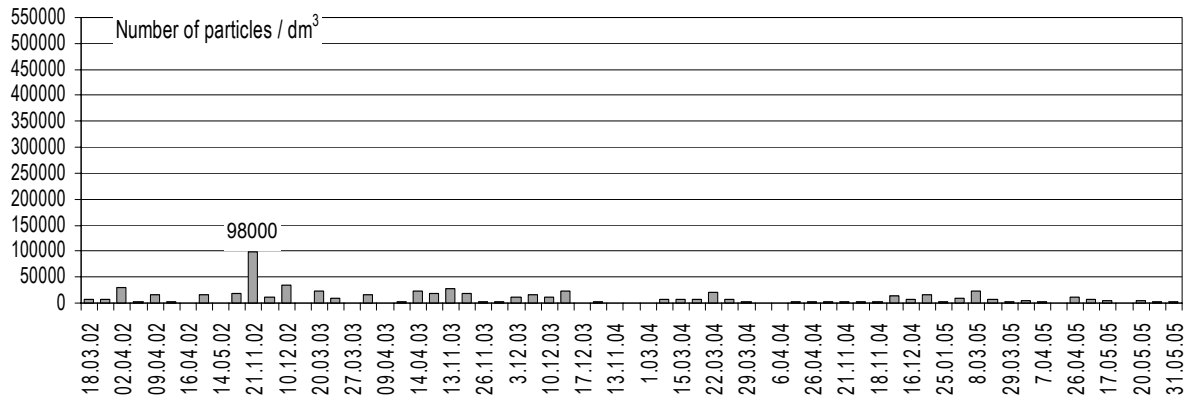
Fig.9. *Particles' concentration (diameter size range 0,7 – 0,8 μm)*
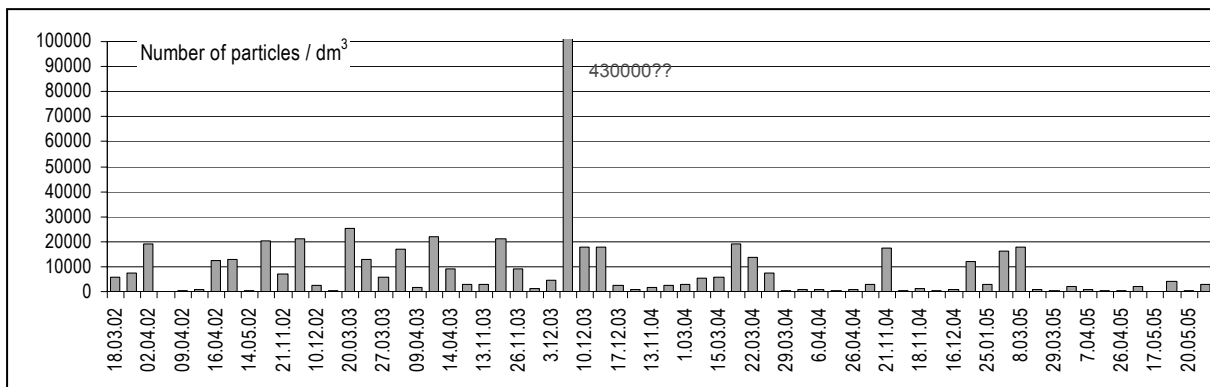
Fig.10. *Particles' concentration (diameter size range 0,8 – 0,9 μm)*
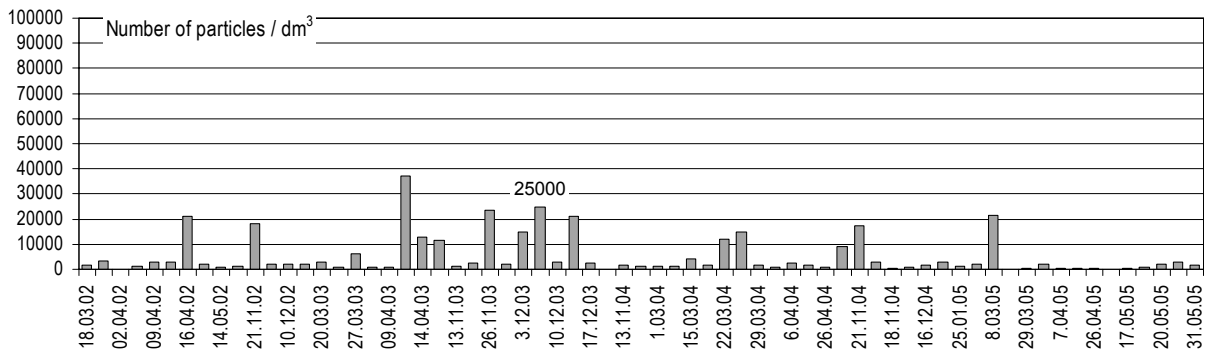
Fig.11. *Particles' concentration (diameter size range 0,9 – 1,0 μm)*
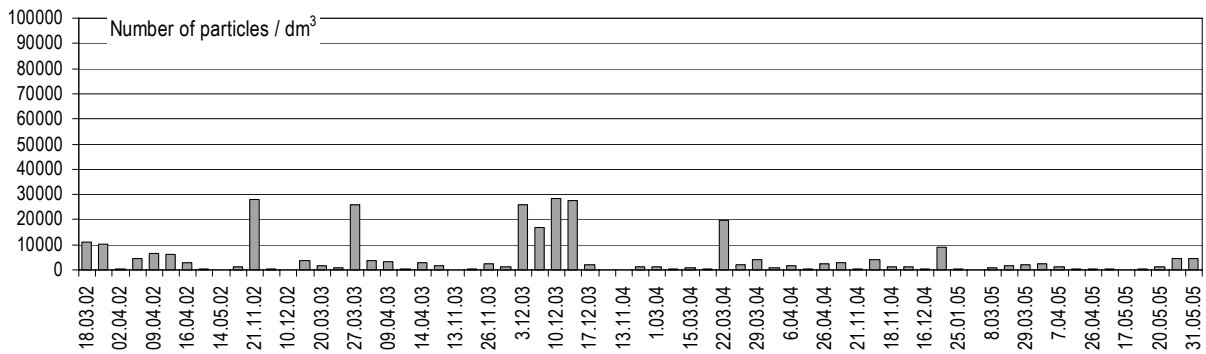
Fig.12. *Particles' concentration (diameter size range 1,0 – 1,5 μm)*
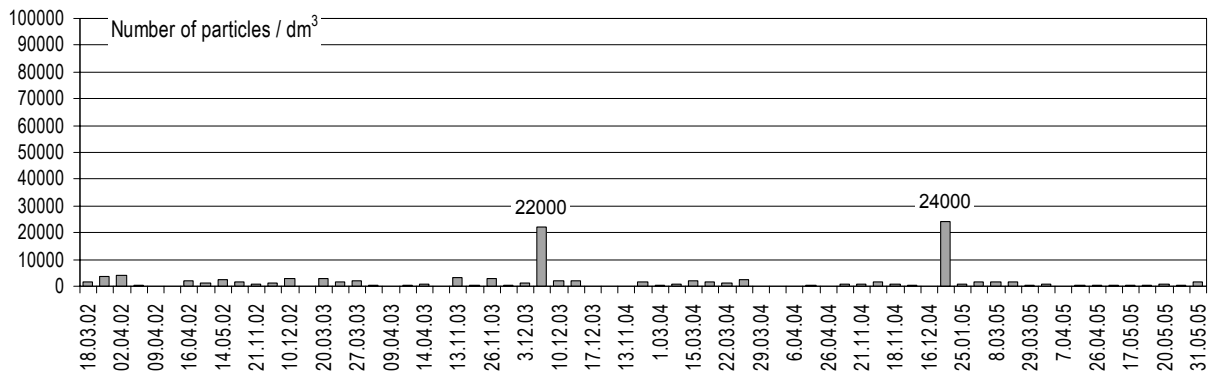
Fig.13. *Particles' concentration (diameter size range 1,5 – 2,0 μm)*
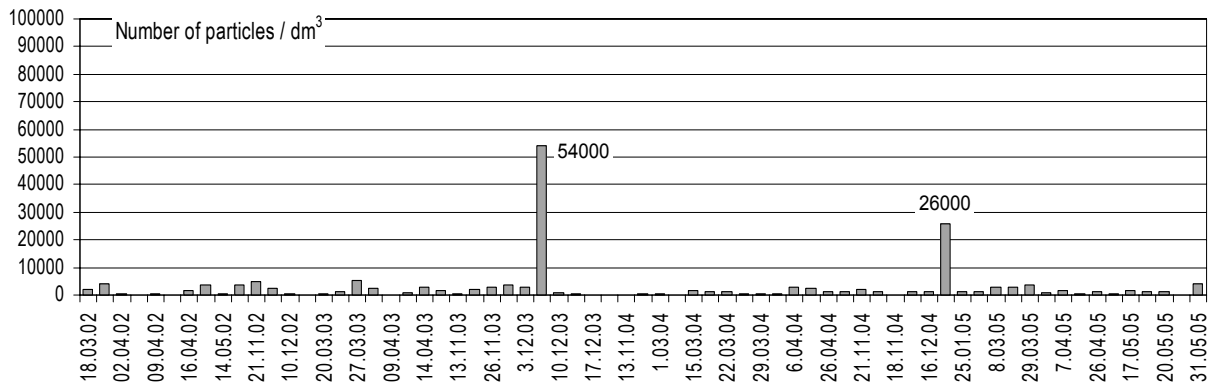
Fig.14. *Particles' concentration (diameter size range 2,0 – 4,0 μm)*
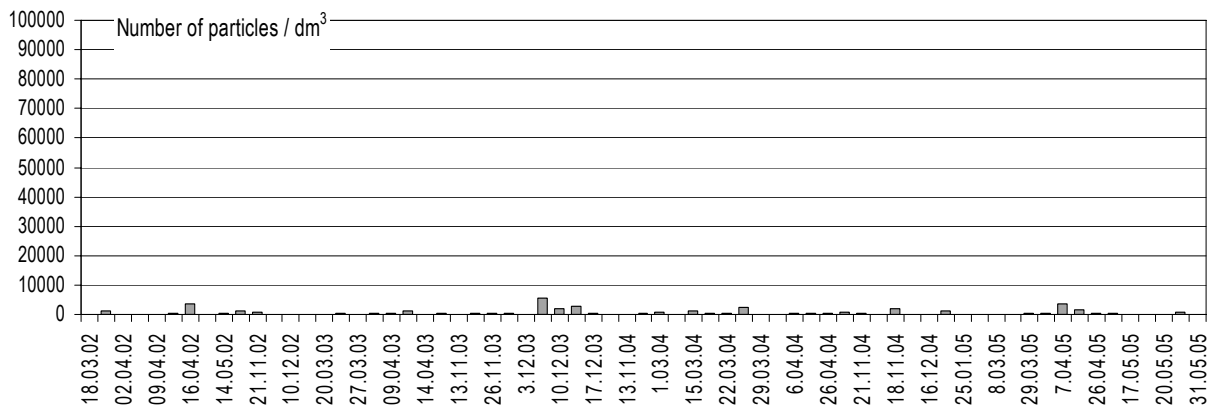
Fig.15. *Particles' concentration (diameter size range 4,0 – 7,0 μm)*
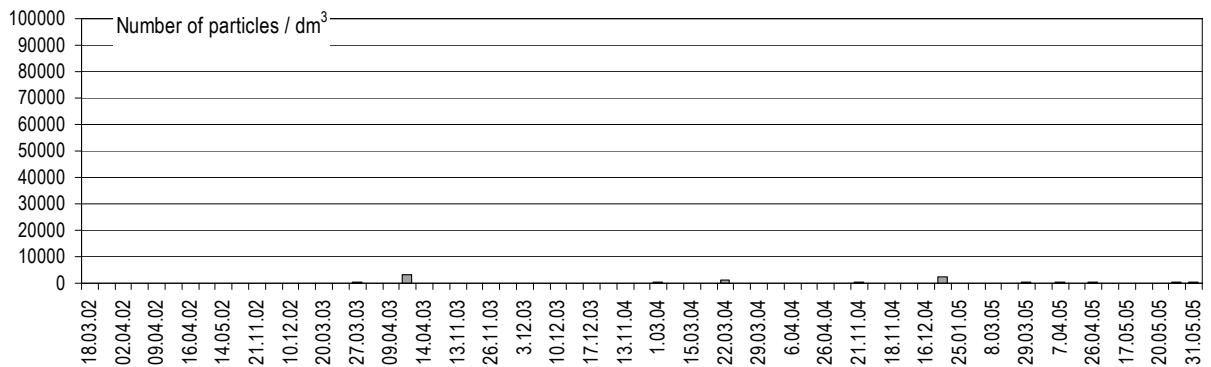
Fig.16. *Particles' concentration (diameter size range 7,0 – 10,0 μm)*

3. Study of the wind direction influence

Wind direction is a crucial parameter for the regional pollution as it indicates the origin of the air mass and the relative position of the measuring sites to the main pollution sources. Information on aerosols concentration size ranges a = (0.4-0.5) μm, b=(0.5-0.6) μm and c = (0.6-0.7) μm was processed. The level of air pollution was determined with respect to wind direction in the area.

This paper analyses the most frequent wind direction dependence of the particle size distribution, as it was noticed that aerosols charge in atmospheric air varies significantly with wind direction.

The experimental data were grouped in four predominant wind directions, as it follows: E~W, N-NW~S-SE, S-N and N-NE~S-SW. The plots below (fig. 4 -7) present the particles concentration distributions (in 1dm^3 of air) for the time period of 3 years and 2 months.
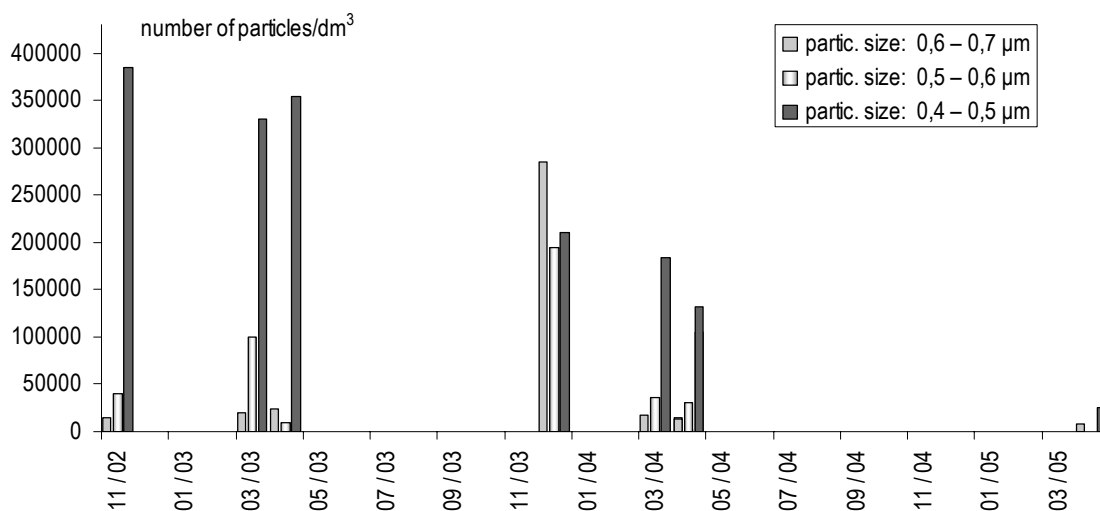
Fig. 17. *The variation of particle concentration (size range 0.4-0.7 μm), for wind direction E~W.*
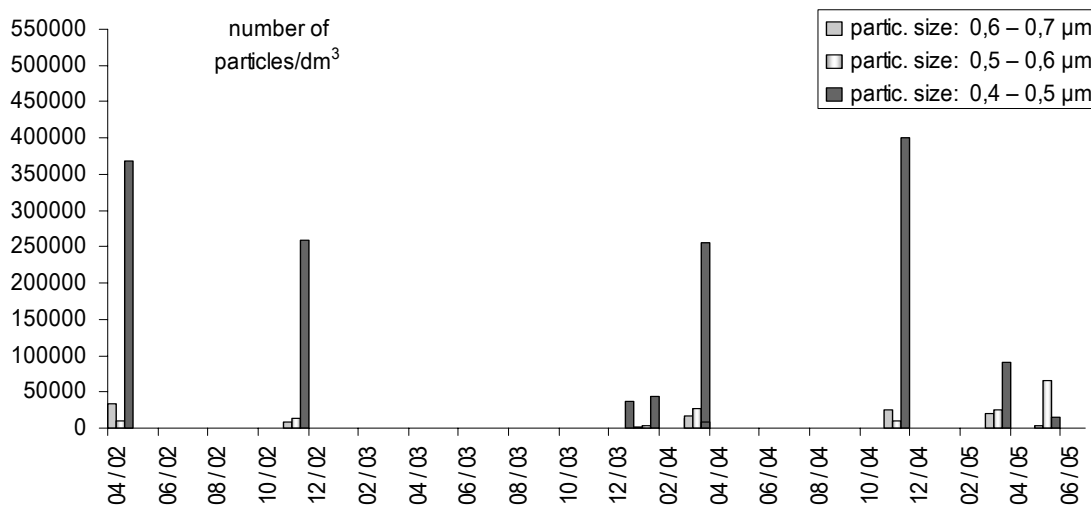
Fig. 18. *The variation of particle concentration (size range 0.4-0.7 μm), for wind direction N-NW~S-SE.*
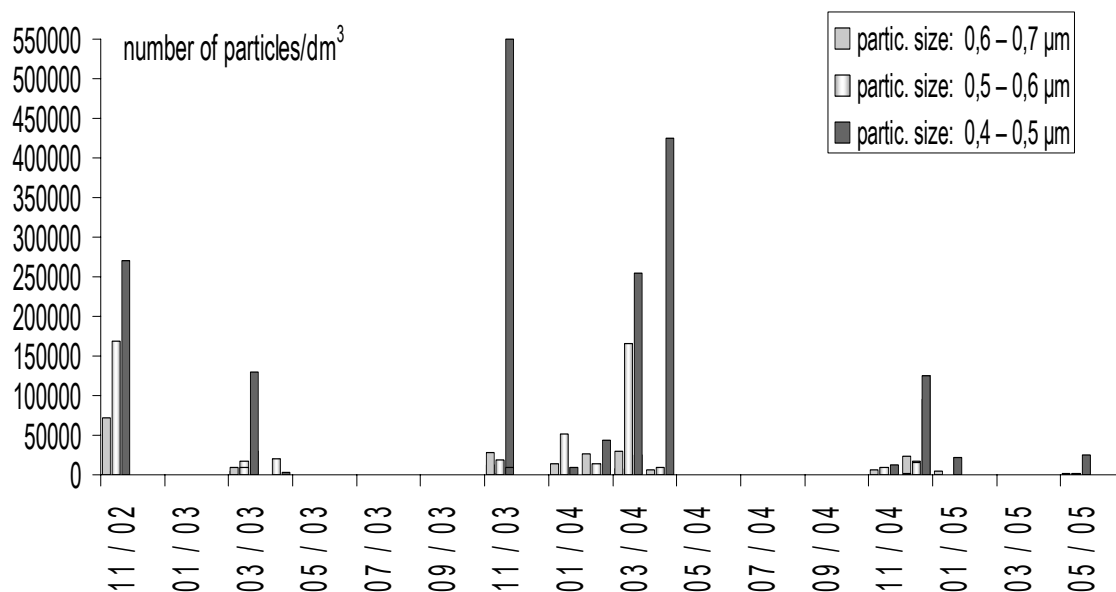
Fig. 19. *The variation of particle concentration (size range 0.4-0.7 μm),*
for wind direction S-N.
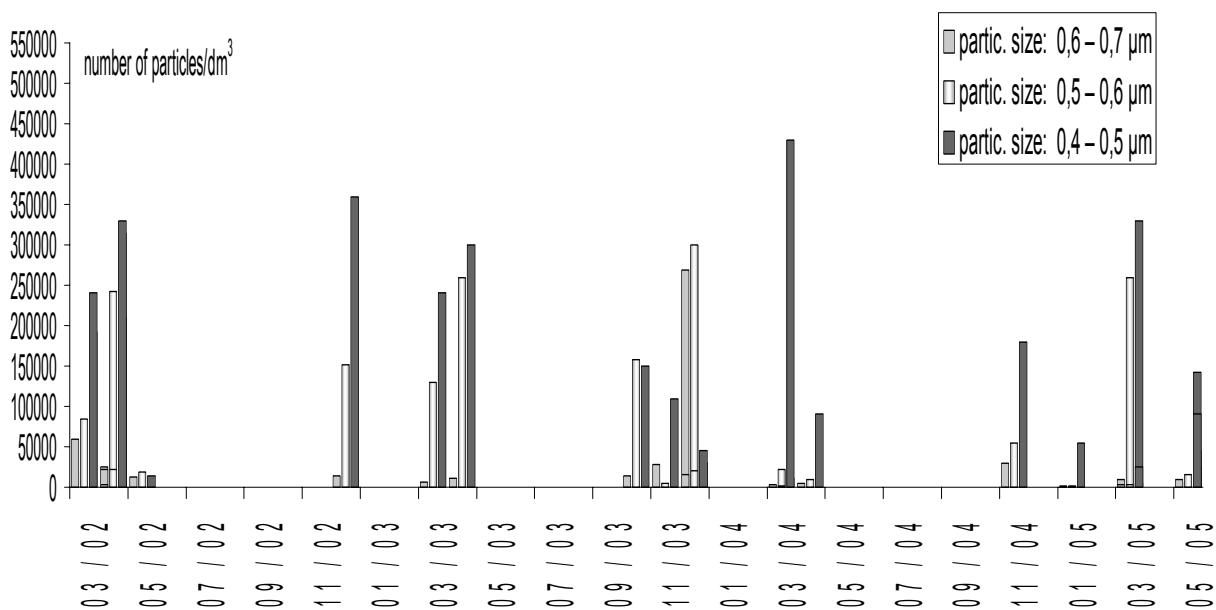
Fig. 20. *The variation of particle concentration (size range 0.4-0.7 μm),*
for wind direction E~W.

4. Discutions

The results of the measurements performed show a temporary situation being influenced by factors with a random evolution in time: intensification of the traffic jam, temperature, pressure, wind speed and direction, humidity.

4.1. *Influence of particles size range*

The data concerning the number of aerosols, registered in the period April 2002 - May 2005 on granulometric classes, guide to following conclusions:

- The particles in 0.4-0.5 µm size range, were in most the cases around value of 400,000 particles/dm^3, but in November 2003 were registered maximum values of 500,000 particles/dm^3;

- To the particles in 0.5-0.6µm size range, were registered several cases around value of 300,000 particles dm^3, and the majority were below the value 50.000 particles/dm^3;

- The particles in 0.6-0.7µm size range, was in most the cases below the value 50 000 particles/dm^3, but in the first half of the month of December 2003 was registered values in the range 250 000 - 300 000 particles/dm^3;

- The particles in 0.7-0.8 µm size range, was bellow 50.000 particle/dm^3;

- The concentration' particles in 0.8-1.5 µm size range, was bellow 20,000 particule/dm^3;

- The particles in 1.5-2.0 µm size range, was in most the cases below 5 000 particule/dm^3, with exception of the first half of the month of December 2003 when was registered ~ 22 000 particles/dm^3 and the beginning of January 2005 when was registered ~ 24,000 particles/dm^3;

- The particles in 2.0-4.0 µm size range, was in most the cases below 5,000 particles/dm^3, with exception of the first half of the month December 2003 when was registered ~ 54,000 particles/dm^3 end the beginning of January 2005 when was registered ~ 26,000 particule/dm^3;

- The particles in 4.0-1.0 µm size range, was in most the cases in insignificant number (<1,000 particule/dm^3);

- As a general observation, after January 2005 the number of the aerosols in natural atmosphere registered important diminutions, below 150,000 particles dm^3, with a singular exception in March 2005, when were registered a growth to 300,000 particles/dm^3 for the particles in 0.4 - 0.5µm size range;

4.2. Influence of wind direction

The number of aerosols registered in the period April 2002 - May 2005 on the most frequently directions of the wind, guide to following conclusions:

1) About the variation of particles number (0.4-0.7 mm size range), for the East - West wind direction:
The particles in 0.4-0.5µm size range, registered the maxims values contained between 300,000 – 400,000 particles/dm^3 in the period November 2002 - April 2003;

- The particles in 0.5-0.6 µm size range and 0.6-0.7 µm size range had an maximum of 200.000 particles/dm^3, respectively 300,000 particles/dm^3 in December 2003;

- After these maximus, the values diminished constantly, and from April 2004 they were insignificant;

2) About the variation of particles number (0.4 - 0.7mm size range), for the Nord – Nord/West ~South/South/East wind direction:

- The particles in 0.4-0.5 µm size range, registered four maxims values in April 2002 of 350,000 particles/dm^3, November 2002 of 250,000 particles dm3, March 2004 of 250,000 particles/dm^3, November 2004 of 400,000 particles/dm^3. After this date the values diminished below 100,000 particule/dm^3;

- The particles in 0.5 - 0.7 µm size range were in insignificant number.

3) About the variation of particles number (0.4 - 0.7 mm size range), South - Nord wind direction:

- The particles in 0.4 - 0.5µm size range, registered four values maxims in November 2002 of 200,000 particles/dm^3, November 2003 of 450,000 particles/dm^3, April 2004 of 450,000 particles/dm^3;

- The particles in 0.5-0.6 µm size range, registered two values maxims in November 2002 of 200,000 particles/dm^3 and March 2004 of 150,000 particles/dm^3;

- In all other time aerosols number had registered insignificant values.

4) About the variation of particles number (0.4 - 0.7 mm size range), Nord – Nord/East~South-South/West wind direction:

- The particles in 0.4 - 0.5 µm size range, they registered the values maxims between 200,000 – 450,000 particles/dm^3 in March April 2002, December 2002, April 2003, March 2004, March 2005, in remainders the registered values were below 100,000 particles/dm^3;

- The particles in 0.5 - 0.6 µm size range, registered the values maxims of 250,000 particles/dm^3 in April 2002, December 2003, March 2005, in remainders the registered values were below 100,000 particles/dm^3;

- The particles in 0.6-0.7µm size range, registered the values maxims of 250,000 particles/dm^3 in December 2003, in remainders the registered values were below 500,00 particles/dm3.

5. Conclusions

- Emissions generated by Mittal Steel metallurgical plant, located in the neighborhood of Galati city, don't have significant influences on the pollution of the city, the circulation air flows from this direction is infrequently:

- The most large amount aerosols transported was registered on the N-NE~S-SW direction, characterized by the most active air flows;
- In the first semester of the year 2005 was ascertained a considerable diminution of the particle number, in 0.4 - 0.7μm size range, which demonstrates the efficiency of some environmental local actions.

References

[1] ALFARRA, M. R., "*Insights Into Atmospheric Organic Aerosols Using An Aerosol Mass Spectrometer*", Ph.D. Thesis, University of of Manchester, 2004.

[2]. APOSTOL, T., "*Strategia şi legislaţia României de protecţie a mediului*", Ed. AGIR, Bucureşti, 2000.

[3]. BALINT L., et al., "*Aspecte privind monitorizarea atmosferei ambientale*", Simp. "Industria şi mediul", IPM Galaţi and Ispat Sidex S.A., Galaţi, 2003.

[4]. BALINT L., et al., "*Aspects regarding the environement atmosphere pollution monitoring*", Proc. of "Conferinţa Naţională de Tehnologii şi Materiale Avansate", Ed. Fundaţiei Universitare Dunărea de Jos, Galaţi, 20-22 nov. 2003, p. 149-163.

[5.] BALINT L., RADU T., BALINT S., NIŢĂ P., CONSTANTINESCU S., "*Poluarea aerului în aglomerări urbane, limitrofe uzinelor metalurgice*" Proc. of the Conf. "*Turnătoria de la rigoarea tehnicii la artă*", Ed. Academica, Galaţi, 2004, pp. 166-168.

[6]. CHANG, H. Y., "*Principles of Air Pollution. Human Health II - Health effects from O3, NOX, SO2, PM, CO, Pb, HAPs*", available at www.envsci.rutgers.edu/~pap_ta/Health%20Effects %20II.ppt (15.03.05).

[7]. DOBRE L.I., PĂTRAŞCU C., "*Monitorizarea imisiilor atmosferice într-o localitate industrială*", Proc. of "Sesiunea de Comunicări Ştiinţifice «35 de ani de activitate a Universităţii Petrol-Gaze la Ploieşti», Ploieşti, 2002.

[8]. KETZEL, M. et al., "*Particle size distribution and particle mass measurements at urban, near-city and rural level in the Copenhagen area and Southern Sweden*", Atmos. Chem. Phys. Discuss. (3) 2003, pp. 5513–5546.

[9]. LĂZĂROIU, GH., "*Tehnologii moderne de depoluare a aerului*", Ed. Agir, Bucureşti, 2000.

[10]. MĂNESCU, S., "*Igiena mediului*", Ed. Medicală, Bucuresti, 1991.

[11]. ROJANSKI, V. et al., "*Protecţia şi Ingineria Mediului*", Ed. Economică, Bucureşti, 1997.

[12]. SEINFELD, J.H., PANDIS, S.N., "*Atmospheric chemistry and physics: From air pollution to climate change*", Ed. John Wiley, New York, 1998.

[13]. UNG, A. et al., "*Satellite data lor air pollution mapping over a city - Virtual stations*", Proc. of the 21th EARSeL Sympozium, Paris, 2001, pp. 147-151.

[14]. DORSEY, J., "*Introduction to Aerosols*", available at http://cloudbase.phy.umist.ac.uk/ people/dorsey/Aero.htm (10.03.2005).

[15]. *** "*Respiratory Deposition*", available at http://aerosol.ees.ufl.edu/ respiratory/ section01.html (8.03.05).

[16]. *** "*Health Aspects of Air Pollution with Particulate Matter, Ozone and Nitrogen Dioxide*", Report on a WHO Working Group Bonn, Germany, 13–15 Jan.

A NEW VISION ABOUT THE DIMENSIONING CALCULUS FOR THE FRAME OF THE COLD MILL MACHINE

Stefan DRAGOMIR, Georgeta DRAGOMIR

"Dunarea de Jos"University of Galati,
email: doromir@email.ro

ABSTRACT

Dimensioning calculus for a rolling mill machine frame, using resistance classical methods allows determines the introduction of errors .For to do a better precisely of calculus we propose to use "Finish Elements Method". In this work also is made a comparison between the classic calculus method and the resistance frame mill calculus with the new method and the implications that result from these.

KEYWORDS: frame, rolling mill, finished element method

1. Introduction

The sheet or strip made from refractory steels and stainless steels are manufactured in a cold or hot rolling mill machine.

The type of rolling mill and afferent equipments are interested because is necessary to obtain a product that respects the specifications for the dimensions and quality.

When we laminated stainless and refractory steels the frame of mill machine is very tensioned and in time appear the "micro crash" –at the inn of the frame corner- who caused major damage at the body cage.

The two frames that are the most important element of the mill cage, are assembled by traverses with screws –for fixed on the plate support of cage-.

The weight of the frame is nearly 450tons and the rolling force in work is approx.120MN.The engines for acctionnary the work rolls have 2x10MW power.

In this work is shown a rigorously dimension calculus for the frame of the reversible cage with dimensions (430x1270x1250mm) and the sheet processed (thickness,1-5mm and breath 1000x2000mm).

In calculus it was taken in consideration the deformability characteristics of laminated sheet, in correlation with cage resistant capacity.

2.Calculus and experiments

Into the classic calculus of dimensioning for the frame the most important force that deformes the frame in time of work is the force of sheet deformation (the direction of action is in a vertically plan).

The formula that was used is (Telicov):
Force of laminated:

$$F = b\sqrt{R \cdot \Delta h} \cdot p_{med} \quad [N]$$

$$\Delta h = h_1 — h_2 \quad [mm]$$

were: b is sheet breath;

R is work roll radius;

h1, h2 are thickness of rolling sheet before and after the rolling mill process; pm is the average resistance for deformation of rolled material.

The frame is made from low alloy cast, with the next characteristic:$Rm=530-790N/mm^2$; $Rp=295N/mm^2$; $A=18\%$.

The section of measured frame column is $0,57m^2$

The preliminary work hypothesis is that the mainly force who can deform the column and traverse of frame is the force on the work roll. In the rolling process is developed horizontal force (small values) in direction of sheet plan.

Because a cage has two frame the mainly force is divided in two like:

$$Fy = Flmax/2$$

In figure no.1 and no.2 is shown the constructive aspects of frame.

After the calculus result the bending moments on the upper traverse $M1 = 11,3 \times 10^9$ Nmm.

For columns the maximum effort (bending and stretching),
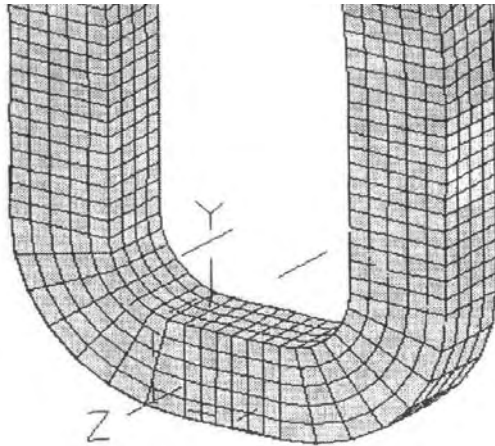
Fig.1. Finish elements structure discretisation

$$\sigma int = \sigma_1 + \sigma_2 = Flmax \ / 2A_2 + Mo / W_2$$
$$[N / mm^2]$$

$\sigma int = 12,8 \ N/mm^2$

were:

W_2 , W_1 is the resistant modulus of column, in cm^3 ;

A_2 – transversal section area of column, in cm^3

E – longitudinal elasticity modulus for cast steel ($E = 1,75 \times 10^6$ N/mm^2).

In the upper traverse the maximum effort of bending through (section I-I, nut zone of pressure screw) can be found :

$$Mo = Fy.l1[1+4r(1,15r.I1/l1I2+1)]/2$$
$$Mo = 8,95 \times 10^8 \ Nmm$$
$$M_1 = Flmax.l1/4 - Mo;$$
$$M_1 = 73,2 \times 10^8 \ Nmm$$

The real stress measured -in the milling process- into the cage frame was:

$\sigma_{int} = 21,7 \ N/mm^2$, on the column of the frame;

$\sigma_{max} = 26.3 \ N/mm^2$, on the traverse of the frame.

The admissible resistance is for the frame material $\sigma a = 45-55 \ N/mm^2$. During the functionary is necessary to take in consideration the durable resistance of frame material.
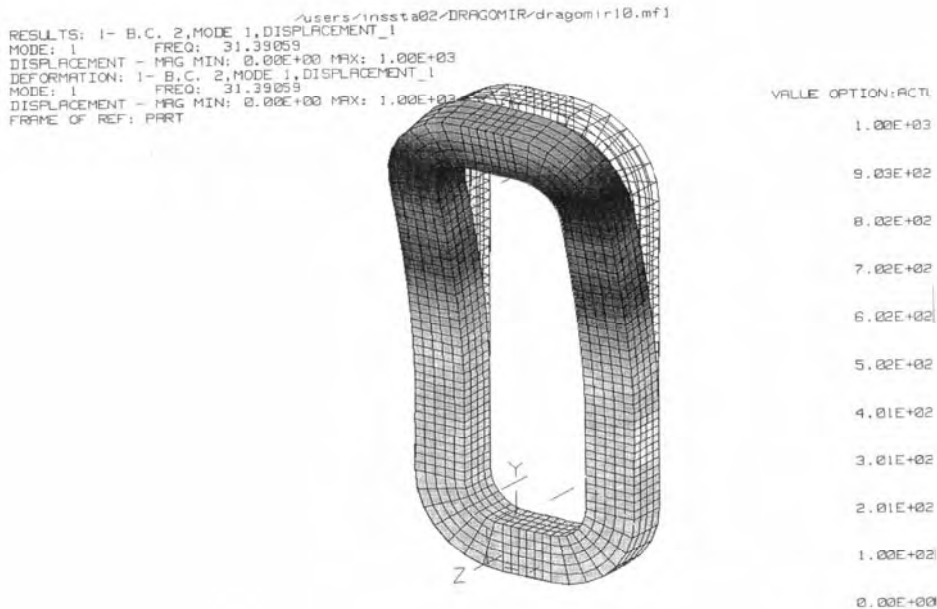
Fig.2. Finished elements method analyzed for the frame cage

On the upper of the frame (superior traverse) is positioned the hole for pressure screw nut. In this zone (section I- I), it is an important stress concentrator.

Using "the method of finished element" we made a complete verification (resistance of material) for the cage frame.

This method offers a calculation algorithm for the frame whose structure was made from bars (three dimensions) and like charges are used static and dynamics tensions.

For apply "the method of finished element" is necessary to discretisation the structure who must be verified in small triangular, rectangular or circular elements with subprogram "MASTER MODELLER".

After the definition of the structure with its geometrically characteristics, we can applies the tensions .The program made automatically redistribution of local "accidents". The program numbers the nodes on which shifting and efforts are calculated (starting from the maximum rolling force), in each side of established element.

3.Conclusions

By comparing the results obtained with a classic calculus (resistance) for the frame of mill cage for cold strip (refractory and stainless steel), and a verifies calculus with method of finished element, we can say that:
-   the columns of the frame have the section with 13,2% increased ;
-   the traverse of the same frame have the section increased with 17.8% (the new method of calculus take in account and the fatigue calculus[3];
-   it can say that the weight of the frame is much that is necessary, because the section is artificially increase and it is a result of the classic calculus;
-   the maximum of tension calculated by this program is in the nut screw zone (upper traverse of the frame);
-   using the method of finit element, the calculus time, is with 60% less than if we applies the classic method of calculus for frame dimensioning.

References

[1].Monaco G. –*Dynamics of Rolling Mills-Mathematical Model and Experimental Results* AISE Year Book 3/1997.
[2].La revue de metallurgie - *Amelioration des performances eppaisseur au train a bandes CIT* septembre 9/ 2003.
[3].Weibul V- *Fatigue testing and Analysis of Result* .Pergamon Press Oxfort London2001.
[4].Programul IDEAS PRO.

ANALYTICAL MODEL OF FORGE CUTTING PROCESS WITH ASYMMETRICAL TOOLS

Nicolae CANĂNAU, Doru HANGANU

"Dunarea de Jos" University of Galati
e-mail: **dhanganu@ugal.ro**

ABSTRACT

In this paper is developed the theory of forge cutting process feasible with asymmetrical tools. The asymmetrical cutting process is different of the symmetrical cutting process. This type of process is necessary to realize the slash of billet when it has one or many steps of diameters, and when is necessary a good precision of slicing.
Based on the mathematical model established above we developed a calculation program that calculates using the MATLAB package.
Force is calculated in three stages, until the penetration is less or equal with high of the oblique zone, and that is uniform.

KEYWORDS: algorithms, simulation, forge cutting process.

1.Introduction

The forging process consists of the deformation operations and cutting operations. The cutting process may be with total or partial separation of the parties of forged body.

For some forge cutting operations the use of symmetrical tool is recommended. In case of other operations the asymmetrical tool is recommended.

The theory of the first case, of the forge cutting with the symmetrical tool, is developed in the [1] reference.

The asymmetrical cutting process is different of the symmetrical cutting process. In this paper is developed the theory of asymmetrical cutting process.

We adopt the following initial conditions:

- The tool body is very hard and consequently, practically the deformation of tool is equal of zero,
- The material of deformation body is homogeneous and isotropous,
- The geometry of active zone of cutting tool is proper of the Figure 1.

The asymmetrical cutting tool has an edge of radius r, an inclined zone of angle γ and the straight zone.

In the developing of the cutting process the first stage is the process of the symmetrical cutting. This process corresponds to the penetration of tool from z = 0 until z = t.

The second stage corresponds to the penetration partial asymmetrical from z = t, until z = r

and the third stage corresponds of the penetration of tool until z = h.
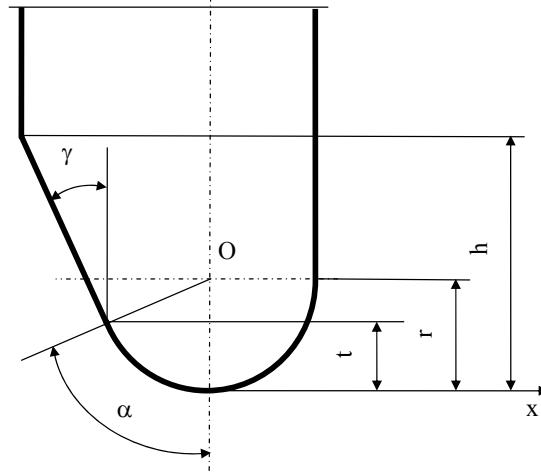
Figure 1. *The geometry of asymmetrical cutting*

2.Theoretical modeling of cutting process

2.1. *In the first stage*

The problem of the theoretical modeling of the symmetrical cutting process is solved in the paper [6]. The geometrical scheme of the cutting process in this stage is sowed in Figure 2.

For $\theta \in [0, \alpha]$ we obtain:
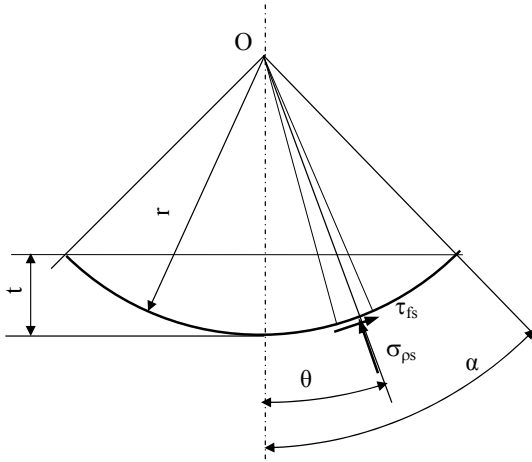
Figure 2. The scheme for calculus of cutting force in the first stage
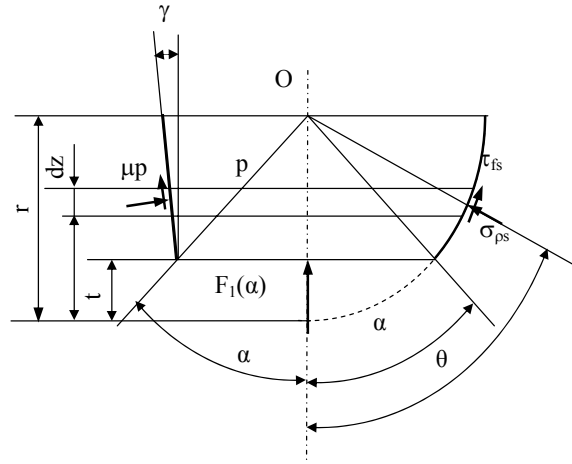
Figure 3. The scheme for calculus of cutting force in the second stage.

Using the equilibrium equation for radial coordinate we obtain for stress $\sigma_{\rho s}$ the relation:

$$\sigma_{\rho s} = -\sigma_0 \left[1 + \mu \cdot \left(2 - \frac{r}{r_\alpha - 1} \right) \cdot (\alpha - \theta) \right] \qquad (1)$$

Relation of elementary force:

$$dF = |\sigma_{\rho s}| \cdot l_t \cdot r \cdot \cos\theta \cdot d\theta + \tau_{fs} \cdot l_t \cdot r \cdot \sin\theta \cdot d\theta$$

(2)

$$F_1(\theta) = 4k \cdot l_t \cdot r \cdot \left\{ \sin\theta + \mu \cdot \left(2 - \frac{r}{r_\alpha - r} \right) \cdot [(\alpha - \theta)\sin\theta + 1 - \cos\theta] + \mu(1 - \cos\theta) \right\} \qquad (3)$$

The signification of the factors from the relation (3):

k – critical stress of the deformed material,
l_t – cutting dimension of the body,
r – radius of edge of the cutting tool,
µ – Friction coefficient,
r_α – radius of plastic deformation zone inside of the body,
α – angle pursuant to figure 3, and depending of penetration on symmetrical zone.

For θ=α we obtain:

We denominate F1 (α) the value of the force what corresponds of the limit of first stage of the cutting process.

Relation defines the force in the second stage:

After integration we obtain:

$$F_1(\alpha) = 4k \cdot l_t \cdot r \cdot \left[\sin\alpha + \mu \cdot \left(2 - \frac{r}{r_\alpha - r} \right) \cdot (1 - \cos\alpha) + \mu(1 - \cos\alpha) \right] \qquad (4)$$

2.3. In the second stage

The geometrical scheme of the second stage of the asymmetrical forge cutting is rendered in Figure 3.

$$F_2(z) = F_1(\alpha) + 2k \cdot l_t \cdot (tg\gamma + \mu)(z - t) +$$
$$+ 2k \cdot l_t \cdot r \cdot \left\{ \sin\theta - \sin\alpha + \mu\left(2 - \frac{r}{r_\alpha - r}\right) \cdot [(\theta - \alpha)\sin\theta + \cos\theta - \cos\alpha] \right\} \quad (5)$$

Between the factors of expression (4) exist the following relation:

$$\alpha = \frac{\pi}{2} - \gamma, \quad \alpha = \arccos\left(\frac{r - t}{r}\right)$$
$$\theta = \arccos\left(\frac{r - z}{r}\right), \quad \theta \in \left(\alpha, \frac{\pi}{2}\right], z \in (t, r] \quad (6)$$

2.4. In the third stage

The geometrical scheme of the third stage of cutting process is presented in Figure 4.

We denominate F2(r) the value of the force what corresponds of the limit of second stage of cutting process. $F_2(r)$ corresponds to z=r, respectively too $\theta = \frac{\pi}{2}$.

Thus we have:

$$F_2(r) = F_1(\alpha) + 2k \cdot l_t \cdot (tg\gamma + \mu)(r - t) +$$
$$+ 2k \cdot l_t \cdot r \cdot \left\{ 1 - \sin\alpha + \mu\left(2 - \frac{r}{r_\alpha - r}\right) \cdot \left[\left(\frac{\pi}{2} - \alpha\right)\sin\theta + \cos\alpha\right] \right\} \quad (7)$$

Relation defines the force in the third stage of cutting process:

$$F_3(z) = F_2(r) + 2k \cdot l_t \cdot (tg\gamma + 2\mu) \cdot (z - r) \quad (8)$$

The mathematical relation (7) is applied for $z \in (r, h]$, h is the active zone of the cutting tool. For z > h to the surface of cutting tool the interaction between materials of body- tool is not developed.

Using asymmetrical tools the transversal surface is perpendicular on longitudinal axes, and material addition is smaller.

Figure 4. *The scheme for calculus o cutting force in the third stage.*

3. The computer calculation of asymmetrical cutting force

Using the mathematical model established above we developed a calculation program that calculates using the algorithm present in this paper.

May be calculate Force versus penetration, in that three phase, using the MATLAB programmer package.

The results of simulation are shown in figure 5.

4. Conclusion

Is possible to see that in first stage force is quickly on the increase and then increase velocity is less, in second stage, and in the third stage it is linear increase. This algorithm is helpful for students from metallurgical and mechanical domains, the engineers from forging wards, or projectors engineers.
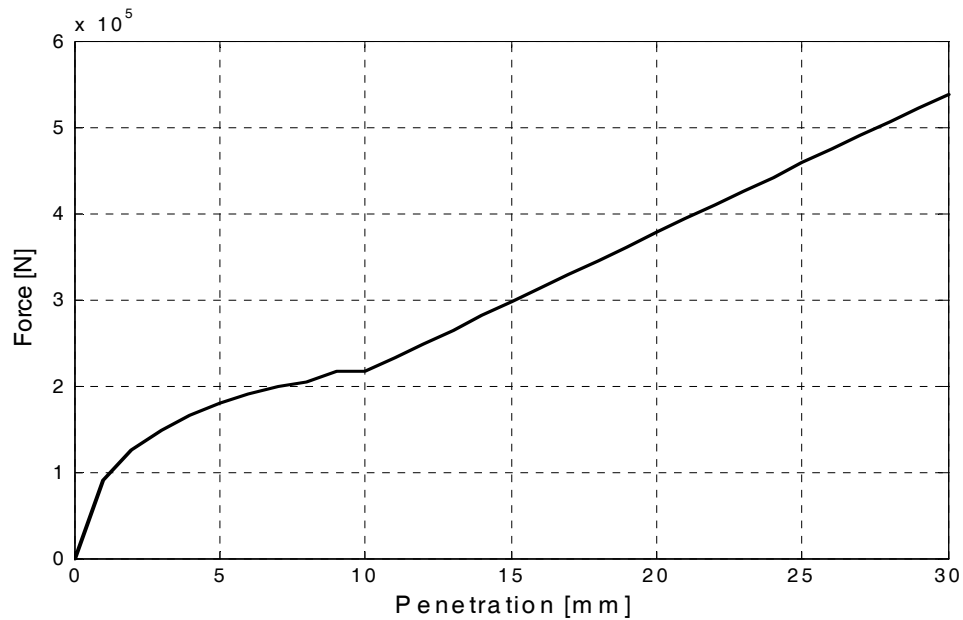
Figure 5. *Force versus penetration of the symmetrical tool*

References

[1] **M. Adrian, S. Badea** – *Bazele proceselor de deformare plastica, Editura tehnică, Bucureşti, 1983;*

[2] **N. Cananau** – *Teoria deformarii plastice, Universitatea din Galati, 1994;*

[3] **M. Ghinea, V. Fireţeanu** – *MATLAB – Calcul numeric-grafică – aplicaţii, Editura Teora, Bucureşti, 1998*

[4] **I. Dragan** – *Tehnologia deformarilor plastice, Editura didactică şi pedagogică, Bucureşti, 1976.*

[5] **N. Cananau,.,a.o.** *Mathematical modeling of the forge cutting process, The Annals of Dunarea de Jos University of Galati, Galati, Romania, fascicle 9, 2004.*

[6] **L. Katchanov,** - *Éléments de la théorie de la plasticité, Editions MIR, Moscou, 1975*

[7] **Rowe,G.W.,** - *Elements of Metalworking Theory, Ed. Arnold, London, 1978.*

COATINGS SYSTEMS: CHROMIUM CARBIDE, NITRIDE AND CARBONITRIDE

Stela CONSTANTINESCU

"Dunarea de Jos"University of Galati,
e-mail: **Stela.Constantinescu@email.ro**

ABSTRACT

The process of the chemical deposition from vaporous implies the adsorption of the mobile atoms (monomers) on the substrate surface, their migration with embryos and stable nucleus formation, followed up by further growth through the adsorption of new atoms on the surface and also by the nucleus coalescence. The final structure of the deposed layer is given by various effects such as, the adsorption of impurities, the incorporation of gaseous, the co-deposition of another elements, the crystallization, etc.

The ultimate properties of the coatings are further dependent on the nature and composition on the substrate. Therefore, in theory a vast number of substrate-coating combinations is possible, with its own set of physical and chemical characteristics.

If the vapor chemical deposition takes place within a tubular continuous reactor, a gas carrying the reacting species is passed over the substrate. At the substrate surface, the reacting elements undergo a number of chemical reactions leading to the product formation. Part of the products are deposited on the substrate and part of it goes back to the gas stream [1].

Before examining the vapor chemical deposition reactions it must be determined if the reaction is possible thermodynamically, if the calculated concentrations (partial pressures) of the reactants under equilibrium conditions are less than their initial values.

KEYWORDS: chemical vapour deposition, substrate-coatings, nitride, carbonitride, chromium carbide

1. Introduction

The basic phenomen of chemical vapour deposition (C.V.D) has been known for centuries in the pack carburizing of iron, although it may not have been recognised as a gaseous or vapour phase process. Indeed the term C.V.D. has, of late, achieved the characteristic of being something of a new process a recent development, particularlywith the application to metal woeking tools of coating of TiC and TiN.

Whether the process is carried out by the long established pack cementation technique or by the more recent, but still well-known, totally gaseous technique, the basic process is still C.V.D. Indeed, to those working with these processes the use of liquid baths is included within the generic term, because the coatings of a given type have such similar properties whichever method is used [1] – [2].

The general characteristics and process techniques of pack, purely gaseous and liquid methods of introducing one element into the solid surface of another, are well known through the very widespread use of the carburization of steel and iron components.

The introduction of elements other than carbon is achieved by using similar techniques. The characteristics exhibited by these coatings result from the differing chemistry of elements involved.

To that end, and before dealing with specific exemples, it is worthwhile to examine some of fundamental differences between the processes used for surface coating.

2. Chromium Carbide

Chromium carbide coatings with a hardness of about 2000 D.P.N. are particularly successful in sliding wear applications, the most often quoted example being the bicycle free-wheel (fig.1).

The life time of the smoll bodies which rotate to lock and unlock the free-whell device can be increased about 20 times for only a small increase in

cost. Many textile machine parts have been similarly   coated.
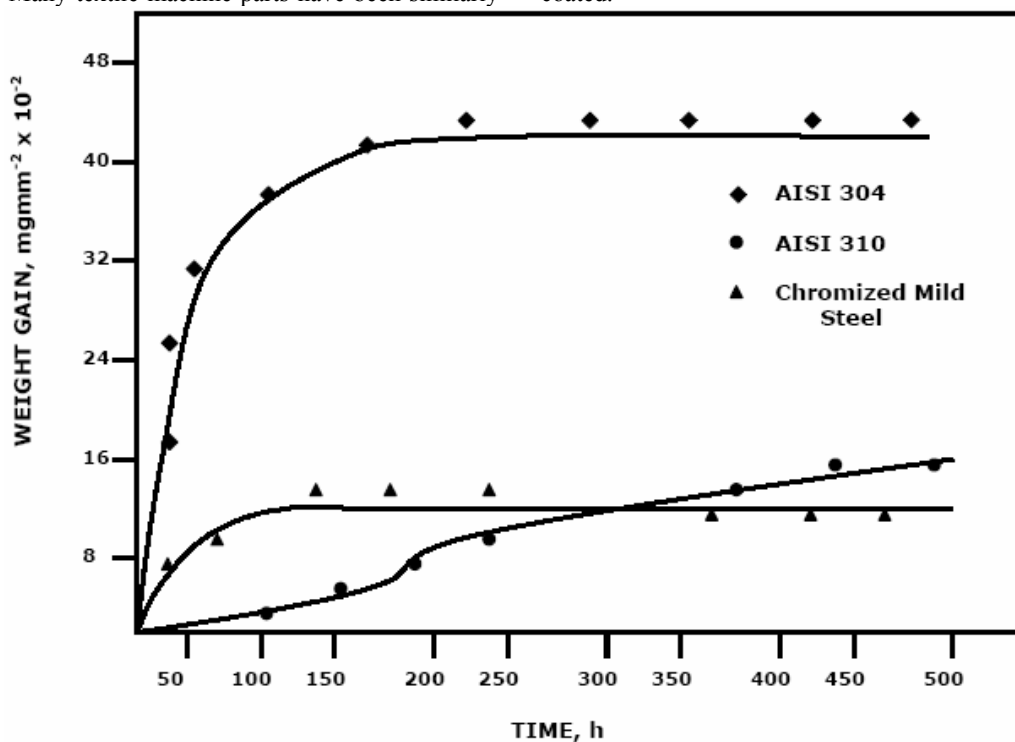
Fig.1.*The oxidation resistance at 1000ºC in air of chromized mild steel wowen wire (0.25 mm wire diameter) as compared with wowen wire samples of austenitic stainless steels.*

3. Titanium carbide.
Nitride carbonitride

Overlay coatings consisting of TiC, TiN and TiC/TiN either separately or as a bonded structure are very widely used on throw-away indexable carbide inserts. TiC and TiN are isostructural and can be formed in continuous solid solution of any composition. These coatings give a surface hardness of around 3000 D.P.N. and their use on carbide containing substrates has simplified the range of carbide compositions necessary to cover all cutting applications.

The properties of TiC and TiN appear to compliment each other in providing resistance to both the slid in wear and crates wear observed on carbide cutting inserts.

The key to their wear resistance on cutting tools is their chemical inertness as well as their hardness. They have no tendency to react with the extremely clean, oxide free, surface of the swarf as it passed the cutting tool. The TiC/TiN combination of coatings is also on carbide forming tools, for example deep drawing dies. The chemical inertness of the coating is important here to reduce tendency for cold welding to occur.

Steel cutting tools been coated with TiC/TiN but with less success than carbide tools. This is caused partly by the lower hardness of the steel substrate which provides less support for the coatings and partly by the necessaty to re-harden steel substrates after coating.

The latter feature is necessary as the C.V.D. process temperature for TiC and TiN is around 1000ºC. With some steels this re-hardening can be combined with the coating cycle, but in most cases a separate vacuum heat-treatment step is required [3]-[4].

TiC coating alone on steel forming tools have been very successful. In this case there appears to be very little advantage in the TiC/TiN combination. All types of punch and die combinations have been coated with TiC to give increased wear life and better surface finishes on the product.

Tool for powder metallurgy have been coated withboth TiC and TiN. In this case the coating act as release agents by reducing the tendency for powder compacts to bond to the tools (fig.2)

DEKTAR 3   VERSION 2.13
PROG FILE NAME: GUILAV.MP
SCAN ROUTINE #: 1
TIME OF SCAN: 01:40:10 Wed
               Jun 26 2 01 02
DATA FILE NAME: .001
Scan ID 0
Scan Length . 1500um
Scan Speed ..... Medium (10 sec)
Data Points 750
Resolution ....2.000 um/sample
Meas. Range ...655 KA
Profile ....Hills&Valleys
R. Cursor ....6644A @ 554.35um
M. Cursor ..... -38513A @ 1080.43um
Vert. Delta .... -45157A
Horiz. Delta 526.09um
ANALYTIC FUNCTIONS:
               R:um   M:um
Film thickness = 8,5 E + 4A = 8,5 μm

Fig.2. Surface profilmeter measurement of the thickness of TiC film for 4 h exposure time.

The choise of the substrate steel is important in the use of TiC and TiN coatings. The TiC coating forms most adherently on steelswith a carbon contecnt over 1%, while TiN is less influenced by the composition of the substrate [5]-[6] .

High speed steels have been used for coating cold forging dies with relatively low dimensional tolerances. For high precision parts where distortion on re-hardening must be minimised.

4. Titanium Nitride

Titanium nitride is a yellow coloured material, and when polished resembles gold. The resemblance can be improved by careful control of the stoichiometry and also by adding traces of carbon. This has caused titanium nitride to be considered for various decorative applications [7].
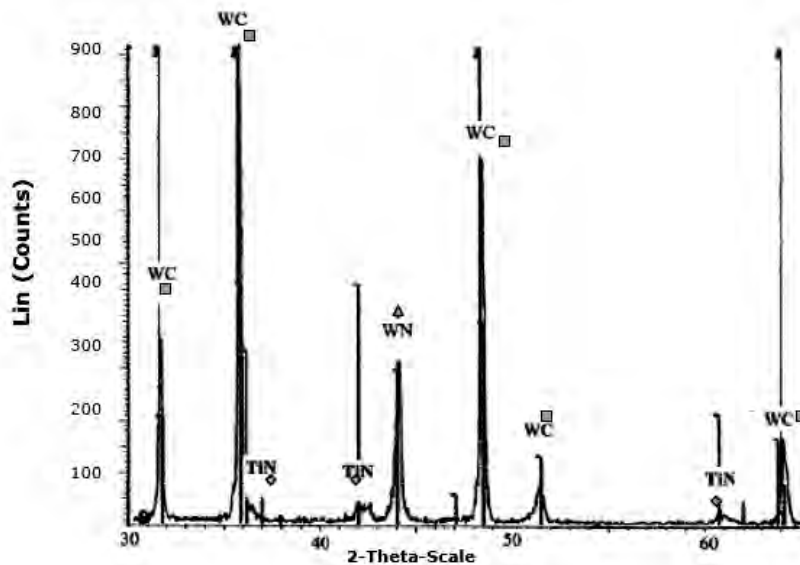
Fig.3. XRD pattern of nitride thin layer for 4 h exposure time.

Watch cases, particularly those made from sintered tungsten, on coated with titanium nitride, and there have been investigations on less expensive items of personal jewellery, cigarette and pens. The hardness of titanium nitride is very suitable for these applications and also its corrosion resistance is adequate for it to maintain a bright appearance even when constantly handled. The largest technical barrier to thewidespread use of C.V.D. titanium nitride as a decorative coating is the necessity to polish the C.V.D. layer. Unless coated parts are designed so that can be polished automatically in large numbers, the cost of polishing is often prohibitive (fig.3).

5. Conclusions

An attempt has been made to highlight some specific cases where C.V.D. coatings have been able to extend the useful life of components used in various industries. It is not always the case that standard processing conditions can be applied to solve the presented problems on any given component. There could be many facets to the problem wich require special alternation to the coating conditions (variations in processing time, temperature, special jigging etc.).

Of the types of coating systems examined, only a few have been developed for practical application. This is in part related to the high coast of coling up specialist plant and the problems of efficient utilization of this plant when operated by a service industry [8] .

Tables 1 some of the C.V.D. coating available commercially along with their typical applications.

An important advantage of the plant used for producing C.V.D. coating is its versatility. It is possible, using the same basic equipment, to alter operating conditions and produce coating of different compositions and characteristics [9].

Table no. 1   *The C.V.D. coating*

Coating material	Typical substrates	Substrate improvements	Typical components
TiC	High speed steels, sintered carbide and tool steels	Wear	Sintered carbide cutting tips, steel press tools, punches and dies.
TiN	As for TiC	Wear, Corrosion	As for TiC and also decorative parts
SiC	Graphite	Oxidation	Heater elements

References

[1]. W. Ruppert, Proc.on C.V.D. The American Nuclear Society, 1972, p.340-423.

[2]. J.P.Chubb and J. Billingham, Engineers Digest, 1980, 41, 27.

[3]. N.P.Suh, Wear, 1980, 62, 1.

[4]. Mitoşeriu O., Constantinescu S., ş.a., Advanced methods of investigation the properties of metallic materials, Universitatea „Dunărea de Jos,, Galaţi 1998.

[5].Constantinescu S.,Radu T., Advanced methods of obtaining thin coats, Ed.Ştiinţifică F.M.R.Bucureşti, 2003.

[6]. Constantinescu S., Metals properties and physical control methods, Didact. and Pedag. Publishing House, Bucharest, Romania, 2004

[7]. Published literature of the Toyo TiC Company, Japan, 1981.

[8] N.J.Archer, Proc.on C.V.D., The Electrochem. Soc., 1981, p.722.

[9]. P.Lavalle, R.Mandelli, E.Lanzoni. Microstruttura e proprieta di rivestiment di carbonitrura di titanio depositati mediante "Lou/plative" su acciaioda utensili.

POSSIBILITIES TO STUDY THE MIXING STATE AND ENERGY DISSIPATION IN METALLURGICAL REACTORS USING A SYSTEM BASED ON COLOURED LIQUIDS

**Petre Stelian NITA, Adrian VASILIU,
Vasile BASLIU**

"Dunarea de Jos" University of Galati
email: pnita@ugal.ro

ABSTRACT

Coloured liquids are used to show the stream lines in aqueous systems used as model liquids, in different chemical reactors, also in metallurgical reactors dedicated to liquid steel processing; ladles represent a class where these principles could be succesful applied .

A blue ink was selected as colouring agent because of the low price, good biological tolerability in contact with the human skin and absence of the necessity to treat the used evacuated water .

As modeling liquid for stee was selected freshly distilled waterl.

Mixing energy dissipation was measured at adequate scales using the transmittance and the absorbance of liquid sampleswith two laboratory spectrocolorimeters (KFK-2 Russia and Spekol-10 Carl Zeiss Jena, Germany). Volumic relative concentrations of the coloured liquids starting with 0,0005%vol. and even bellow are measured using this technique and the mentioned devices.

Two model vessels, representing two types of metallurgical reactors, were usd in the present set of experiments. The experimental systems provide enough precise data because of using an adequate and accesible system of image recording and capture, based on a performant commercial web video camera.

KEYWORDS: colouring agent, transmittance T(%), ladle reactor.

1. General aspects

There are many reasons to insist on the physical measurements in mixing phenomena research, generally in liquid, also in liquid alloys.

Firstly, the physical properties of the liquids are not of the same values in the different regions of the mixing reactors, even in the absence of any mixing action. Only especially insulated reactors are isolated and it can be supposed that the liquid contained in the reactor can, reach every moment a perfect equilibrium, the condition of absence of any external or internal perturbation. Ladle reactors are frequently either open, either covered, but the most frequently they are exposed to the normal temperature of the environment. Every time, in this situation it will be a convection movement in the ladle because of the differences between temperatures of the steel, from a central region and the wall region. Even at high values of mixing energy input there are important decreasing of the flow rates toward the walls of the ladle.

Because of a lot of simplifications of the physical reality, sometimes mathematical models are less performant and precise. These simplifications are introduced under the form of the initial imposed conditions and frequently are due to the steady state diffusion coefficients of different species which are considered valid in turbulent conditions; such situations are as it follows:

- in tranzitoric regimes, from zero mixing energy dissipation (recipient in thermal equilibrium with the environment) up to the point when the flow pattern, for a selected plug and a fixed rate of bubbling gas, reaches the next stage –the permanent mixing regime;

- permanent mixing regime – the mixing regime obtained using a selected and well specificated pieces, modellind the porous plug, and an input of bubbling gas rate.

In this moment, a huge amount of research work is done in the field of investigating new methods to improve the predicting performance of the different

models, using new experimental techniques and sensors.

The reason for a such attitude is a consequence of the fact that simply mathematical models based on conservation of quantum and energy are too general and use values of the physical, physico-chemical and thermodynamical properties of fluids, which are not quite corresponding to the reality.

Non homogeneity at macro and micro scale is the responsible for all these non-conformities of the models describing mixing phenomena and the adiacent engineering processes in industrial vessels.

A short inventory of the identified tendencies in the study of the mentioned problems shows that mixing is an actual problem in research even in well studied systems; these directions of research uses techniques as it follows:

- reactive tracers to probe macro mixing and macro-segregation in stirred vessels at plant scale [2].

- addition position of a tracer in agitated vessels influences the mixing time obtained by simulation [6].

- special and particular effects are used to study and to perform measurements during mixing in different conditions. Fluorescence is used in study of circular impinging jets [3], and a new reaction pair is used for micromixing study in gaz-liquid systems with large vapour generation [5].

- electrical resistance tomography (ERT) of the agitated vessels is used to perform measurements of mixing gas-liquid [1], as state or associated with visualised reactive tracers technique [4]. In this respect, a novel electrical sensor for monitoring the phase distribution in industrial reactors, was developed [7].

As it results a single technique or procedure to mark the mixing aspects in a qualitative manner is unsatisfactory or incomplete.

Chemical reactions based on gas-vapor generation or precipitated coloured and dispersed phases, associated with sudden changing of properties and colour are used as tracers, markers or devices to visualise the direct effects or associated effects [2] – [5] [8].

In the paper [8] color changes are used in diagnostic of mixing time by visualization of liquid(red) –liquid(blue) mixing processes which produce a yellow liquid; an adjacent indicator(the pH of the instant solution) is used for mixing time, resulting a dual indicator system.

2.Colour as principal indicator of mixing state and energy dissipation

Study of the colour in solutions, as transmittance of the collected small volumes from stirred modelling liquid in the reactor vessel is a measure of the characteristics of the mixing process from the point of view of the following point of views:

- intensity of energy dissipation ε/unit mass, or ε'/unit time;

- uniformity of the dissipation of mixing energy and the special distribution by the liquid low, macro and local distribution;

- time of perfect or partially agreed degrees of mixing, in reactors.

There are many reasons to use colour as indicator of mixing degree and associated sensitive quantities. In order to be understood, values as figures, obtained by simulations and numerical analysis must be shown and positioned in space. Human being is a senzitive one and needs to see a general image in order to compare.

An agglomeration of numbers only rarely is able to promote a fast understanding of the represented phenomena or process evolutions.This is a reason for which, in electric resistance tomography used to model mixing phenomena, as mentioned before, data representing and showing the macro and micro-segregation in mixing under different conditions, in stirred vessels are represented in terms of colours, varying as intensity and changing gradually. Because of the fact that at the end of all this attempts and techniques there is a sensation = colour and a perception of this, using difference, it is normal to take into account the colour and its dissipation in liquid as a measure of different mixing aspects. The main problem in measuring colour of liquid is to do this in a non invasive and non-perturbative manner.When measuring mixing aspects in stirred vessels with segregated region and short-circuits, in permanent established regime, this problem is almost satisfactory solved.

Despite all these difficulties, a kind of tomographic map of mixing could be obtained although using direct measuring of an adequate indicator of the colour intensity. Under the aspects of the quantity of necessary samples in measurements there are devices using enough small amounts to be considered as non-perturbative for the general and local pattern flow.

Using cuvettes of adequate length of the optical path, small liquid samples must be collected rapidly (within less 1 second) while to measure a conductance or a specific resistance around a point is a more complicated procedure.

In the same time, a collected sample is a physical evident probe at the disposition of the researchers a long period of time with adequate conservation precautions. If the colored liquid has an enough long time of stability, there are not problems.

Sets of colored liquids can be analyzed how many times is necessary, without to repeat the whole experiment. If the coloring action of an agent is enough strong, low concentrations are necessary and

they are comparable with the concentrations of different elements in steels.

3. Technique and experimental conditions

Initial experiments which were performed have pointed that the analysis of colour in mixed vessels is sensible starting with concentration of 50 μl/l or the equivalent concentration 0,005% vol. Working carefully, the concentration could be decreased with an order of magnitude and so it could be referred to the concentrations of microalloying elements in HSLA steels. As colouring agent named in this paper colour marker and ink it was selected and used a commercial quality blue bright ink Pelikan®, usually used for pens. This ink has no adverse effects in using, handling even when swalling and as a joke, it was found on the net, that despite of this, this ink it is not quite exactly recommended to be used as an aliment. This has permitted us to do experiments without to agress the environment, without any risk for persons involved in experiments and whithout costs and operations for depollution. The modelling liquid was freshly distilled water which provide a good behaviour as stability and sensitivity for blue coloured solutions even at very low dilutions. The rate of decreassing the transmittance of the solutions in the range of low additions of blue marker ink was experimentally established at the value of 6,4 +/_0,2 (%)/ml ink, for the range of aditions representing 0,01-0,1%vol. The range +/_0,2% is due to the imprecision in exact dividing of a the base unit of 1ml blue marker ink. To measure the transmittance of solutions was used an electric photocolorimeter of concentration KFK-2 (Russia, Bashkortostan)(fig.1) at the length of 490nm, in the blue region of the light spectrum, where it was obserwed the maximum value of absorbance and consequently the minimum value of the transmittance in the whole range of working concentrations.

Fig. 1. General image of the electric photocolorimeter KFK – 2, including the chamber of measuring and etalon cuvettes, in working position.

This device presents the possibility to analyse transmittance of liquid colored solutions using also cuvettes of 100mm length, that means an increasing of the sensitivity starting with volumic concentrations of 0,0005%vol. Cuvettes of optical glass presenting an active length 50,0100mm, one for the etalon distilled water the other for the studied solution were used (fig.3). A Carl Zeiss Jena Spekol 10 using the module EK5 for cuvettes of 5cm length was also a solution to be used because it ask only 5ml liquid for analysis (fig.2).
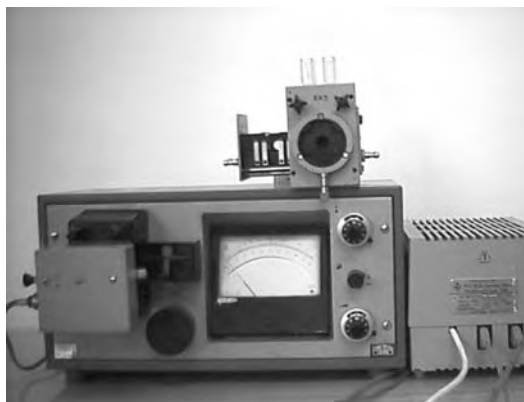
Fig. 2. General image of the spectrocolorimeter SPECOL 10 containing properly named device with measuring device EK1 and electric suppling source. Upper positioned is the measuring device EK5.

Fig. 3. Pairs of cuvettes of 50 mm optical path used in transmittance measurements based on KFK2 electric photocolorimeter (right positioned pair) and on SPECOL 10/EK5 (left positioned pair). Optical path or capacity of cuvettes may be read directly in the image.

The experimental trials were performed in two laboratory vessels. The first one is a paralelipipedic perspex vessel of dimensions

H=250mm (experimentally used 186mm), L=176mm (front view), T=102mm (thickness) as it can be seen in the fig.4-10.

Fig. 4. *t = 0 s*

Fig. 5. *t = 1 s*

Fig. 6. *t = 12 s*

Fig. 7. *t = 46 s*

Fig. 8. *t = 52 s*

Fig. 9. *t = 60 s*

Fig. 10. *t = 70 s*

Fig. 11. *t = 74 s*

In the fig.13-16 is presented the second vessel, having inner height H=250mm and the inner diameter D=210mm. In the same figures are presented other experimental data regarding the experimental conditions.

Up to this moment all presented data are totally dedicated to the establishing of some experimental limits in the range of the low and very low concentrations of the blue marker ink in distilled water and of the used deviced to produce mixing in experimental conditions similar to some real metallurgical reactors as tundish and ladle, in condition of stirring induced by different devices.

All data regarding images of stirring in both model reactors were recorded using a performant web camera, of commercial quality, provided with the necessary softwear for all necessary image processing.
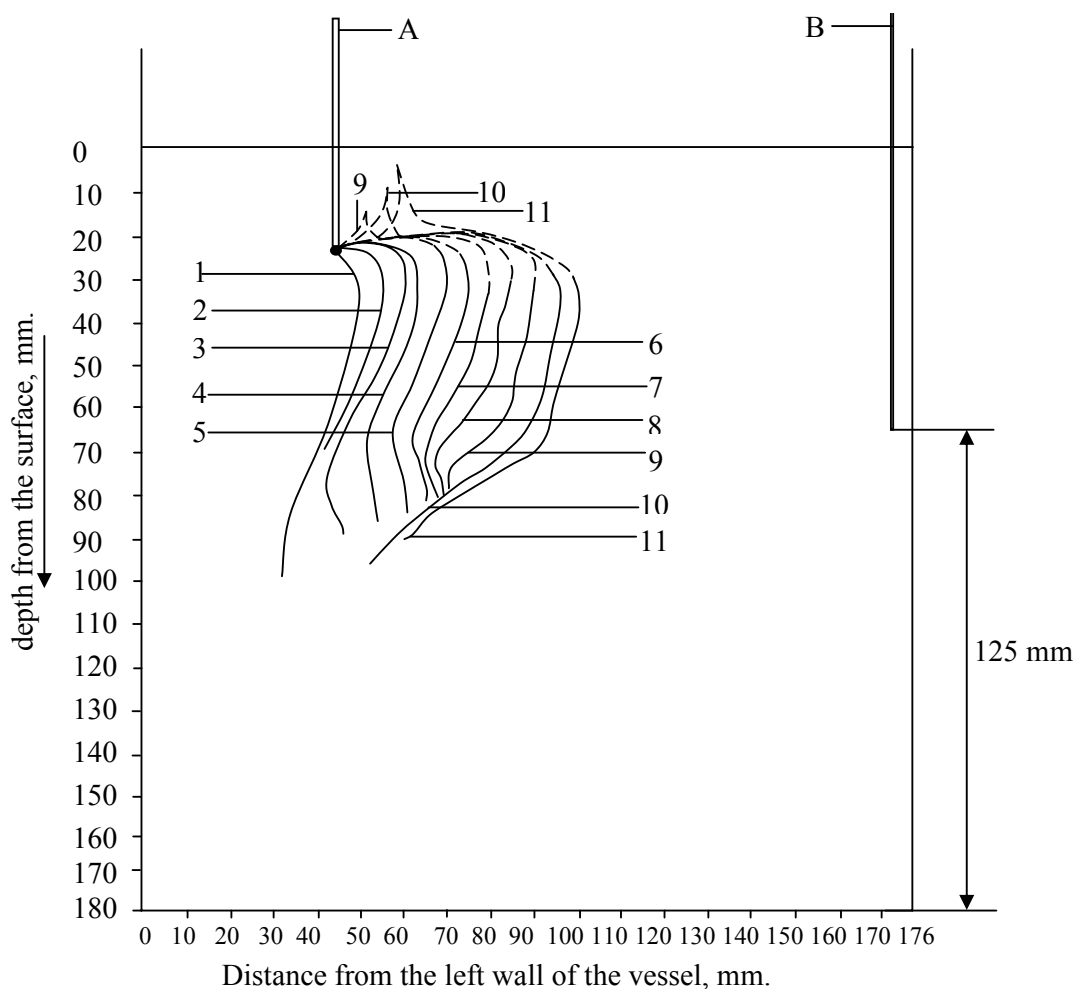
Fig.12. *The evolution of the marker ink stream line under the circulation induced by the injection of 20 ml distilled water in 5 seconds.*
Curves (1 – 12) correspond to an image captured at an established moment (t , seconds).
(1 – 52 s, Fig. 8 ; 2 – 54 s ; 3 –56s; 4 – 58 s; 5 – 60 s, Fig. 9; 6 – 62 s; 7 – 64 s;
8 – 66 s; 9 – 68 s; 10 – 70 s, Fig. 10; 11 – 72 s)
A – injection needle marker ink (blue);
B – injection needle 20 ml distilled water.

Fig. 13 Water model vessel.
Dimensions and data.
Inner height Hi = 250 mm
Inner diameter Di = 210 mm.
Diameter of the bubling nozzle 0,8 mm.
Water column height 220 mm (for ascendent bubling by nozzle).
Precision thermometer 0 – 50ºC (±1ºC)
Possibilities to use bubling by vertical lance.

Fig. 14. Bubling by nozzle.
Air pressure 2.105 N/m2.
Before colour marker ink (t = 0 s).
Reference value of transmittance for distiled water T = 100 %.
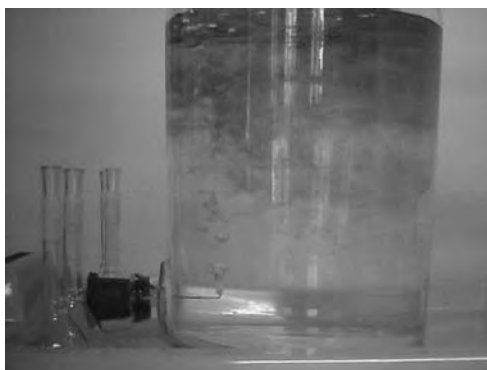
Fig. 15. Bubling by nozzle.
Air pressure 2.105 N/m2.
30 seconds after smooth injection of 4 ml marker ink. (t = 5 s).
Value of transmittance for liquid in the central region T = 98,5 %.
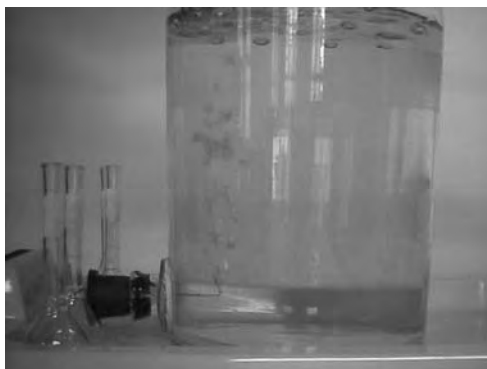
Fig. 16. Bubling by nozzle.
Air pressure 2.105 N/m2.
60 seconds after smooth injection of 4 ml marker ink.
Value of transmittance for liquid in the central region T = 98,2 %.

4. Experimental results and visualisation of the mixing process

In the fig.4-fig.10 an imagistic analysis is done regarding the initial stability and the dispersion of a thin stream of blue marker ink formed at the orifice of a calibrated tube 0f 1,00 mm inner diameter. The realised experimental system has provided results as it was programmed. So, as it was expected, it can be seen in the fig.10 the small quantum to introduce a small amount of blue marker ink did not a deviation fron the strait vertical line. An impulse produced by the injection of 20ml water had produced a deviation evoluting according to the fig.12. It is very inportant that the visual recording using a common, but of good quality web camera, provided a succesion on the liquid circulation in the upper region of the rectangular vessel.

Trials on the water model of the bubble argon stirred ladle proved that, despite the intesity of mixing, the colour in the vessel is stongly segregated in the first minute and only at the end of the second minute of mixing there is a fast tendency to the complete homogenisation. Mesurement were performed in a singe point at it resulted the necessity to analyse also the evolution of the colour concentration in other points at different levels.

The position of the active extremity of the tube for gaseous phase introduction , also that of the colour introduction is extremely important for the morphology og the mixing zones and require a detailed schedule of trials and mesurements.

Also using this technique , data must be completed and compared with mixing predictions based on macroscopic models for stirred ladles[9].

5. Commentaries and conclusions

Colored liquid technique, recommended by many researchers of the mixing processes also can be used in mixing processes researches based on water models of the metallurgical reactors.

The proposed method in this paper consists in measuring essential and quatitative aspects of mixing by measuring transmittance T(%) of the colored solution sample collected at an established moment.

A such determination is representative for the physical state of mixing in the established region only if the sample is carefully collected, in order to avoid any perturbation of the induced pattern of flow and mixing.

The method is sensitive when studying mixing phenomena and rates in the range of very low concentrations, being useful for study of the elements homogenisation in low alloyed steels (HSLA).

The technique is non-poluting and non-toxic for human health; neutralisation of the persistent colour can easily done using drinking water of common quality.

The developped system of research composed from working liquid, colour marker, device and method to measure the transmittance , vessels representing the metallurgical reactors at scale, and opto-electronic system, based on web camera are adequate to study more complex mixing phenomena.The influence of the way, speed and place where alloying elements are introduced and modes of dissipation of mixing energy are some of them.

Our team offers all cooperation for enlarged groups of researches in Romania and abroad.

References

[1]. **Wang M., Dorward A., Vlaev D., Mann R.** "Measurements of Gas-Liquid Mixing in a Stirred Vessel Using Electrical Resistance Tomography (ERT)." *1st World Congress on Industrial Process Tomography*, Buxton, Greater Mancester, April 14-17, 1999, p 78-83.

[2]. **Wabo E, Mann R.** "Using Reactive Tracers To Probe Macro-Mixing and Macro-Segregation in a plant-Scale Stirred Vessel, p 1-16." *The 7th Conference of Mixing Fluid Mixing 7*, 10-11 July 2002, University of Bradford, UK.

[3]. **Ding R., Revstedt J., Fuchs L.** " LIF Study of Mixing in Circular Impinging Jets Effects of Boundary Conditions." *Proceedings of PSFVIP – 4*, June 3-5, 2003 Chamonix, France, p 1-13.

[4]. **Wabo E., Kagoshima M., Mann R.** " Batch Stirred Vessel Mixing Evaluated by Visualised Reactive Tracers and Electrical Tomography." *Chemical Engineering Research and Design* vol 82, Issue A9, Sept 2004, p 1229-1236.

[5]. **Zhao D., Müller-Steinhagen H., Smith J.M.** "New Reaction Pair For Micro-mixing Measurements in Gaz-Liquid Systems with Large Vapour Generation." *The 7th Conference of Mixing Fluid Mixing 7*, 10-11 July 2002, University of Bradford, UK.

[6]. **Bujalski J.M., Jaworski Z., Bujalski W., Nienow A.W.** " The Influence of the Addition Position of a Tracer on CFD Simulated Mixing Times in a Vessel Agitated By a Rushton Turbine." *The 7th Conference of Mixing Fluid Mixing 7*, 10-11 July 2002, University of Bradford, UK.

[7]. **Bolton G.T., Oin C.H., Wang M.** "A Novel Electrical Tomography Sensor For Monitoring The Phase Distribution in Industrial Reactors." *The 7th Conference of Mixing Fluid Mixing 7*, 10-11 July 2002, University of Bradford, UK.

[8]. **Melton A. L, Lipp C.W., Spradling R.W., Paulson K.A.,** "DIMST-Determination of Mixing Time through Color Changes" *Chemical Engineering Communmications* (2001).

[9]. **Mazumdar D., Evans J.W., "**Macroscopic Models for Gas Stirred Ladles" *ISIJ International*, Vol.44(2004), No.3, pp.447-461.

LASER CLADDING OF Ni-Cr-B-Fe-Al ALLOY ON A STEEL SUPPORT

Sanda Maria LEVCOVICI[1], Dan Teodor LEVCOVICI[2], Constantin GHEORGHIEŞ[1], Simona BOICIUC [1]

[1]University "Dunarea de Jos" of Galați
[2]S.C. Uzinsider Engineering S.A. Galați
e-mail: dslevcovici@pcnet.ro

ABSTRACT

Multilayer coating by injection of powder with 8.9% Cr, 4.5% Fe, 5.1% B, 2.4% Al, 0.6% Cu; all reminded of Ni, as chemical composition, in melted bath by CO_2 continuous wave laser connected to x-y-z coordinate table was tested in order to rise the wear and corrosion resistance of 0.45% C superficial steel layers. Layers made by different laser running were characterized by macro and microstructure analysis, as well as phase quality analysis by X ray diffractometry, micro hardness analysis and hardness finding on coated layer surface in order to establish the optimal deposit running.

KEYWORDS: laser, cladding, nickel, microstructure, microhardness, difractometry

1. Introduction

550°C temperature hot rolled tape is lined up on winding reel by some manipulators having the wearing plates in touch with moving tape edge.

Quick abrasion and oxidation wearing of these plates result. In order to enlarge their useful life, it is requested the coating of a superficial layer of material with higher wear and oxidation resistance.

Gas-thermal coatings (oxy-gas flame, spreading in plasma) by powder based on nickel from systems Ni-Cr-B-Si, Ni-Cr-Al, Ni-Mo-Si and others, for parts working under large thermal and mechanical loads in aggressive environments are known [1] ÷ [3], Researches made on thermal spread coatings from Ni-Cr-B-Si alloys, lately melted by laser, pointed out rising of hardness and fatigue resistance, decreasing of friction coefficient, lapping period and seizing trend compared to coatings made by flame melting [2], [4].

Researches more recent shows the laser cladding structure and properties of some nickel alloys from predeposed or injected powder [4] ÷ [15].

Hereby paper work gives the results of multilayer coating by injection in laser melted bath by nickel alloy powder from Ni-Cr-B-Fe-Al system.

2. Experimental conditions

For coating „Alliages Speciaux 7569 Alliajes Frittes, Franța" powder with 8.9% Cr; 4.5% Fe; 5.1% B; 2.4% Al; 0.6% Al; All reminded Ni was used. By sieving the granulometric fractions, inside 80÷90 μm interval, were separated in order to be used as addition material. Powder had spherical shape that provided a fluid floating of addition material through the injection system. Powder dried at 110°C temperature for 15 minute before feeding the addition material into injection system tank. Coatings were performed on 25 x 25 x 15 mm^3 samples made of 0.45% C carbon steel in improved condition.

Laboratory trials were performed in a CO_2 continuous wave laser installation as GT type of 1400 W (made in Romania), with coordinate working table and computer program for running, provided by powder injection system onto laser melted surface.
For laboratory tests it was used a 1150 W power laser beam by 1,8 mm in diameter on machined surface, which deposed the parallel partly superimposed strips by 1.5 mm transverse motion pass. Final layer thickness resulted by superimposing of 4÷5 layers. In order to establish the optimal coating laser run there were changed the adittion material flow, sweeping speed of charging surface and initial sample temperature. In table no. 1 are given the layers running condition and thickness for several experimental running.

Table 1 Experimental conditions and layer thickness

Sample code	Addition material flow [mg/s]	No. of superimposed passes [initial sample temperature]	Sweeping speed [mm/s]	Layer thickness [mm]
1	55,5	5 [T_P=20°C]	9	1,50
2	105	4 [T_P=20°C]	7,5	2,07
3	105	4 [T_P=20°C]	11	0,59
4	63,9	4 [T_P=60°C]	11	0,42
5	63,9	4 [T_P=60°C]	7,5	0,35

Deposited layers were tested by: macroscopic analysis on both coated layer surface and cross section in laser processing direction, after its metallographic preparation; microstructure analysis and $HV_{0.98}$ (0.98N load) micro hardness profile drafting in cross section of laser strips; phase quality analysis by X ray to coated layer surface made by DRON 3 diffract meter using: copper anticathode; monochromatic diffracted beam; U=34kV; I=30mA; F_1=2mm; F_2=0,5mm; ω=1°/min; s_{trip}=720mm/h, for diffraction angle variation between 2θ = 20°....75° limits.

3. Results and discussion

Macroscopic analysis pointed out the coated surface quality, tightness, coated layer thickness and its adherence on support. Thick layers may be observed with good adherence on support, tight and with a plain surface of deposited layer (figure 1), as lately mechanical work to be minimally. Regarding to running influence on surface quality, tightness and thickness of coated layer, good results were obtained in a very large running range. It was found the lack of any support influence upon chemical composition throughout deposited layer depth after five passes. Figure no.2 shows the coated layer microstructure aspect for the sample 2, when multiply by x500. Good coated layer adherence to the support may be seen. In fusion line there are no tightness defects or non-metallic inclusions.
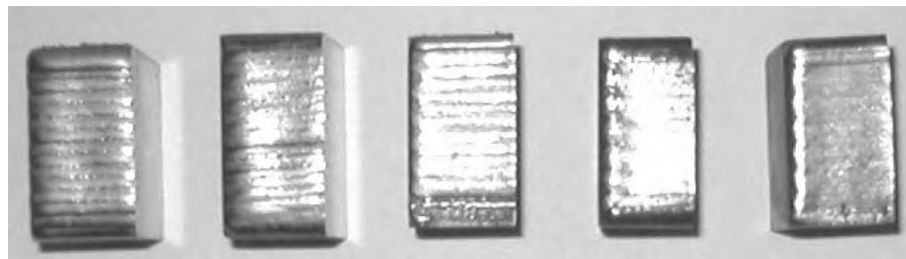
***Figure1.** Samples coated by thick layers of nickel alloy*
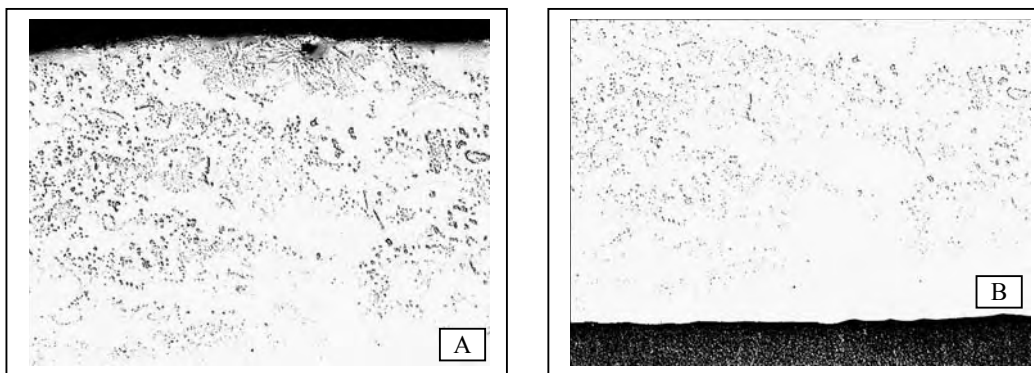
***Figure 2.** Nickel alloy microstructure deposed onto sample 2. A-layer surface; B-base deposed layer and support (x500). Nital attack 2%.*

According to phase quality analysis (figure 3), deposit microstructure includes solid solution based on nickel and eutectic colonies of boride like NiB, Ni$_2$B, CrB, Cr$_3$B$_4$ and FeB, main hardening phase being CrB. In the layer bottom a nickel-iron narrow dilution area may be seen, without eutectic carbides that make transition to support material.

Figure 3 Diffractometer diagram for deposed layer on sample no. 2
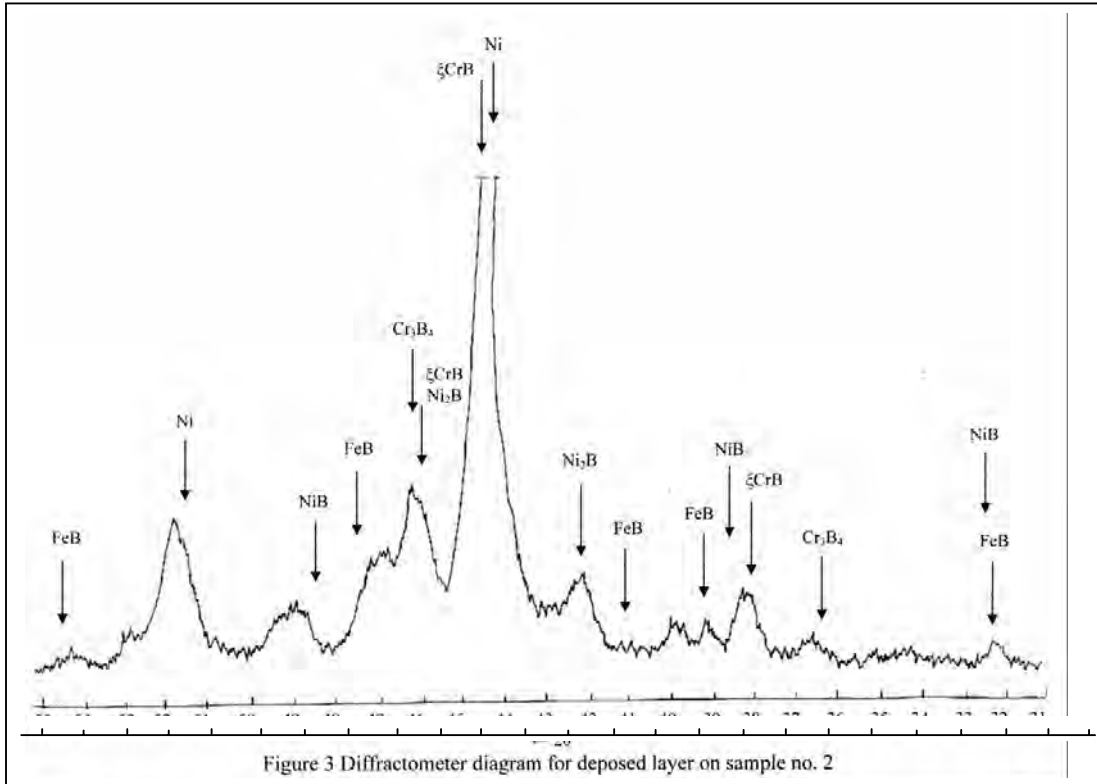
Figure 3 Diffractometer diagram for deposed layer on sample no. 2

Figure 4 shows HV$_{0.98}$ micro-hardness variation through laser deposited layer depth in samples with code 1, 2 and 3, without support preheating. Maximum layer hardness and thickness were found at sample no.2, where the minimum sweeping speed was and maximum addition material injection volume was. Sample preheating to 60^{0}C (samples no. 4 and 5) decreases the coated layer hardness and thickness, more emphasized in slow sweeping speeds because of superficial temperature rising and vaporization processes intensifying. As laser beam mainly gives the energy required to melt the addition material, the sweeping speed has to be correlated to addition material flow. The larger addition material flow determine the smaller the sweeping speed that provides maximum deposited layer thickness.

Optimal running (of sample no.2), was used in order to get the wearing plates of winding system manipulators of hot rolled stripes. Figure 5 gives a wearing plate on which nickel alloy in active area was deposed.

4. Conclusions

When multi layers coating by continuous wave laser beam, thick layers nickel alloy may be achieved to be wear and corrosion resistant, from Ni-Cr-B-Fe-Al system, dense, with good adherence to under-layer by dilution decreased layer. Laser coating by powder injected in melt bath is a complex process of mass and heat transfer, which is efficiently in condition of a powder injection system in continuous flux with steady flow. In condition of coating by powerful laser beam with given dimensions, hardness and thickness of deposited layer depend on addition material flow, surface sweeping speed, initial sample temperature, number of superimposed layers and laser strips superimposed degree. Dilution degree is influenced by powder flow and power factor used.

Optimal nickel alloy coating running (sample no.2) achieved a 2 mm in depth dense layer with HV$_{0.98}$ micro hardness varying between 9543MPa and 12 640MPa.
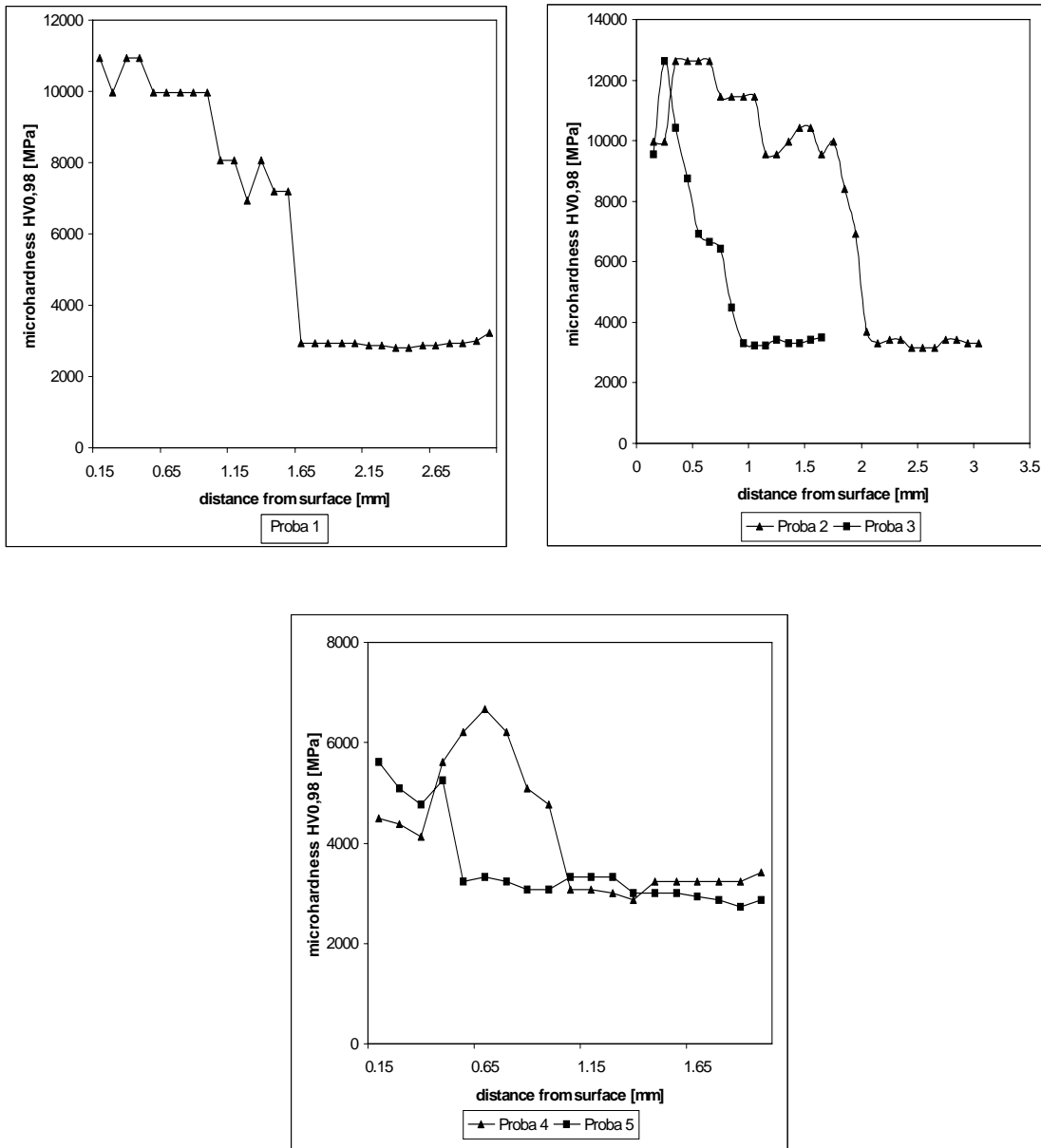
Figure 4. *Vickers micro-hardness variation in relation with distance since deposed layer surface, samples no. 1, 2, 3, 4, 5.*
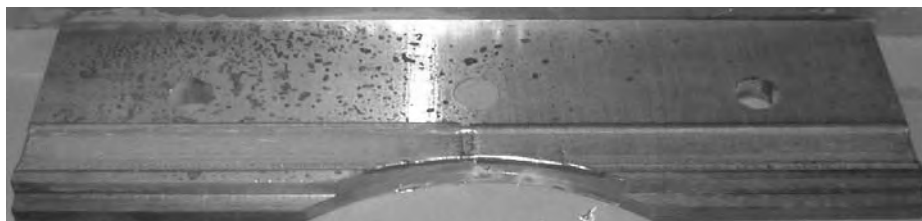
Figure 5. *Wearing plate of winding system manipulators of hot rolled stripes*

References

[1].Boris, I.S, Harlem, I.A., Sidorenco S.L., Ardatovskaia E.N., *"Gazo-termiceskie pocritia iz poroshkovih materialov"*-Spravocinik, Kiev, Naukova Dumka, 1987, page 253-280

[2].Spiridonov, N.V., Kobiakov, I.L., Kupriakov, I.C., *"Plazmennie i lazernie metodi uprocinenia detalei mashin,* Vişcisia scola, Minsk,1988

[3].Cai, G., Molino, G., *"Comparison Between Cladding by Means of Plasma Spray and the More Recent Technologies of Plasma Transferred Arc, Plasma Semi-Transferred Arc and Laser on Traditional Filler Material and New Nickel Base Boron-Free Alloys"*, Proc. Laser-6, 1990, page 79-90

[4].Lugscheider, E., Oberländer, B.C., Meinhardt, H., *"Laser Cladding and Laser Surface Remelting of Nickel-base Hardfacing Alloys"*, Proc. ECLAT '90, 1990, page 555-568

[5].Yang, X.C., et al., 1988, *"Microstructure and Performance of Laser Cladding NiCrSiB Alloy"*, Proc. ICALEO '87, page 209-220

[6].Singh, J., Mazumder, J, *"Effect of Extended Solid Solution of Hf on the Microstructure of the Laser Clad Ni-Fe-Cr-Al-Hf Alloys"*, Acta Metall., vol. 35, no. 8, 1987, page 1995-2003

[7].Sircar, S., Ribaudo, C., Mazumder, J., *"Laser Clad Nickel Based Superal loys: Microstructure Evaluation and High Temperature Oxidation Studies"*, Laser Beam Surface Treating and Coating, SPIE, vol. 957, 1988, page 29-41

[8].Damborenea, J. de, Vázquez, A.J., Fernández, B., *"Laser-clad 316 Stainless Steel with Ni-Cr Powder Mixtures"*, Materials & Design, vol. 15, no. 1, 1994, page 41-44

[9].Grünenwald, B., et al., *"Laser Cladding with a Heterogeneous Powder Mixture of WC/Co and NiCrBSi"*, Proc. ECLAT '92, 1992, page 411-416

[10].Kar, A., Mazumder, J., *"Extended Solid Solution and Nonequilibrium Phase Diagram for Ni-Al Alloy Formed During Laser Cladding"*, Metall. Trans. A, vol. 20A, 1989, page 363-371 Schneider M.F., "Laser cladding with powder", Ph. D. Thesis University of Twente, Enschede, Haarlem, 1998.

[11].Bruck, G.J, *"High Power Laser Beam Cladding"*, J. of Metals, vol. 39, no. 2, 1987, page 10-13

[12].Ollier, B., et al., *"Cladding with Laser Radiation: Properties and Analysis"*, Proc. ECLAT '92, 1992, page 687-692

[13].Chabrol, C., Hernandez, J., Vannes, A.B., "Determination of Internal Stresses in Laser Treated Surfaces and Cladding", Laser Treatment of Materials, 1987, page 91-99

[14].Cooper, K.P., *"Surface Treating by Laser Melt/Particle Injection"*, Laser Beam Surface Treating and Coating, Proc. SPIE, vol. 957, 1988, page 42-53

ASPECTS REGARDING THE BIOCORROSION OF THE PAPER MANUFACTURED MACHINES

Constantin STANCIU, Marian BORDEI

"Dunarea de Jos" University of Galati
e-mail: **stanciu.constantin@ugal.ro**

ABSTRACT

This paper presents the main microorganisms causing biocorrosion, the concentration, their effects and a series of measures for their reduction.

The conclusion is that the sulpho-reducing bacterius are responsible for the majority of defects that take place in the paper industry.

KEYWORDS: widia plates**,** thin layer, cutting

1.Introduction

The metals corrosion consists in the spontaneous, partial or total distruction of the metals as a results of some chemical, biochemical or electro-chemical reactions happened during their interaction with the environment.

It is estimated that 20% of the serevising expenses in the cellulose and paper industry are due to the corrosion problems. The concept of microbiological corrosion (chemical corrosion, biochemical) can be controversial, because there are few cases when physical and chemical phenomena do not take place. Bioccorosion is determined by the activity of the different microorganisms that use the metal as a medium of culture (vital metabolic element) representing a resultant of a asssembly of metabolic reactions catalysed by enzymes.

The types of microorganisms that affects the unit from the cellulose and paper industry are inferior form members of vegetable life, mainly the bacteriums, algas and the fungies.

2. The causes of the microbiological corrosion

The micreobiological corrosion can be caused by three phenomena:

-a "chemical" attack because of the metabolic products with agresive activity over metalssuch as sulphuretted hydrogen, sulphuric acid or organic acid;

-a "physical" attack under the form of deposits that isolate locally the metal, prevent the inhibits of corrosion, or simply create the conditions for a corrosion differential aeration;

-an "enzime" attack directly responsible for the enzime equilibrum dispalcement, by means of a depolarfization action of a micoorganism at the anode (the case of bacteriums of iron).

In reality the microbiological attack of the metals is translated by an assembly of electrochemical reactions and it is a special case of corrosion in watery medium, at a temperature compatible with the micoorganisms activity, in the presence of the molecular oxygen or under anaerobic conditions and in a large scale of pH from 1 to 10. among the microorganisms, the sulpho-oxidizing, the sulpho-reducing and ferruginous have the greatest contribution to the corrosion.

3. Experimental data

The paper industry is a "wet" industry that vehiculates by quantities of water (10-50 m^3/t paper). Water is the main source of microbiologic infection of the paper mill system and of the paper products. A bacterium/ 1 ml of water correspends already to 10^6 bacteriums/m^2 and taking into account the specific consumption of water per tone of paper, there are billions of bacteriums that contaminate daily the paper machine.

A temperature close to the incubation temperature, nutrients in big quantities leads to a exponential rise of the bacteriums.

Taking into account this fact, it was required the identification of the main microorganisms responsible for biocorrosion and the affected installations. Among the sulpho-reducing bacteriums, the most frequent species in the papers mills is the bacterium Desulphovibrio desulfuricans. The sulpho-reducing bacteriums are anaerobic bacteriums, that grow better at a pH = 5.5 – 8.5, in the presence of organic substances and of a moderate concentration of sulphate.

Desulphovibrio desulfuricans, being a bacterium gram negative uses hydrogen from organic

substances, reduces sulphates, sulphites, tiosulfite at H_2S, being able to produce up to 3100 mg H_2S/l.

Some anaerobic bacteriums such as Clostridium spp. and Desulphovibrio spp., create secondary corrosive produces that can completely make holes in the stainless steel of ¼ inch in several months or even weekes.

Figure 1 presents the aspect of the Clostridium and Desulphovibrio bacterium.
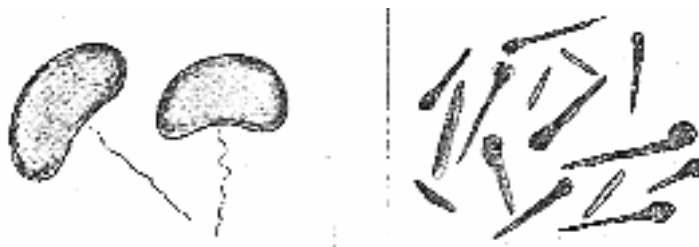
Fig.1. *The aspect of Clostridium and Desulphovibrio bacteriums.*

These bacteriums caused the corrosion of the headbox, of the Gautsch roles make of stainless steel, of the pipes and pumps.

Figure 2 presents the corrosion of some metallic stainless surfaces caused by the sulpo-reducing bacteriums.
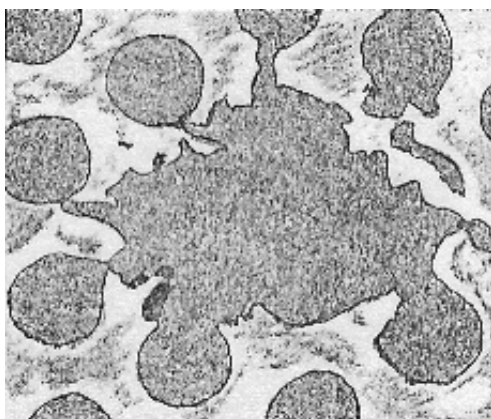
Fig.2. *The corrosion of some stainless steel metallic surfaces provoqued by sulpho reducing bacteriums.*

The ferro-bacterium or the ferric bacteriums are aerobic bacteriums that takes the energynecessary to the metabolism from the oxidizing the ferrous salts in feric salts.

This transformation is favoured by an enzyme suitable to those bacteriums.

The reactions that takes place are the following:

$$FeCO_3 + 3/2\ H_2O + 1/2O2 = Fe(OH)_3 + CO_2 + 92{,}5\ cal.$$
$$2FeO + O + 3H_2O = Fe(OH)_3 + 353\ cal.$$
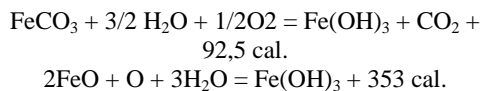
$Fe(OH)_3$ is deposited under filament form at the Leptothrix (fig.2.), Cronothix, and at the Gallionela under the forum of bands.

Fig.3. *Ferruginous bacteriums of Leptothix type isolated from the water supplying pipes.*

These bacterium tend to a row fast and to form deposits that adhere to the inside of the pipes, tanks, nozzles preventing the following and contributing to the corrosion process is represented by the anaerobic conditions created and that ensures a favourable medium for the growth of the sulpho-reducing bacteriums.

The algae are nexious to metals on the one hand through metabolism produces that modify pH and the water purity and on the other hand through their provinently growth cause deposits of substances with a gelatinous aspect or under the form of crusts that represent substratums for the growth of other microorganisms. The acummulations of algae can ostruct the filters, sieves, nozzles, and pipes can cause indirectly corrosion located in the growing areas. The most frequent algae are the green and blue-green ones.

Figure 4 presents the blue-green filamentous alga, called Lyngbya ussually found in reservoirs and clarifiers.

Fig. 4. Blue-green fillamentous algae.

Fylamentous blue-green algae Lyngbya usually found in reservoirs and clarifiers.

Among the fungus, some species of moulds are implied in corrosion phenomena, they act on the substractum mainly through a series of metabolism produes. Thed moulds identified on the circuits of the paper machine are show in figure 5.

The weight of the microorganisms found on the fabrication circuits causing corrosion is represented by bacteriums. Table 1 presents the content of microorganisms in the paper fabrication.

The content of microorganisms in the paper fabrication. (nr. of microorganisms/ 1 g dry substance or 1 ml. licquid).

Table 1. The content of microorganisms in the paper fabrication
(nr. of microorganisms/ 1 g dry substance or 1 ml. liquid).

Sample	Bacterims [millions]	Fungus [thousand]
Industrial water	0,14	0,02
Paper paste	49,56	65
Greasy water	17,60	100

Fig. 5. Moulds identified on the paper machine.

In order to combat the microorganisms causing corrosion, a great variety of chemical ageents can be used, agents knows as biacids, which act on the enzyme systems of the microbical cells or a bioprocessual technology.

This biproseccual technology experimented by us consists in the introduction of some culture of selected bacteria (BIOLEN IS 80) on residual waters circuits, which have the capacity of degrading the organo-sulphirized products (without H_2S evolution and sulphide formation) have influences over the corrosion and smells reduction.

Tabelul 2 presents the reduction of S^{2-} and SO_2^{2-} content in the residual water at BIOLEN IS 80 using.

Table 2. *The reducing of S^{2-} and SO_4^{2-} content at the BIOLEN IS 80 using*

Components	Initial	Samples with BIOLEN		
		After 24 h	After 48 h	After 72 h
S^{2-}, mg/l	5,3	4,5	4,3	4,2
SO_4^{2-}, mg/l	56	5,3	50	50

The sulphide content decreased with 18,9%, after 48 hours and with 20,8% after 72 hours, but the sulphide content decreased with 5,35% after 48 hours.

4. Conclusions

Bioccorosion is a complex problem that require the detailed analysis of the deposits existant on the fabrication circuits. The greasy water characteristics may have an important role in the corrosion and deposit problems. The construction materials of the system may also help the generated problems. The possibility of the corrosion appearance will be significantly increased by the deposits presence. The sulphide-reduction of sulphur bacteria are responsible for a great amount of defects that take place in the paper industry.

References

[1]. **Blankenburg I., Schulte J.**, PPI, 39, (6), 67 (1997).
[2]. **Simons B.,** La Papeterie, (261), 12 (2004).

MECHANICAL AND TRIBOLOGICAL PROPERTIES OF TiC_xO_y THIN FILMS

Daniel Munteanu[1], Bogdan Borcea[1], Alexandru Munteanu[1], Rodica Cozma[2], Filipe Vaz[3]

[1]Dept. of Technological Equipment and Materials Science,
Transilvania University of Brasov – ROMANIA,
[2]Dept. of Product Design and Robotics,
Transilvania University of Brasov – ROMANIA,
[3]Dept. of Physics, Minho University, Guimaraes – PORTUGAL
muntean.d@unitbv.ro

ABSTRACT

The main purpose of this work consists on the preparation of single layered titanium oxycarbide, TiC_xO_y, thin films, deposited by d.c. reactive magnetron sputtering. The depositions were carried out from a TiC solid target, on (AISI M2) steel substrates at 200^oC, under the variation of two process parameters, such us time deposition and flow rate of reactive gas O_2. The O_2 flow varied between 0.5 and 7.5 sccm and the deposition time between 3600 and 6000 s. In terms of film colours, the most interesting colour tones have been observed if the oxygen flow increased. Static friction coefficient, wear and residual stresses are characterized and discussed as a function of both process parameters (oxygen flow and time). The results reveled a good correlation between compressive residual stress level in the films and the oxygen flow. A compressive residual stress state has been observed if the O_2 flow is bigger than 1 sccm. Generally, the addition of oxygen till 7.5 sccm leads to an increasing of this compressive stress level to -17.7 GPa. For an oxygen flow rate higher than 2 sccm and a high compressive residual stress level, the deposited films presented a good wear behaviour. However, the best wear results were registered for a moderate value of the residual stress (-1.18 GPa) and an oxygen flow rate of 2.5 sccm.

KEYWORDS: TiCO, Sputtering, Friction, Residual stress, Wear

1. Introduction

The increasing importance and use of surface coatings for improving component performance brought an increasing need for fundamental understanding of their properties if the optimum coating for a particular purpose is to be selected. The solutions to achieve a coating tailored for a particular task will essentially depend on the ability to establish knowledge of the interrelationship between their physical, structural and mechanical properties. In modern science, a new field is emerging with increasing application possibilities – the so-called decorative thin films.

Decorative hard coatings were first introduced on small consumer products such watches, writing instruments, eyeglass frames, pens, wristwatches, kitchen and bathroom equipment, as well as jewelry parts. While enhancing the appearance and lending attractive coloration to surfaces, the films are supposed to provide scratch resistance, protection against corrosion and durability.

As a result of technological progress in recent years, a new challenge was passed onto decorative hard coatings. The growing demand for low-cost products and reduced material resources imply that the continuous change in target materials and basic PVD deposition procedures to obtain different coloured films is clearly unsuitable [1,2]. At the same time, from the decorative aspect point of view, the attainable colour tones are largely restricted to some golden yellows, various shades of grey and black tones [3,4], although some attempts have been made to obtain other colours [2,4].

Taking these restrictions into consideration, recently two new classes of materials has been

gaining importance for both decorative and tribological applications, the so-called metal oxynitrides Me(N,O) and metal oxycarbides Me(C,O) (Me = early transition metal). Their importance results from the presence of oxygen that allows the tailoring of film properties between those of nitride or carbide and the correspondent oxides.

Despite the huge amount of published scientific works on thin films of metallic nitrides and oxides over 10 years, the area of metal oxynitrides and, especially of metal oxycarbides is poorly explored so far and knowledge of the fundamental mechanism that explains the observed behaviour, both structural and mechanical, is yet insufficient [5]. In fact, a basic understanding of the gase-phase and thin-film oxygen and carbon (or nitrogen) incorporation chemistries facilities the processing of oxycarbides (oxynitrides) nanostructures with desirable properties.

Taking into account these features, the aim of the present research is to establish a general basis allowing the interpretation and the prediction of reactively d.c. sputtered TiCO coatings as a function of different preparation conditions, such as those of oxygen flow and deposition time. The sets of deposited samples allowed studying the evolution of the mechanical and tribological properties (thickness, residual stress, static friction coefficient) as a function of the different deposition parameters. The correlation with the wear characteristics is also an important parameter in this work.

2. Experimental details

The TiCO thin-films were deposited by reactive dc magnetron sputtering, onto polished high-speed steel (AISI M2) and stainless steel (AISI 316) (samples) substrates. The first samples (manufactured from AISI M2 - Φ25x5mm) were used from the tribological tests and the second ones (manufactured from AISI 316 - Φ25x0.5 mm) for establishing the thickness and residual stresses.

The depositions were carried out in a "home-made" apparatus under Ar/O_2 atmosphere. The system consists of two vertically opposed rectangular magnetrons (unbalanced) in a closed field configuration. Prior to depositions, the substrates were *ex situ* ultrasonically cleaned and *in situ* sputter etched for 15 min. in a pure Ar atmosphere, using a pulsed power supply: I ≈ 0.35 A; V ≈ 300 V; f = 200 kHz.

A turbo molecular pump was used to achieve a base pressure of 2E-4 Pa (before introducing the gas mixture). The substrate temperature during deposition was approximately 200°C, while the substrate bias voltage was kept at the ground state.

The base pressure in the deposition chamber was typically in the order of 10^{-4} Pa and rose to values around 3×10^{-1} Pa during depositions.

The experiments were carried out with the TiC target coupled to a dc power supply: I = 0.5 A/cm²; V ≈ 480 V and the oxygen flow rate varied from 0.5 up to 7.5 sccm. The argon flow was kept at 12 sccm. Table 1 presents, first the oxygen flows used for depositions and second the deposition time.

Film thickness was obtained by "Ball Cratering" technique. This technique, ex-situ, consists, basically, in the erosion of the coating by rotating sphere. A typical mathematical model allows calculating the coating thickness based on dimensions of gotten crater [6]. An average number of five "Ball Cratering" experiments were carried out in each sample to determine its thickness.

Table 1. *The oxygen flows and time deposition values typically of the studied coating conditions*

Sample	Oxygen flow [sccm]	Deposition time [s]
TiCO 1	7.5	3600
TiCO 2	2.5	3600
TiCO 3	5	6000
TiCO 4	0.5	5400
TiCO 5	1	5400
TiCO 6	1.5	5400
TiCO 7	2	5400
TiCO 8	3.5	5400

The technique used for residual stress measurements is based on the curvature or deflection of the substrate. The major advantage of the thin film approximation is the possibility of calculating the coating residual stress using Stoney's equation [7]:

$$\sigma_{res} = -\left[\frac{E_s}{6(1-\nu_s)} \cdot \frac{t_s^2}{t_c} \right] \cdot \left(r_a^{-1} - r_b^{-1} \right) \qquad (1)$$

where $E_s/(1-\nu_s)$ is the biaxial modulus of the substrate's material (in this case, stainless steel, E_s=215 GPa, ν_s=0.3), t_s and t_c are, respectively, the thickness of the steel substrate and coating, r_b and r_a represent the radius of the curvatures of the substrate before and after deposition. The curvature of the samples was analyzed with a laser displacement meter (Keyence LC-2100). The thickness of the substrate was measured using a digital micrometer.

In order to establish the static friction coefficients for all the coatings, a typical method such as the inclined plane slope was used [8]. This system can estimate the static friction coefficient value based on typical linear size measurements, involving the correlation between the friction angles *α,* and the static friction coefficients μ_s.

Within the frame of this method, the friction couple, which is in a rest position, is inclined by the aid of a plane with variable vertical adjustment, until

the sliding phenomenon appears in the couple. The angular value α_l for which the sliding occurs, is in direct correlation with the static friction coefficient μ_s according with:

$$tg\,\alpha_l = \mu_s \qquad (2)$$

The static friction coefficient values were established, for each sample, in three-friction condition, using a plane fixed half-couple made by heat treatable steel (AISI B7), in normalizing heat-treatment conditions. In the first case the friction plane fixed half-couple had an average roughness R_z = 0.4 μm, in the second 2.25 μm and in the last 2.5 μm. The work with the three roughness values of fixed plane half-couples is important in order to could take into consideration the possible influence of roughness on friction process and to have finally an average value of static friction coefficient.

Before the tribological tests, the samples were first degaussed and then alkaline cleaned and wiped. The fixed half-couple was also degaussed and periodically alkaline cleaned and wiped. According to the method description, 10 friction tests were performed for each sample on each half-couple: 5 in one direction and 5 abeam, such as the one-way roughness would not influence the moving of the samples. In each case, the utmost values were eliminated.

The wear behavior of the coatings (abrasion wear) has been estimated using a custom made pin-on-disk tribosystem [8].

For all wear tests, the annular type wear surface was characterized by an average diameter of approximately 13 mm. According to the technical arrangements, the friction distance length was estimated as 40.82 mm / one rotation cycle. The normal load applied by the pin on the sample surface was 10 N. For each sample, the wear test consisted in 5 minutes of holding load.

The wear distance length created in each sample was calculated as 17.55 m, with a plateau rotating speed of 86 rpm. Before the tests and after each rotation cycle, the samples were gravimetrically measured using an analytical balance Sartorius Master U11206-30 type. The environmental conditions of tribological tests were: T = 23.5 °C and 63% humidity.

3. Results and discussion

Table 2 presents the thickness values of deposited films and the static friction coefficients. Generally, referring to the second parameter, for each sample a small increase in roughness of plane fixed half-couple generally leads to a small decreasing of

friction coefficient. Nevertheless, the last column of table 2 presents a general average value of this friction parameter that covers these small variations.

Table 3 shows the results of wear tests and the residual stress levels.

Fig. 1 presents the values of static friction coefficients for different oxygen flows used for preparing films.

This graph shows that, there is no a clear dependence between the oxygen flow (which is a deposition technological parameter) and friction coefficient.

Table 2. Thickness and static friction coefficients of deposited films.

Sample	Thickness [μm]	R_z [μm]	μ_s	μ_s (general average value)
TiCO1	0,6	0,4	0,1632	0,1355
		2,25	0,1242	
		2,5	0,1192	
TiCO2	1,4	0,4	0,2233	0,1876
		2,25	0,1825	
		2,5	0,1570	
TiCO3	0,9	0,4	0,2714	0,246
		2,25	0,2096	
		2,5	0,2572	
TiCO4	1,8	0,4	0,2585	0,2565
		2,25	0,2558	
		2,5	0,2552	
TiCO5	2,2	0,4	0,1882	0,1847
		2,25	0,1964	
		2,5	0,1697	
TiCO6	2,5	0,4	0,1844	0,1891
		2,25	0,1833	
		2,5	0,1996	
TiCO7	1,1	0,4	0,3491	0,3308
		2,25	0,3786	
		2,5	0,2648	
TiCO8	0,7	0,4	0,3774	0,2994
		2,25	0,3537	
		2,5	0,1671	

Table 3 shows the results of wear tests and the residual stress levels.

Fig. 1 presents the values of static friction coefficients for different oxygen flows used for preparing films.

This graph shows that, there is no a clear dependence between the oxygen flow (which is a deposition technological parameter) and friction coefficient.

Table 3. *The wear test results and the residual stress levels.*

Sample	Initial mass M_0 [g]	Final mass M_f [g]	$\Delta M = M_0 - M_f$ [g]	Residual stress [GPa]
TiCO1	19.7186	19.7184	0.0002	- 17,703
TiCO2	19.5474	19.5473	0.0001	- 1,188
TiCO3	19.6133	19.6130	0.0003	- 8,105
TiCO4	19.4422	19.4402	0.0020	+ 4,692
TiCO5	19.7143	19.7110	0.0033	+ 23,616
TiCO6	19.7070	19.7061	0.0009	- 2,472
TiCO7	19.7537	19.7530	0.0007	- 7,364
TiCO8	19.4957	19.4952	0.0005	- 17,057

The minimum values of friction coefficient were observed for the films prepared with an oxygen flow of 7.5 sccm and the maximum ones for 2 sccm.
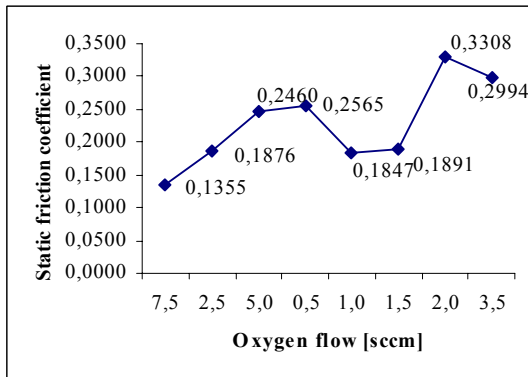
Fig.1. *Evolution of the static coefficient of friction (μ_s) of the deposited films as a function of the oxygen flows used for preparing coatings.*

The evolution of residual stress levels as a function of the oxygen flows is illustrated in Fig. 2.
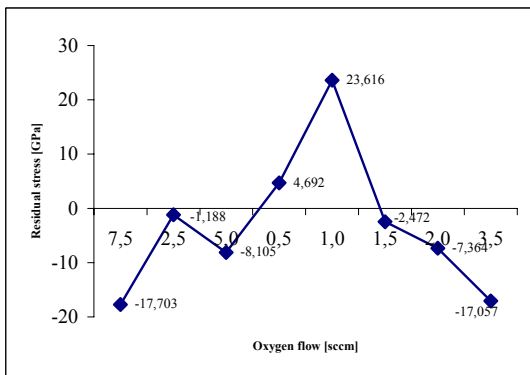
Fig.2. *Variation of the residual stress level of the deposited films as a function of the oxygen flows used for preparing coatings.*

The maximum value of these residual tensile stresses was observed for an oxygen flow of 1 sccm, but also for 0.5 sccm the tensile level of residual stresses is active yet in the films. Generally, it is clear that a developing of compressive residual stress level in the films follows an increase in oxygen content.

The first conclusion that can be drawn from these results shows that the using of oxygen flows lower than 1 sccm leads to the inducing in the films of important residual tensile stresses.

Fig. 3 summarizes the wear behaviours of the coatings after the pin-on-disk wear tests under the applied load of 10 N.

In terms of total mass loss during wear tests, the best results (the minimum mass loss) were obtained in the case of films which have been prepared with an oxygen flow of 2.5 sccm. However, acceptable wear strength was observed for the films prepared with oxygen flows higher than 2.5 sccm. In all these cases, especially for TiCO 2 and TiCO 1 samples, the films presented a very good adherence to the substrate.
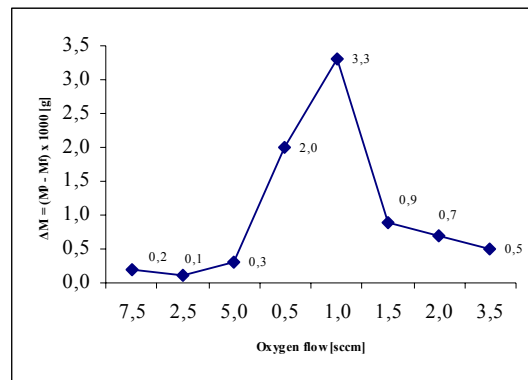
Fig.3. *The total mass loss of the deposited films after wear tests as a function of the oxygen*
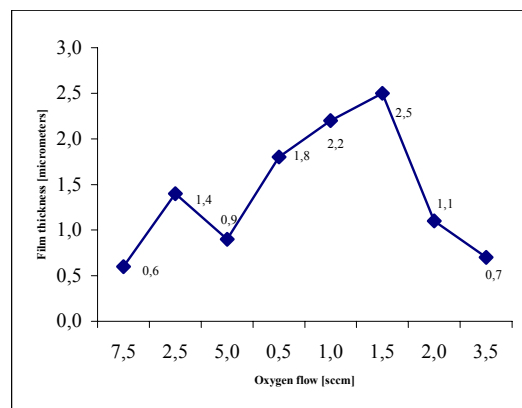
Fig.4. *The thickness of the films as a function of the oxygen flow.*

According with fig. 1, these samples were characterized by a small friction coefficient, which could be a possible explanation of their good wear behaviour. No good results are registered for TiCO 4 and TiCO 5 samples.

These films presented a brittle behaviour during the wear tests, which led to the generation of wear debris on the friction contact surface and also to the direct metal-to-metal contact. It is clear that this wear behaviour is in correlation with the residual tensile stress state registered in both two cases of TiCO 4 and TiCO 5 samples.

According with the results of thickness measurements (fig. 4), it is clear that there is no a real dependence between the films thickness and the deposition time so long as the oxygen flows varied. But the graphic dependence between oxygen flow and thickness leads to the conclusion that doesn't exist a linear correlation between these two parameters. From the above experimental results the maximum thickness values were registered for oxygen flows between 0.5 and 1.5 sccm. For all these three cases, the deposition time was the same, 5400 s.

Taking into consideration the graphics from fig. 3 and 4, an interesting conclusion could be drawn: the good results of wear strength are associated with an increased presence of oxygen. At the same time in these cases the films thickness presented moderate values, maximum 1.4 μm for the best results.

Referring to the colour tones of the films, it has been observed that an increase of oxygen flow leads to a strong colour changing (apparition), as follows: for small oxygen flow values (0.5, 1 sccm) the films present a silver metallic colour (mirror aspect); for oxygen flow values between 1.5 and 2 sccm the coatings become silver blue towards dark blue. For 2.5 sccm oxygen the film colour goes to a non-pronounced mixture between golden-green and pink. The both colour tones (golden-green and pink) are equal in area for an oxygen flow of 3.5 sccm and, if the oxygen flow increased to 5 sccm this colour aspect is kept but the pink tone become prevalent.

An interesting change in colour was observed for an oxygen flow of 7.5 sccm. Thus, the general prevalent tone of colour is yellow-green but the pink reflection disappeared and is replaced with a brightness-blue tone.

A final worthwhile observation is the possible influence of the residual stresses in the colour tone aspects. In fact, there is a remarkable difference in the colour of the sample prepared with an oxygen flow of 7.5 sccm (which develop in the films the highest compressive levels of residual stresses) than the other samples for which are used lower oxygen flows and the level of residual stresses has lower compressive values or tensile values. High compressive stresses are known to affect the microstructure of a material

and thus influence all the properties depending of them.

4. Conclusions

Thin films within Ti-C-O ternary system were prepared by reactive dc magnetron sputtering.

Friction characterization results generally reveal a good dependence between the oxygen flow used for films preparation and the static friction coefficient. Generally, the films prepared with more oxygen reveled a smaller static friction coefficient value (μ_s = 0.1355 for maximum oxygen flow used - 7.5 sccm) than the film, which contain less oxygen.

Residual stresses measurements revealed a good correlation between oxygen flow rate and the level of residual stresses. Generally, an increase of oxygen flow is followed by an increase in the residual (compressive) stress level. If the oxygen flow rate is under 1 sccm the residual stress level become a tensile stress level.

Regarding the wear behaviour, it is essential, however, to point out that an acceptable wear strength is influenced by the presence in the film of a residual compressive stress level. A moderate compressive stress level and confer to the films prepared with more than 2 sccm flow of oxygen a small wear rate and a good adhesion to the substrate. In contrast, the presence of the residual tensile stresses in the films leads to a brittle behaviour of these during the wear tests and increase clearly the wear rate.

Referring to the colour aspect, with the increase in the flow rate of the oxygen reactive gas from 0.5 to 7.5 sccm, the film colour rises slowly from silver-metallic colour to a pronounced mixture tone of yellow-green and blue.

Acknowledgements

References

[1]. **F. Vaz, P. Carvalho, L. Cunha, L. Rebouta, C. Moura, E. Alvez, A.R. Ramos, A. Cavaleiro, Ph. Goudeau, J.P. Riviere**, *Thin Solid Films* 469 - 470 (2004), p. 11.

[2]. **E. Budke, J. Krempel-Hesse, H. Maidhof, H. Schussler**, *Surf. Coat. Technol.* 112 (1999), p. 108.

[3]. **B. Zega**, *Surf. Coat. Technol.* 39 - 40 (1989), p. 507.

[4]. **C. Mitterer, J. Komenda – Stallmaier, P. Losbichler, P. Schmolz, W.S.M. Werner, H. Stori**, *Vacuum* 46 (1995), p. 1281.

[5]. **R. Fraunchy**, *Surf. Sci. Rep.*, 38 (2000), p. 195.

[7]. **G.G. Stoney**, *Proc. R. Soc.*, London A82, 172, (1909).

[8]. **D. Munteanu, A. Munteanu**, *Proc. of 3rd Conference "THE" Coatings*, section "Tribology", Thessaloniki – Greece, 28 – 29, (2002), p. 493.

EXPERIMENTAL STUDIES ON STRUCTURE PROFILE OF CAST ALUMINUM ALLOYS

Alina-Adriana MINEA, Adrian DIMA

Technical University "Gh. Asachi" Iasi, Romania;
e-mail: adima@tuiasi.ro

ABSTRACT

This paper presents experimental studies regarding the behavior after heat treatment of two cast aluminum alloy. So, we selected a typical charge for studying the structure profile. The studies that we have done can reveal the advantage of controlling the heating process at heat treatment of aluminum alloys.

Doing the studies that are described in the paper, we have obtained the microstructure profile that can express the importance of the process.

KEYWORDS: aluminum, heat treatment, microstructure profile, experimental model, cast alloys

1. Introduction

Heat treating on its broadest sense, refers to any of the heating and cooling operations that are performed for the purpose of changing the mechanical properties, the metallurgical structure, or the residual stress state of a metal product. When the term is applied to aluminum alloys, however, its use frequently is restricted to the specific operations employed to increase strength and hardness of the precipitation – hardenable wrought and cast alloys. These usually are referred to as the "heat – treatable" alloys to distinguish them from those alloys in which no significant strengthening can be achieved by heating and cooling. Heat treating to increase strength of aluminum alloys is a two – step process:

- quenching heat treating: dissolution of soluble phases and development of supersaturating;
- aging (age hardening) heat treating: precipitation of solute atoms either at room temperature (natural aging) or elevated temperatures (artificial aging or precipitation heat treating).

2. Experimental results

To take advantage of the precipitation – hardening reaction, it is necessary first to produce a solid solution. The objective of this process is to take into solid solution the maximum practical amounts of the soluble hardening elements in the alloy. The process consists of soaking the alloy at a temperature sufficiently high and for a time longs enough to achieve a nearly homogenous solid solution. Nominal commercial quenching heat treating temperature is determined by the composition limits of the alloy and an allowance for unintentional temperature variations.

The time at the nominal quenching heat treating temperature (soak time) required to effect a satisfactory degree of solution of the undissolved or precipitated soluble phase constituents and to achieve good homogeneity of the solid solution is a function of microstructure before heat treating. This time requirement is variable with the part dimensions.

After quenching, hardening is achieved either at room temperature or with an artificial aging. Artificial aging heat treating generally is low – temperature, long – term processes. Temperatures range from 115 – 190 °C; times vary from 5 to 48 h. Choice of time – temperature cycles for artificial aging should receive careful consideration. Larger particles of precipitate result from longer times and higher temperatures; however, the larger particles must, of necessity, be fewer in number with greater distances between them. The objective is to select the cycle that produces optimum precipitate size and distribution pattern. Unfortunately, the cycle required to maximize one property, such as tensile strength, is usually different from that required to maximize others, such as yield stress and corrosion resistance. Consequently, the cycles used represent compromises that provide the best combination of mechanical properties (it can be referred at a combination of hardness and mechanical stress).

Temperature control and uniformity present essentially the same problems in artificial aging heat treating as they do in quenching heat treating.

Good temperature control and uniformity throughout the furnace and load are required for all precipitation heat treating. Recommended

temperatures are generally those that are least critical and that can be used with practical time cycles.

The general methods for heat treating aluminum alloys include the use of molten salt – baths, air – chamber furnaces and induction heaters. The choice of heating equipment depends largely on the alloy and the configuration of the parts to be processed. The type of heat treating can also influence the choice of heating equipment.

Air furnaces are used more widely because they permit greater flexibility in operating temperature. Air furnaces are also more economical when the product mix includes a few parts; holding temperature of a large volume of salt in readiness for an occasional part is far more expensive than heating an equal volume of air. Also, induction methods can provide high heating rates, which affects transformation behavior.

In air furnaces, careful attention should be given to arrangement of the load. Air flow and natural temperature distribution within the furnace should be arranged to:

-offer minimum resistance to air flow

-produce the least disturbance in the natural temperature distribution

-afford constant replenishment of the envelope of air around each part.

This paper presents two cast aluminum alloys, which is used for aeronautical parts. These alloys are heat treated in order to establish the optimum mechanical properties, and we are referring especially at microhardness, tensile strength and elasticity. So, we took 10 parts, of identical measures, from this alloy and we apply the final heat treating. At the end we were studying structural properties, in order to establish the optimum technology.

The experiments were made using modern equipment, which is assisted by computer in order to control the process and to reduce energy consumption, especially at heating for quenching and artificial aging.

Experimental results are shown in fig. 1 and fig. 3 for the two aluminum alloys in cast conditions and in fig. 2 and fig. 4 for heat treating conditions.

necorodat

corodat

ATCSi10Mg

Fig. 1. Structure of a cast aluminum alloy – ATCSi10Mg.

140°C, 11h, corodat   **160°C, 9h**   **160°C, 7h, corodat**
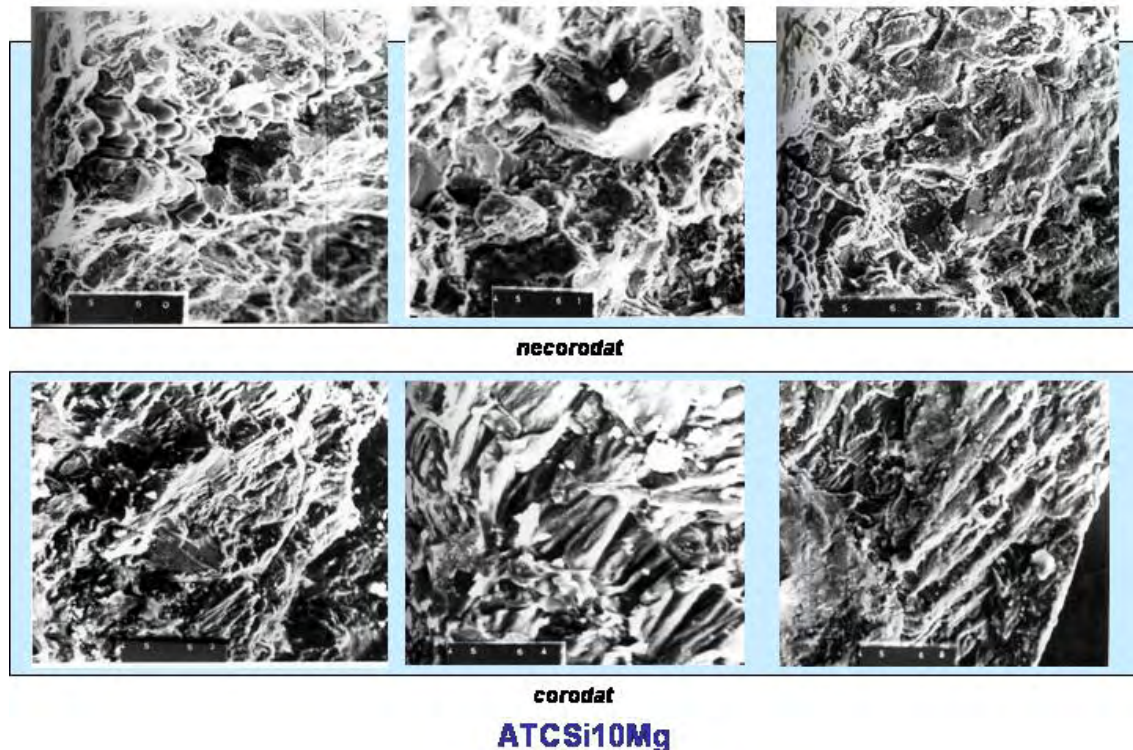
ATCSi10Mg quenched and artificial aged
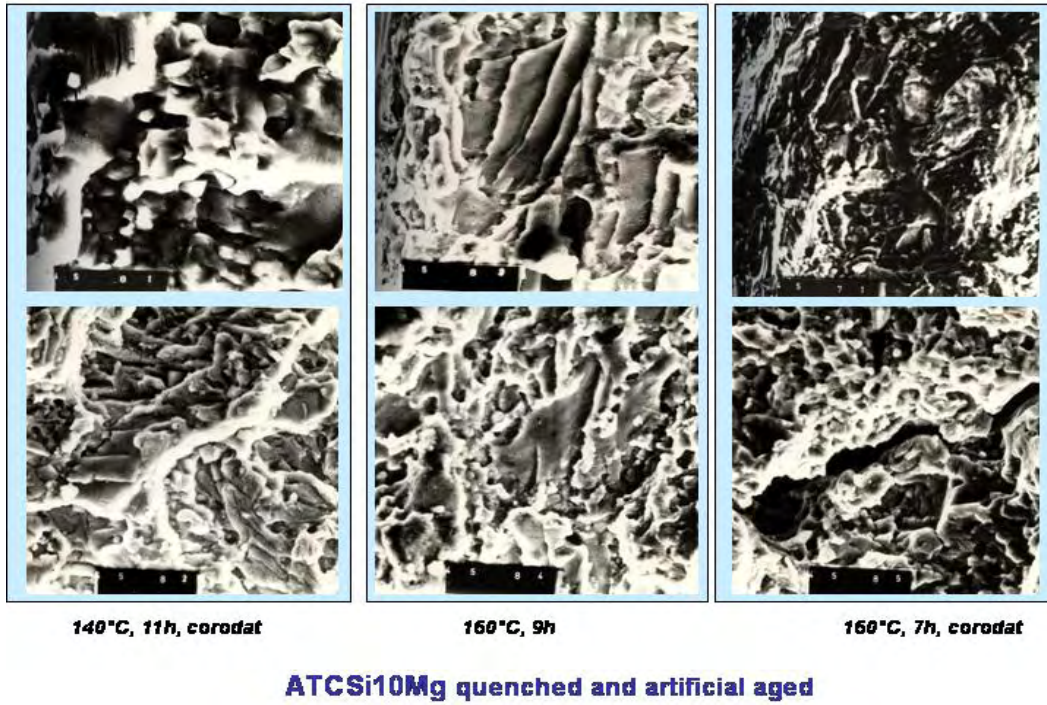
Fig. 2. Structure of a cast aluminum alloy – ATCSi10Mg, in heat treating conditions

necorodat

corodat

ATCSi5Cu1

Fig. 3. Structure of a cast aluminum alloy – ATCSi5Cu1.

180°C, 11h, corodat   140°C, 8h, corodat
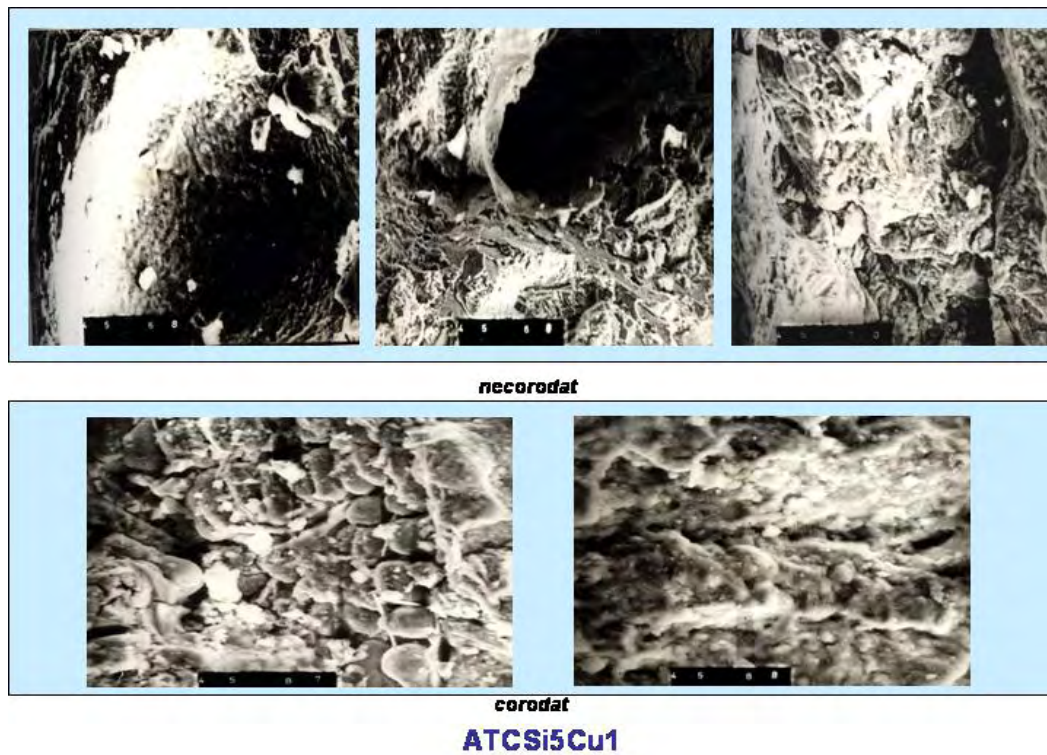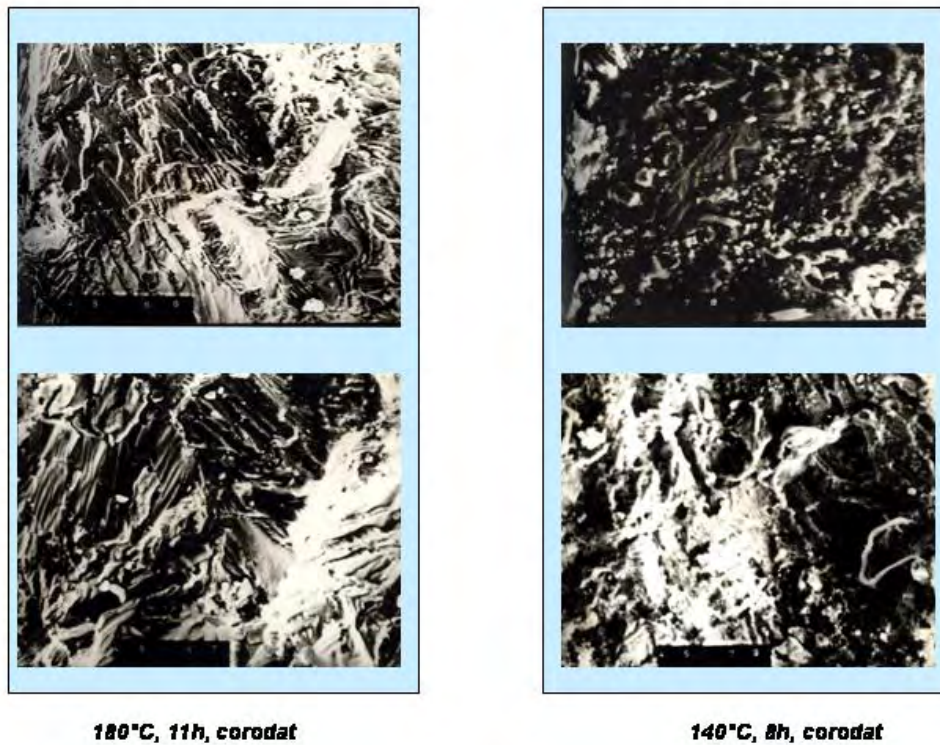
ATCSi5Cu1 quenched and artificial aged

***Fig. 4.** Structure of a cast aluminum alloy – ATCSi5Cu1, in heat treating conditions.*

Otherwise, for improvement of aluminum alloy final heat treating technology we care about aspects like:
- applying methods that can eliminate human work;
- eliminating manuals commands by using smart systems;
- reducing heat losses by using correct isolations.

3. Conclusions

This paper contains a study regarding the improvement of heat treating parameters, which determine a better heat treating technology for aluminum alloys and low energy consumption.
In this paper is presented the variation of structure characteristics with aging and quenching heating temperature.
We consider that the researching methodology choused is original and allow realizing the experiments to reveal the following improvements of the final heat treating technology for an aluminum alloy:

- correct calculation of the final heat treating technology for the studied alloy;

-choosing a performant heating furnace, an air chamber furnace with controlled heating;
-using modern equipment for testing the final heat treated parts, and we are referring at mechanical stress and hardness;
-correct programmed experiments and interpretations.

In this context, final heat treating technology optimization for aluminum alloys, with a high degree of predicting the mechanical characteristics of the working parts is an important contribution in the industry field.
As a conclusion, the paper presents the algorithm for applying the optimum heat treatment in order to obtain the necessary properties for the working parts.

References

[1].**Golubev, A.I**. , 1966, „Rolul compusilor intermetalici", I. D. T. Bucuresti
[2].**Mocanu, D.R**., 1982, „Incercarea materialelor", vol.1, E.T. Bucure[ti
[3].**Gadea, S**., 1965, „Aliaje neferoase", E. T. Bucuresti
[4]. **A.A. Minea, O. Minea, P. Dumitras**, 2003, „Studies about AlCu2Mg1,5Ni behavior at heat treatment", Elektronaia obrabotka materialov, Revista Academiei de Stiinte a Moldovei, Republica Moldova, no.6, pp.82-84, ISSN 0013-5739.

THE INFLUENCE OF THE THERMOMAGNETIC TREATMENTS ON THE HARDNESS NUMBER OF STEELS AND THE SUPERFICIAL LAYERS NITRIDED DURABILITY

Carmen-Penelopi PAPADATU

"Dunarea de Jos" University of Galati,
e-mail: **PCARMEN-PENELOPI@email.ro**

ABSTRACT

Two types of steels subjected to a nitriding thermo-chemical treatment after thermomagnetic treatments. The structural aspects into superficial layer of these steels are studied during friction process by using of an Amsler machine, taking two sliding degrees, different contact pressures and testing time. I tried to determine the durability of these materials, the surface structure evolution at different tests after thermomagnetic treatments.

KEYWORDS: thermomagnetic treatements, hardness number, wear process, durability

1. Introduction

The friction or wear processes are complex, being of physical, chemical, mechanical or metallurgical nature. These processes appear during dynamic or static contact between surfaces of two solid bodies where can be or not be a gaseous atmosphere, liquid (or solid) lubricant. The depth of the superficial layer varies between some atomic layers, in case of wear and chemical processes, and can attain up to 50-100 μm – in case of dry friction.

An important domain for laboratory researches and industry activity is the heat treatments domain. Here we can add the thermo-chemical treatments domain. Overlapping a magnetic field on Conventional heat treatments (the hardening and the recovery processes → the improvement process), the energy of magnetic field interferes in global energy balance of solid stage transformation. This magnetic field changes (thermodynamic change), the transformations mechanism and cinetics – obtaining the thermomagnetic treatment.

In the end, it can be obtained the change of the mechanical properties and the change of structure configuration for these materials. Interciding with a surface treatment (thermo-chemical treatment) like nitriding with plasma (ionic nitriding), the resistance to wear increase [8] and the resistance to corrosion too.

In this paper, it was made the balance- sheet looking at the advantages/disadvantages between: classic improvement and ionic nitriding and the improvement in different regimes of magnetic field (continuous or alternative current), different cooling regimes and ionic nitriding.

Until 1932, the martensitic structure of steels – after hardening process, it was considered the principal materials for the magnets [6]. Minkievici, Stark and Zaimovski, Erahtin, Komar and Tarasov studied roentgenographic, these alloys.

They demonstrated that, the optimal magnetic properties are a consequence of their variable structure-that appear in the initials processes stages by order.

Because variable structure, the materials has individuals micro-volumes of different phases. Each of these micro-volumes of ferromagnetic phase, has a spontaneous magnetization and a marked magnetic anisotropy (a single axes by light magnetization). These micro-volumes are isolated magnetic layers, un-magnetic layers or, easily magnetic layers. Result, a big coercitive force which depends by the grain size and the temperature.

For the stable magnetic texture making, are preferred two methods:
a). The cooling regime in outside magnetic field → thermo-magnetic treatment;
b). The cooling regime based on overlap to unilateral elastic tensions → Thermo-mechanic treatment.

2. Experimental tests

It was considered two few alloy steels, for improvement treatments, useful in metallurgical

industry: 42MoCr11 (code V) and, 38MoCrAl09 (code R). These materials are presented in table 1.

Table 1: The chemical composition

Steel grade	C(%)	Mn(%)	Si(%)	P(%)	S(%)	Cr(%)	Cu(%)	Mo(%)	Al(%)
42MoCr11 (code V)	0,38- 0,45	0,60- 0,90	0,17- 0,37	Max. 0,03	0,02- 0,04	0,90- 1,20	Max 0,30	0,15- 0,30	0,02
38MoCrAl09 (code R)	0,35- 0,42	0,30- 0,60	0,20- 0,45	Max. 0,03	0,02- 0,035	1,35- 1,65	Max 0,30	0,15- 0,25	0,70- 1,10

The heat and thermo-chemical treatments applied are:

t_1= Martensitic hardening process (at 850 ˚C for code V and 920˚C – for code R) and high recovery (at 580˚C –for code V and 620˚C – for code R)), without magnetic field (classic treatment: H =0). T1= t_1 + ionic nitriding (at 530˚C);

t_2= Complete martensitic hardening process in weak alternative magnetic field (cooling in water) and high recovery process (just cooling in water, in strong alternative magnetic field –H=1300 A/m). T2 = t_2 and ionic nitriding;

t_3= hardening process (cooling in water, in strong alternative magnetic field) and high recovery process (cooling in water, in strong alternative magnetic field – more then 1300 A/m). T3 = t_3 and ionic nitriding;

t_4= hardening process (cooling in water in strong continuous magnetic field) and high recovery process (cooling in water in strong continuous magnetic field). T4 =t_4 and ionic nitriding.

T_5= t_1 + laser nitriding (t= 5 ms);
T_6= t_1 + laser nitriding (t = 5 ms);
T_7= t_4 + laser nitriding (t = 5 ms);
T_8= t_3 + laser nitriding (t = 5 ms).

The usual methodology for the machinery parts study (roller wheel) useful in the metallurgical industry, presents the theoretic contact like a point (point contact) or, a line (linear contact).

On Amsler machines [7], I tried to determine the durability of rolls, the surface structure evolution at differents tests. Not must be neglect the other factories which influence the wear process: the geometric forms at contact machinery parts (roll on roll, roll on ring), the technological parameters (the surface quality, the heat treatments,) or, the exploitation conditions (the solicitation temperature – for example).
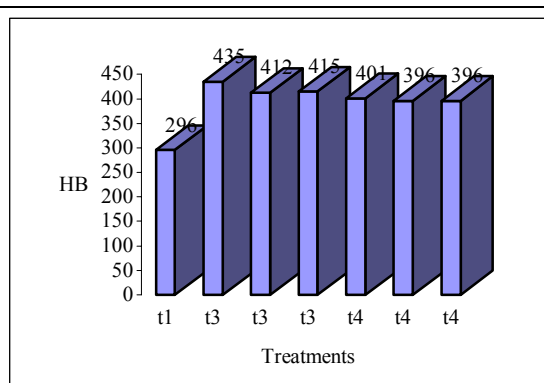
Figure 1: The influence of the magnetic field applied on the hardness number, for code V (42MoCr11)
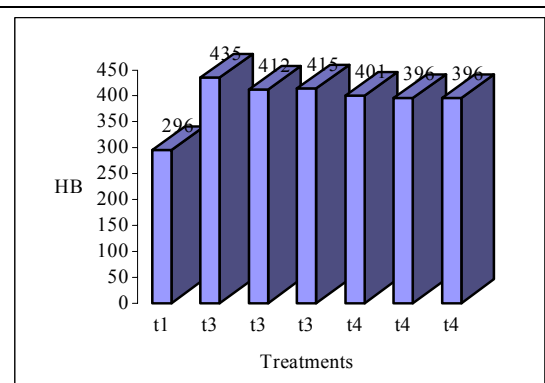
Figure 2: The influence of the magnetic field applied on the hardness number, for code R (38MoCrAl09)

It were submissive at wear process on Amsler machine from University "Dunarea de Jos" of Galati –Romania, rolls with different diameters and, different materials (code V, code R) which suffered

differents regimes like: T_1, T_2, T_3, T_4, T_5, T_6, T_7, T_8. The forces Q_i are variable from a roller to another one, and the wear process period, is variable too.

The partial results are presented in table 2

Table 2

Code material	Code treatment	Sliding degree (%)	Q_i [daN]	Initial size D_0' [mm]	Uh_f Wear depth [mm]	T[h] Total Wear time	Δt [h] Wear time
42MoCr11	T_1	10	-	40	-	0	0
"	T_1	10	75	40	-	1	1
"	T_1	10	75	40	-	2	1
"	T_1	10	75	40	0.10	3	1
"	T_1	10	-	40	-	0	0
"	T_1	10	150	40	-	1	1
"	T_1	10	150	40	-	2	1
"	T_1	10	150	40	0.12	3	1
"	T_1	20	-	44	-	0	0
"	T_1	20	150	44	-	1	1
"	T_1	20	150	44	-	2	1
"	T_1	20	150	44	0.13	3	1
"	T_1	20	-	44	-	0	0
"	T_1	20	190	44	-	1	1
"	T_1	20	190	44	-	2	1
"	T_1	20	190	44	0.3	3	1
"	T_2	10	-	40	-	0	0
"	T_2	10	75	40	-	1	1
"	T_2	10	75	40	-	2	1
"	T_2	10	75	40	0.07	3	1
"	T_2	10	-	40	-	0	0
"	T_2	10	150	40	-	1	1
"	T_2	10	150	40	-	2	1
"	T_2	10	150	40	0.09	3	1
"	T_4	20	-	48	-	0	0
"	T_4	20	150	48	-	1	1
"	T_4	20	150	48	-	2	1
"	T_4	20	150	48	0.11	3	1
38MoCrAl09	T_1	10	-	40	-	0	0
"	T_1	10	75	40	-	1	1
"	T_1	10	75	40	-	2	1
"	T_1	10	75	40	0.09	3	1
"	T_1	10	-	40	-	0	0
"	T_1	10	150	40	-	1	1
"	T_1	10	150	40	-	2	1
"	T_1	10	150	40	0.14	3	1
"	T_1	20	-	44	-	0	0
"	T_1	20	190	44	-	1	1
"	T_1	20	190	44	-	2	1
"	T_1	20	190	44	0.18	3	1
"	T_1	20	-	44	-	0	0
"	T_1	20	150	44	-	1	1
"	T_1	20	150	44	-	2	1
"	T_1	20	150	44	0.13	3	1
"	T_3	20	-	44	-	0	0
"	T_3	20	150	44	-	1	1
"	T_3	20	150	44	-	2	1
"	T_3	20	150	44	0.065	3	1
"	T_3	20	-	44	-	0	0
"	T_3	20	190	44	-	1	1
"	T_3	20	190	44	-	2	1

"	T_3	20	190	44	0.1	3	1
"	T_6	20	150	40		0	0
"	T_6	20	150	40		1	1
"	T_6	20	150	40		2	1
"	T_6	20	150	40	0,16	3	1
"	T_7	20	150	40		0	0
"	T_7	20	150	40		1	1
"	T_7	20	150	40		2	1
"	T_7	20	150	40	0,125	3	1
"	T_8	20	150	40		0	0
"	T_8	20	150	40		1	1
"	T_8	20	150	40		2	1
"	T_8	20	150	40	0,105	3	1
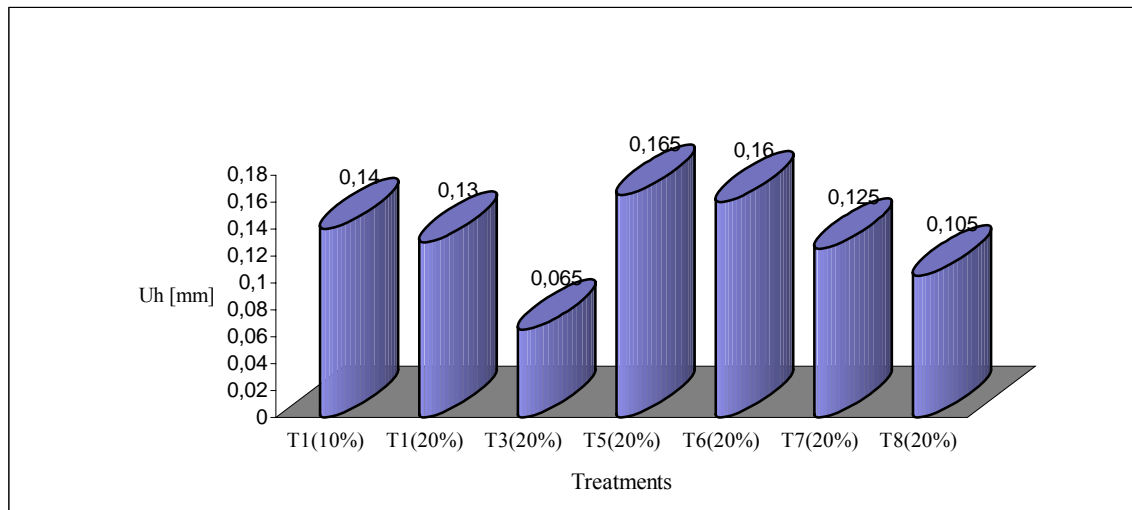
Figura 3: *The worn-out layer depth evolution as a function by the treatments applied for 38MoCrAl09 (code R) steel grade.*
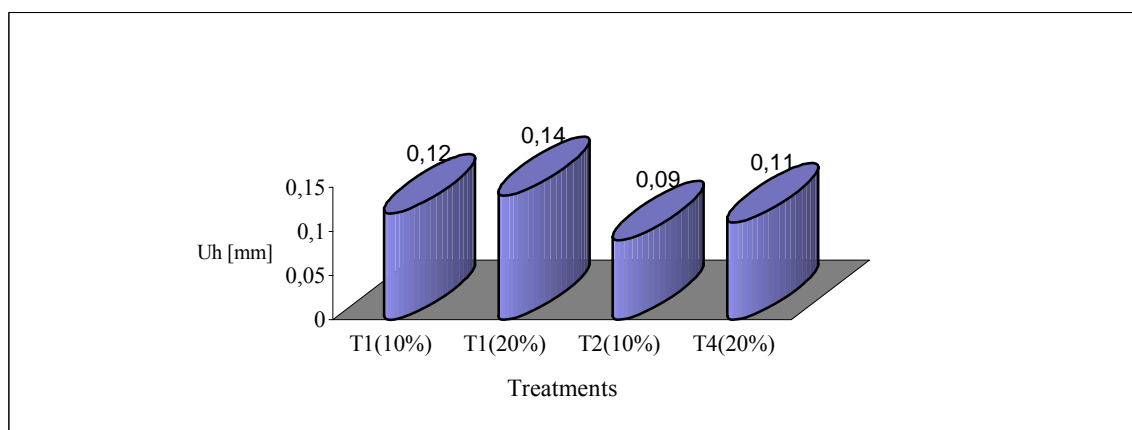
Figure 4: *The worn-out layer depth evolution as a function by the treatments applied for 42MoCr11 (code V) steel grade.*

3.Conclusions

The worn-out layer depth decrease and the hardness number of steels increase for the thermomagnetic treatments case.

This study may be considered like a fundamental research as it shows the necessity to perform typical studies for each kind of material and thermal or thermo chemical treatment applied.

References

[1] Crudu I., Gheorghies C., , *Incercarea materialelor*, Editura Tehnica, Bucuresti; 1986

[2] Crudu I. s.a., *Structural modification in the superficial layer of the material in wear and fatigue processes* », Nagoya, Japan; 1990,

[3] Gheorghies C., Crudu I., - *A Cybernetic Structural Model Applied to the Study of Friction Process"*, NORDTRIB 2000, 11-14 IUNIE Porvoo, Finland;

[4] Gheorghies C., *Modificari structurale in procese de uzura si oboseala,* Editura Tehnica, Bucuresti;

[5] Drugescu, E.- Teza de Doctorat;

[6] Vonsovski: *Teoria moderna a magnetismului*, Editura Tehnica, Bucuresti, 1956, pag.311;

[7] Stefanescu,I., s.a.-*"Organe de masini"*, Indrumar de laborator, Editura Fundatiei Unioversitare "Dunarea de Jos'' din Galati, 2002

[8] Papadatu,C, Stefanescu, I: -*Experimental study on the behaviour of some non-conventional treated steels during friction process* », Analele Universitatii "Dunarea de Jos" din Galati, Fasc.VIII-Tribology, 2004.

THERMOMECHANICAL PROCESSING OF MICROALLOYED STEELS USED FOR NAVAL AND OIL INDUSTRIES

**Ana DONIGA, Elisabeta VASILESCU,
Miltiade ISTRATE, Silviu MACUTA**

"Dunarea de Jos" University of Galati
e-mail: **doniga.ana@ugal.ro**

ABSTRACT

This paperwork shows the laboratory experiments made on X60 and X65 steels with several intercritical thermomechanical treatment application.

Two variants were used: "down-up" thermomechanical treatment with heating and rolling in the intercritical range and "up-down" thermomechanical treatment with preliminary complete austenitizing and rolling in the intercritic interval. High values of the strength characteristics and a good plasticity were gotten. A comparison was made with gotten results of the classical thermal treatment application (normalizing).

KEYWORDS: thermomechanical treatment, rolling, intercritic interval.

1. Introduction

The present world conjuncture regarding the plate products offers and costs imposed (to keep the markets) the making of the new technologies of the processing and thermal treatments that lead to the diminution of the energy consumption. The siderurgy is placed between the industrial branches with high level energy consumption therefore, the aim of this paper-work is to settle the reduction solutions of the energy consumption in the final stage of the plate-products thermal-treated.[1]

The study of the national and international standards, that establishes the manufacturing conditions, mechanical and technological characteristics of the siderurgical products made of the hypoeutectoid steels, showed that there are cases when the thermal treatment characteristics are not precised. In these cases first of all, and when the treatment characteristics are not precised, the researches could be achieved to settle the reducing ways of the energy consumption by temperature decrease or final thermal treatment elimination.

It is supposing a nonconventional approaching of the thermal treatment process by studies thoroughly regarding transformation mechanism and kinetics in the intercritic field of the structural steels and a better correlation to the previously stage – plastic deformation.[2]

In the practice of the thermal treatments the conservative positions are shown that imposes the hypoeutectoid steels to be complete austenitized to achieve the normalizing annealing or quenching.

Long time it was considered that the incomplete austenitizing to such steels leads to the fatigue strength worsening and to the transition temperature increase at brittle fracture.

For all that some domestic and abroad researches introduce the incomplete austenitizing for normalizing of the naval plates or some structural steels quenching and of the welded joint thermal influence zones for some low Carbon Ni-Mo or Ni-Mo-V steels.

It was established that, by thermal treatment temperature reducing a certain values increase of the material strength and plasticity, and metal loss reduction due to oxidation during thermal treatment were gotten.

By study thoroughly and systematisation of this field research-results, a new orientation could be traced in the practice of the hypoeutectoid steels, thermal treatment, and answers better to the purposes for which these siderurgical products are made.

The thermal treatment of the steels and cast-irons, based on the austenite getting and, subsequent, transformation (annealing, quenching), are made traditionally, with complete austenitizing (for hypoeutectoide steels) or incomplete austenitizing (for eutectoide, hypereutectoide and ledeburite steels).[3]

From austenitizing temperature point of view, the respective treatment of the hypoeutectoide steels could be considered "overcritic" (above Ac_1-

Ac_3 interval), and for the other steels "intercritic" (in Ac_1-Ac_{cem} critic interval).

By heating, in the balance condition of a hypoeutectoide steel, in A_1-A_3 interval, its microstructure, pearlitic-ferrite initially, will become austenite-ferrite. Carbon concentration of the austenite and austenite ratio, as well, will depend on steel carbon content and heating temperature. The

highest possibiliyties of controlable variation of such characteristics, the steels with extend A_1-A_3 range present, those with 0,10 – 0,30%C, respectively. [4]

Moreover, the fact should be specified that the studies balance situation could be achieved on the other ways as: by steel heating in the austenite field (total austenitizing) and by show cooling up to a temperature placed in A_3-A_1 interval (fig.1).
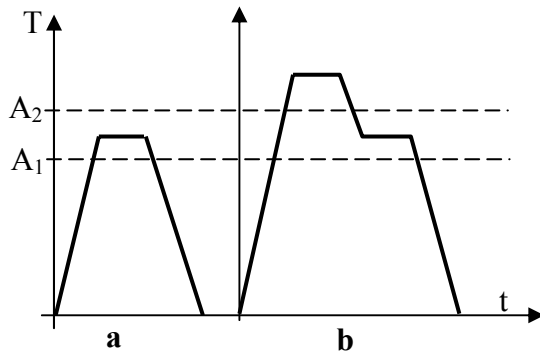
Figure 1. Practical ways of an intercritic treatment for an hypoeutectoide steel:
a) heating from the ambient temperature in A_3-A_1 interval (down-up)
b) preliminary austenitizing and precooling in A_3-A_1 interval (up-down)

This kind of the treatments were named intercritical thermal treatments and are used for thermal influenced zone recovery from electroslag welding of some Ni-Mo or Ni-Mo-V steels (with low carbon) and dual-phase steels, as well.

The latest paper-works of speciality show that the intercritical thermal treatment could be used for some hypoeutectoide steel, as well, those with high Ni content, carbon-steel, and low alloyed steels for naval constructions.[5]

2. Laboratory experiments

Having in view the importance of the naval-plates from the total production of S.C.ISPAT-SIDEX Galati, it is considered that the reduction of the energy consumption will be important using the intercritic conditions. Combining the thermal treatment with a plastic deformation in the intercritic field, an intercritic thermal mechanical treatment was achieved. For experiments X65 steel test pieces were used having the following characteristics (mentioned in table no.1 and 2)

Table 1. Chemical characteristics of X65 steel (%).

C	Mn	Si	V	Al	Ni	Mo	Ti	Nb
0,1	1,53	0,26	0,03	0,07	0,01	0,003	0,02	0,04

Table 2. The imposed mechanical characteristics steel grade.

Steel	R_m,min [N/mm^2]	$R_{p0.2}$,min [N/mm^2]	A,min [%]	KV, min [J]
X65	413	331	22	27

The intercritic thermo-mechanical treatment was used by the direct heating in the intercritic + deformation field (down-up) and deformation in

intercritic condition after a preliminary austenitizing (up-down) - fig.2.
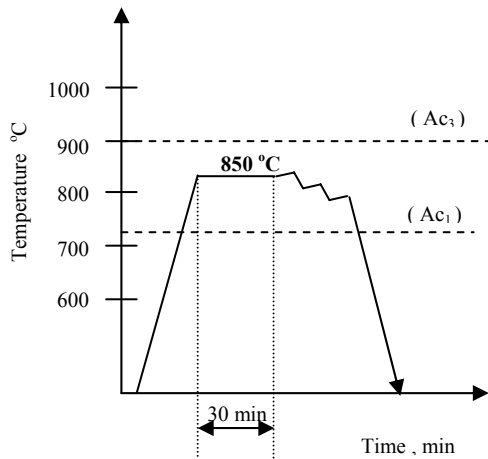
Figure 2. *Intercritical thermo-mechanical treatments*

a – down-up;
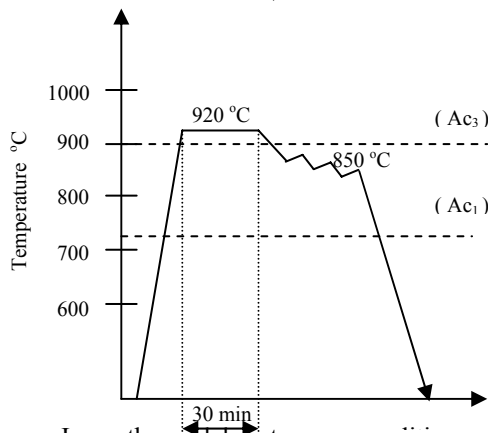
b – up-down

In the laboratory the thermomechanic treatment consisted of:

- heating in the austenitic or intercritic conditions;
- one passing rolling with a ε = 30% and 20% reduction degree on the laboratory rolling mill having barrell diameter of D = 129mm;

- the rolling was achieved in the intercritic field (temperature of 850^0C and 800^0C) for both treatments: "down-up" and "up-down";
- the cooling after rolling was made in air or water.

On the test specimen, thus gotten, the mechanical characteristics and structure was determined. The results are shown in table 3.

Table 3. *The experimental conditions of the intercritical treatments*

No. exp.	Experimental variants of TT/TTM	Mechanical characteristics				
		ε [%]	Rm [N/mm^2]	Rp$_{0,2}$ [N/mm^2]	A5 [%]	HB
1	Heating to 920° C + cooling air (normalizing)	30	546	368	29	278
2	Heating to 920°→cooling 850°+ rolling→ water	30	804	764	22	292
3	Heating to 920°→ cooling 850°+ rolling → air	30	637	579	29	191
4	Heating to 920°→ cooling 800° + rolling → water	30	803	753	20	285
5	Heating to 920°→ cooling 800°+ rolling → air	30	577	412	26	174
6	Heating to 850°→rolling→ water	20	834	685	26	292
7	Heating to 850°→rolling → air	20	686	566	32	202
8	Heating to 800°→rolling→ water	30	1027	852	20	329
9	Heating to 800°→rolling → air	30	651	498	20	215
10	Heating to 800°→rolling→ water	20	933	756	20	315
11	Heating to 800°→rolling → air	20	651	498	20	215
12	Heating to 920°→cooling 850°+ rolling→ water	20	880	696	20	301
13	Heating to 920°→ cooling 850°+ rolling → air	20	636	526	26	148

3. Results and discussions

First experiment consisted in a clasic normalizing treatment for results comparison (table 3, regime 1).

Second experiments group consisted of "up-down" treatments where working conditions were different by the cooling way and deformation degree:

- austenitizing temperature $T = 920^0C$;
- cooling at 850^0C;
- rolling with $\varepsilon_1 = 30\%$ and $\varepsilon_2 = 20\%$;
- cooling water and air.

It is remarked that Rm and $Rp_{0.2}$ mechanical characteristics values exceeded the values provided by the norms (table 2). In turn, the elongation is not framing, in all cases, in the values required by the norms.

Deformation degree didn't influence appreciably the mechanical characteristics.

In case of such treatment the best results are gotten in domains 3 and 5 (table 3) with austenitizing temperature $T = 920^0C$, cooling 850^0C, rolling $\varepsilon_1 = 30\%$ and air cooling. The water cooling results the low elongation values. The structure are shown in fig.3a and 3b.

The third group of the experiments consisted of "down-up" treatment thus:

- heating at 850^0C and 800^0C;
- rolling at these temperature;
- air or water cooling;
- deformation degree $\varepsilon_1 = 30\%$ and $\varepsilon_2 = 20\%$.

The best results were gotten in the domains 6 and 7 (table 3) with heating at 850^0C, rolling with $\varepsilon_2 = 20\%$ and air / water cooling.

High values are gotten for both Rm and $Rp_{0.2}$ and elongation as well (32% to the min 22% provided by norms).

The structures are shown in fig.3c and 3d.

4. Conclusions

- All the experiment variants of the thermomechanical treatment lead to the increase of the mechanical characteristics values of the strength (Rm, $Rp_{0.2}$) and some of them to the improvement of the plasticity characteristics (Ar %);
- The experiments variants of the thermomechanical treatment with water cooling after deformation result the high values for strength characteristics (over 2 times higher than "rolled" condition) but determinate the elongation decrease even under 20% (smaller than "rolled" condition);
- The experiment variants of the thermomechanical treatment with air cooling after plastic deformation result the mechanical characteristics improvement both: strength and plasticity:

$R_m = 577 \div 686$ N/mm^2;
$Rp_{0.2} = 412 \div 566$ N/mm^2;
$A_5 = 20 \div 29$ %, frecvent 26 %.

Studying the possibility of the thermomechanical treatment with air cooling after plastic deformation the following remarks are mode:

- regarding the heating way: "up-down" or "down-up", the variants with preliminary austenitizing result the highest values of the plasticity characteristics $A_5 = 26 – 29\%$ when mechanical characteristics are kept at high values:
(Rm = $577 \div 637$ N/mm^2; $Rp_{0.2} = 412 \div 579$ N/mm^2).
In the frame of these experiment variants could be seen that the deformation degree, ε, in limits of 20…30% hasn't an important influence on the characteristics.

- the experiment variants of the thermomechanical treatment without preliminary austenitizing ("down-up") determinate a decrease of the elongation from 26% to 20% even though the mechanical characteristics of strength are high, with remark that the deformation degree from 20% to 30% doesn't influence meaning fully:

- regarding the plastic deformation temperature established between intercritic interval of the studied steel could be remarked:

a) in the experiment variant with preliminary austenitizing and deformation at 850^0C having deformation degree $\varepsilon = 30\%$, a good assembly of mechanical characteristics is achieved (Rm = 637 N/mm^2; $Rp_{0.2} = 579$ N/mm^2; $A_5 = 29\%$) in comparaison to the temperature of 800^0C (Rm = 577 N/mm^2; $Rp_{0.2} = 412$ N/mm^2; $A_5 = 26\%$);

b) the experiment variant without preliminary austenitizing ("down-up"), also, demonstrated that temperature of 850^0C leads to the good results of the characteristics indifferent to the deformation degree.

In conclusion, the experiment results show that X65 microalloyed steel is sensitive to the mechanical processing and the value of the mechanical characteristics are modified to the rolled condition or to the conventional thermal treatment but the optimum experiment variants that lead to the establishing of the technological conditions in keeping with the studied steel grade are characterized by the following parameters:

1) preliminary austenitizing at 920^0C;
2) plastic deformation temperature 850^0C;
3) deformation degree about 30%;
4) air cooling after deformation.
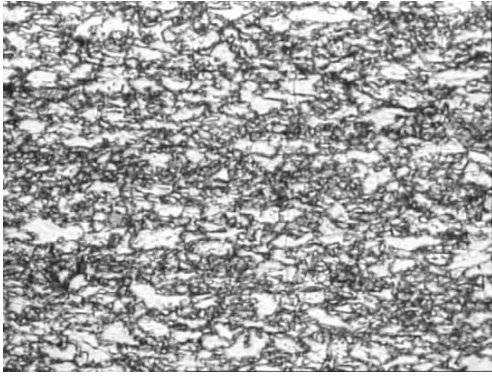
Figure 3. *Specimen microstructure with intercritic thermomechanical treatment* (table 3) *(x 500 magn., Nital etch 2%)*

a) regime 3;
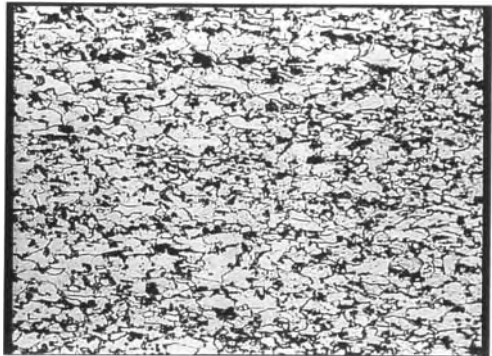
b) regime 5
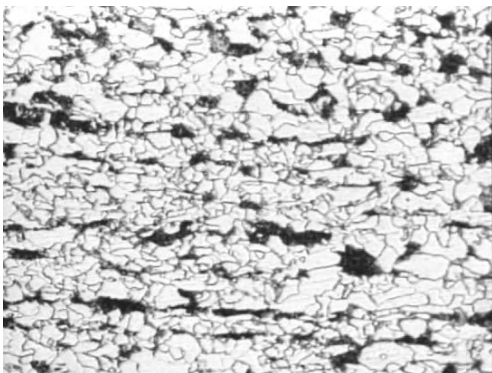
c) regime 6

d) regime 7

References

[1] **Leger J.** - *Etudes des traitements intercritiques (A$_1$-A$_3$) des aciers hypoeutectoides* Mem. Scient. Met LXVII, nr. 5 , 1971
[2] **Vasilescu E.** - *Tratamente termice si termochimice* (note de curs).

[3] **Nicolae Popescu s.a** - *Tratamente termice neconvenționale* (București, Editura Tehnică 1990).
[4] **Suzana Gâdea şi Maria Petrescu** - *Metalurgie fizică si studiul metalelor* (București, E.D.P. 1983)
[5] **Doniga A., Vasilescu E.** - *Bazele tratamentelor termomecanice* E.D.P. 2004.

BEHAVIOR OF 1% Cr STEELS AT FLUIDIZED BED NITROCARBURIZING

Sorin DOBROVICI[1], Nelu CAZACU[1], Adolf BÂCLEA[2], Elena DRUGESCU[1]

[1]Universitatea "Dunărea de Jos" din Galați,
[2]S.C. Cosena S.R.L Constanța
Sorin.Dobrovici@ugal.ro

ABSTRACT

Paper is based by nitrocarburizing experiments made on pilot installation. For experiments were used different samples of steel at different nitrocarburizing regimes. Influence factors were: temperature and ammonia concentration. Treatment time had a constant value 2h30min. Influences of factors were investigated by: samples mass modifications, surface structure (micrograph), layer depth to all samples and hardness HV5 on the surface. The results confirm possibility to use fluidized med like nitrocarburizing media and good behavior of steel.

KEYWORDS: Nitrocarburizing, fluidized bed, steel

1. Introduction

After nitriding, nitrocarburizing became the most usual treatments for pieces at lower temperature. Nitrocarburizing and oxynitrocarburizing became alternative technologies for parts of car industries. After this thermochemical treatment a surface layer with properties approaching at nitriding treatment is obtained, [2]. If a post oxidation is used to obtaining a Fe_3O_4 superficial a porous layer, which increases corrosion resistance of parts. Porous layer offer a good adherence for different sealant that conduce to one order increasing for a corrosion resistance. For efficiency of nitrocarburizing treatment evolution shows tendencies for quality and low costs. A complex processes are performed in fluidized bed. Gasses (ammonia and methane in different proportion) in active zone, near over separation plaque, are thermal decomposing in contact with hot solid granular.

The homogeneous reactions are possible to continue on the high of bed, but equilibrium is established at higher uniform regimes temperatures. A secondary stage is for heterogeneous reactions at surface samples, with adsorption of nitrogen and carbon atoms. As results of these two stage of reactions chemical compositions of gasses having major modifying: hydrogen and nitrogen and rests of methane and ammonia. These gasses produced normal fluidizations in bed and that maintaining a normal and a constant gas dynamics for constant properties of fluidized bed. A fluidized bed technology (FBT) for heat and thermo chemical treatments offers a low costs for investments and an acceptable quality [3]. The most important characteristics of fluidized bed are influenced by: chemical compositions of fluidization gas through physical gas properties and the solid granular properties (physical characteristics, shape, dimension)

High values for heat and mass transfer coefficient conduce to shorter treatment time and this technology may have applications for small enterprises and for small series of pieces.

2. Experimental conditions

*Nitrocarburizing was made
on the pilot conditions (*

Fig. 1). The fluidized bed furnace has minimal conditions for nitrocarburizing. The furnace working up to 1000°C and a various gas mixtures is possible to use for different heat and thermochemical treatments. Fluidized beds are made from burned clay and a gas mixture by methane and ammonia, with different proportion of methane. Nitrocarburizing in fluidized bed is based by repeatability of process, [4]. The nitrocarburizing media was made in fluidized bed. In this case the internal and external properties of

fluidized bed are important for treatment, because a large exchange surface is formed between fluidized bed and parts (samples). After fluidization, at outlet from furnace, gases were burned.

For nitrocarburizing experiments three steels with 1%Cr were used: 21TiMnCr12, 18MnCr10 and 40Cr10 (Romanian standards). Chemical compositions are showing in Tab. 1. The critical points for transformation for all steels are showing in Tab. 2. For all steels nitrocarburizing are a sub critical treatments, that's have not influence over core structure and properties.
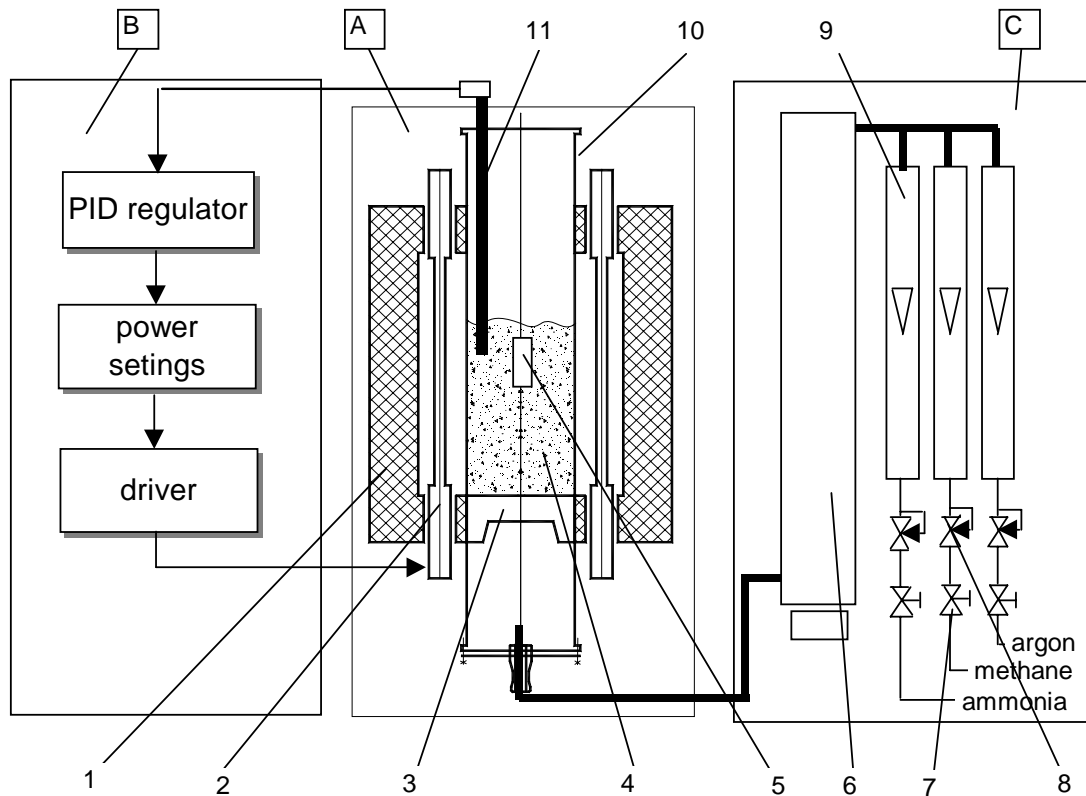
Fig. 1. *Schematic representation of fluidized bed furnace: B-automatization unit,*
A- furnace unit, C-gas unit, 1-isolation, 2-resistors, 3-fluidiszation plaque,
4-fluidized bed, 5-samples, 6-silicogel column, 7-valves, 8-gas regulators,
9-rotameters, 10-fluidized bed furnace, 11-K thermocouple

Tab. 1. *Chemical composition for steel used in experiments*

Steel	Chemical composition,%.							
	C	Mn	Si	P	S	Cu	Cr	Ti
21TiMnCr12	0,20	0,95	0,28	0,014	0,016	-	1,05	0,06
18MnCr10	0,18	1,05	0,22	0,035	0,035	-	1,05	-
40Cr10	0,40	0,65	0,27	-	-	-	1,00	-

Tab. 2. *Critical points for steels used in experiments*

No.	Steel	Ac1	Ac3
m.u.	-	°C	°C
1	21TiMnCr12	740	840
2	18MnCr10	765	838
3	40Cr10	743	782

Tab. 3. Nitrocarburising in fluidized bed regimes

No.	Temperature	Time	gas composition
	°C	h, min	%
1			25% ammonia + 75% methane
2	550	2h30min	15% ammonia + 85% methane
3			5% ammonia + 95% methane

Tab. 4. *Hardness measurements on the nitrocarburizing surface*

steel	ammonia contents (rest methane)	HV_5
m.u.	%	kgf/mm^2
21TiMnCr12	5	667
	15	752
	25	655
18MnCr10	5	524
	15	623
	25	549
40Cr10	5	655
	15	713
	25	677
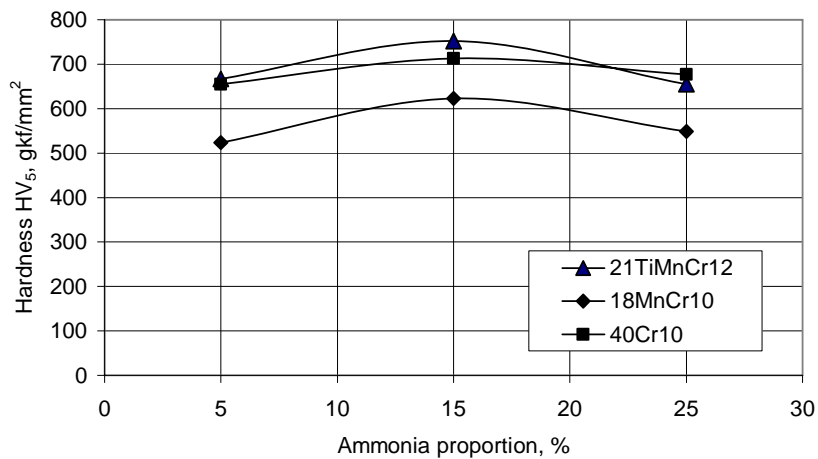
Fig. 2. Hardness on the nitrocarburizing surface.

Because ammonia is more expensive gas the proportion was varied between 5 and 25%, and the influence of ammonia proportion over experiments was studied (Tab. 3).

3. Results

The hardness on the surfaces is the technological properties that are usual determined. All steel having in chemical compositions approximate 1%Cr. That conduced to hard combinations at temperature and nitrogen presence in surface. As a normal result for all samples hardness (HV5) having higher values (***Tab. 4***, **Fig. 2**). For 15% ammonia contents in gas mixture for fluidization a maximum values were obtaining for all samples. Measurements of layer thickness for all nitrocarburizing samples are showing in **Fig. 3**. A normal increasing of layer depth by ammonia proportion is presence to all steel samples, but having different behaviour. The structure and properties of nitrocarburizing layer is determined

by chemical compositions that conduced to particular   behaviour of each steel samples.
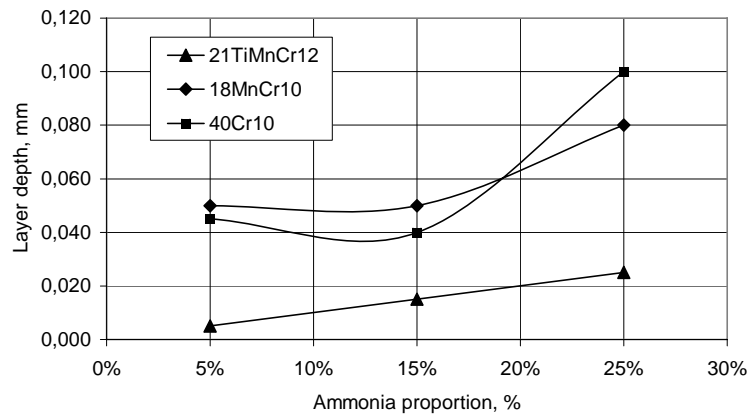
Fig. 3. *Nitrocarburizing layer variation with ammonia proportion*
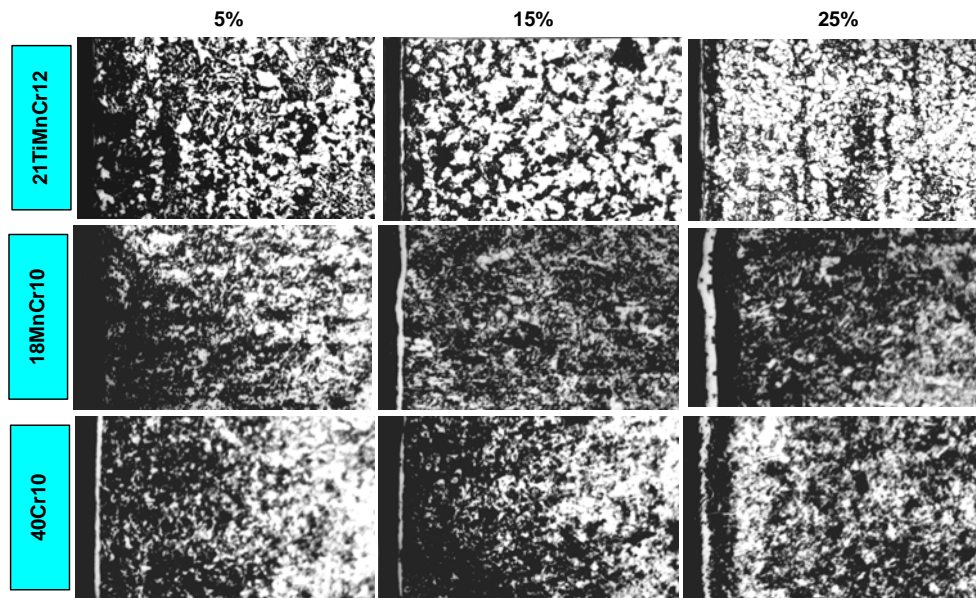
Fig. 4. *Representative microstructure for nitrocarburizing in fluidized bed layers*
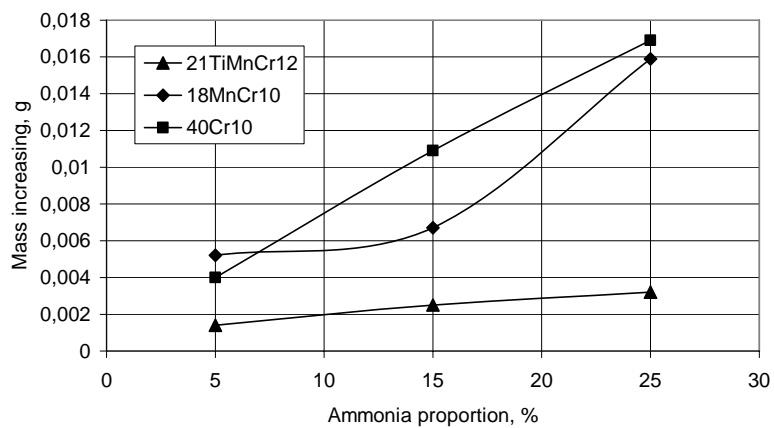
Fig. 5. *Mass increasing of nitrocarburizing samples*

For all steel samples representative microstructures are showing in **Fig. 4**. Combination layer has a normal increasing with ammonia proportion. Mass increasing for all steel samples was calculated by difference between final mass an initial mass, when the samples having identical shape and identical dimensions. The results are showing in **Fig. 5** Increasing of ammonia proportions in initial fluidization gas mixture conduced to mass increasing to all samples

4. Conclusions

Nitrocarburizing experiments made in fluidized bed over the samples from 1% Cr steels confirm fluidized bed capacity for mass transfer at higher temperature. Nitrocarburizing layer was formed for all regimes, and structures and properties of layer is depending by ammonia proportion in initial gas mixture. A maximum values for hardness is in 720…750 kgf/mm^2 interval, which is higher values for 150min nitrocarburizing time at 550°C temperature. A shorter treatment time is the most important characteristics of fluidized be d technology.

References

[1]. **Dulcy M., Gantois M.,** *Principe de base de la cementation et de la carbo-nitruration*, Traitements termique No.289, 1996, p.46-54

[2]. **Roland A**, *Oxicad (R) NT en four a tapis, Nitrocarburation Oxidation Trempe*, Traitement thermique No.346/Avr 2003, pg.37

[3]. **Willing R, Faulkner C,** *Nouvelle facon d'utiliser le bain de sel en nitrocarburation*, Traitement thermique No.333/ Aou-Sep 2001, pg.33

[4]. **Beguin Cl, Crevoiserat O**, *Controle des processus de nitruration et de nitrocarburation gazeuses avec la sonde Datanit*, Traitement thermique No.352/Janv-Fevr 2004, pg.33

ZINC LAYER REMOVAL AT THE STEEL APPLIANCES SCRAPS

**Lucica BALINT, Anişoara CIOCAN,
Simion BALINT**

"Dunarea de Jos" University of Galati
e-mail: **aciocan@email.ro**

ABSTRACT

All appliances contain an important quantity of steel and iron. These can be further recycled at the end of product usefulness. A component of the appliances is the bodies. These are made from galvanized steel. A study for the zinc coated layer removal from the surface of the galvanized steel, prior to recycling the steel scrap by melting in the steelmaking process is presented.

KEYWORDS: appliances, zinc removal, galvanized steel, air and chlorine atmosphere

1. Introduction

Appliances include washing machines, dryers, dishwashers, ranges, air conditioners, refrigerators, freezers and water heaters. A most part of the appliances components is made from steel. By weight, the typical appliance consists of about 65 % steel. Appliances are, in fact, systems of mechanical and electrical components encased in steel shells or bodies. This steel, and the iron components, is recyclable. All appliances contain a minimum of 25 % recycled steel that can be further recycled at the end of product usefulness. To extend the life of landfills and encourage appliance recycling, several states have enacted landfill bans for large appliances (known as „white goods") thereby forcing the contained steel into the post consumer scrap stream.

The use of coated sheet with zinc from old appliances as raw material increases the amount of zinc in dust. The zinc is a volatile metal, which concentrates in the fumes of the steelmaking reactors and ends up in the dust, or in the sludge, if wet collection is used. Zinc oxide, either zincite or more complex spinels, is the chemical form of zinc found in the dust. If can be sent back to the zinc smelters, but the concentration is usually too low (typically less than 5 % in the oxygen steelmaking dust, or more than 25 % in the EAF dust) to qualify as a substitute for ore concentrate, which has a grade of 60 %. [1]

When the concentration of zinc in materials for recycling is comparatively low (less than ~ 35 %) it may not be economically viable. Therefore, a process must be carried to increase its zinc content to at least 55-60 % at which concentration zinc recovery becomes economically viable.

For this reason, the best method for separate and recover both the original metals, iron and zinc is the removed of the zinc coated layer from the surface of the galvanized steel, prior to recycling the steel scrap by melting in the steelmaking process. This work present the laboratory studies for converting galvanized scrap into clean scrap for new steel making by the air and chlorine mixture in the dezincing process. Also, the recovery of the zinc is easily.

2. Thermodynamically data

The experimental conditions can be established if the thermodynamically parameters are analyzed. Figure 1 shows the equilibrium specification of Zn and Fe in a system air and chlorine mixture. Thermodynamics data shows that zinc chloride is more stable than its oxide, and the reverse is true for iron. [2].

The possible reactions together with their respective standard free energy changes (ΔG^0) are given in the table 1.
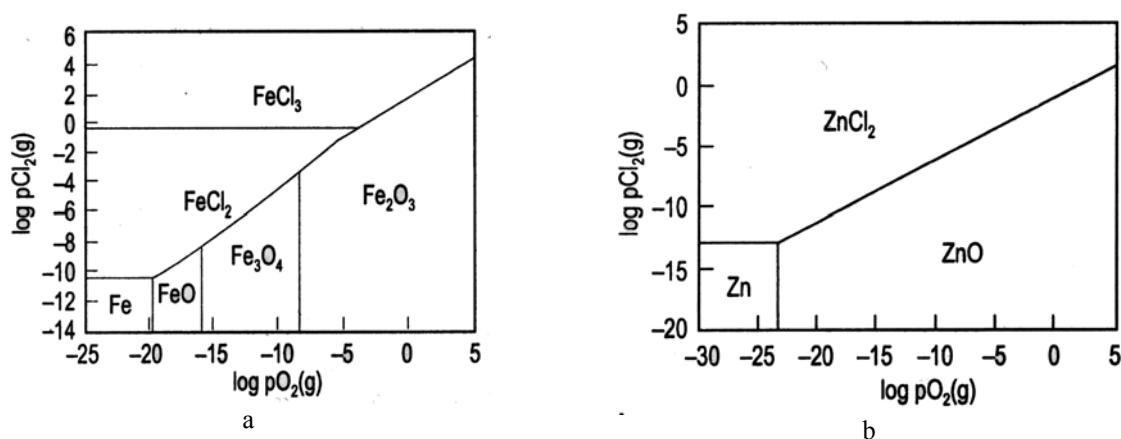
Figure 1. *Phase stability diagrams at 800 ^{0}C for the*
(a) Fe-O$_2$ –Cl$_2$;
(b) Zn-O$_2$ – Cl$_2$ system [1]

Table 1. *Standard free energy changes, ΔG^0*

Eq.no.	Reactions	ΔG^0, kJ/mol (at 800 ^{0}C)
1	$Zn(l) + Cl_2(g) \rightarrow ZnCl_2(g)$	- 272.430
2	$Zn(l) + 1/2\ O_2(g) \rightarrow ZnO$	- 240.160
3	$ZnO + Cl_2(g) \rightarrow ZnCl_2(g) + 1/2\ O_2(g)$	- 32.270
4	$Fe + 1/2\ O_2(g) \rightarrow FeO$	- 202.347
5	$3\ FeO + 1/2\ O_2(g) \rightarrow Fe_3O_4$	- 163.111
6	$2\ Fe_3O_4 + 1/2\ O_2(g) \rightarrow 3\ Fe_2O_3$	- 86.371
7	$Fe_3O_4 + 9/2\ Cl_2(g) \rightarrow 3\ FeCl_3(g) + 2\ O_2(g)$	+ 73.550
8	$Fe_2O_3 + 3\ Cl_2(g) \rightarrow 2\ FeCl_3(g) + 3/2\ O_2(g)$	+ 77.831

The thermodynamically data show that at the typical operation temperature of 800 ^{0}C and under reducing conditions only volatile zinc is thermodynamically stable, whereas under oxidizing conditions solid ZnO and volatile ZnCl$_2$ are present in about equivalent amounts.

After the removal of the zinc coating, iron is oxidized to form mostly Fe$_2$O$_3$ with a small amount of Fe$_3$O$_4$. This iron oxide is a protective layer that resists attack from chlorine. [2, 3]

3. Experimental

Materials. Samples of the galvanized steel, obtained by dipping in the melting zinc are utilized. An iron-zinc alloy coating with excellent adhesion and variable zinc content on the depth layer is present on the sheet sides. The structure phases and the microhardness variation on the depth layer are shown in figures 2 and 3. [4, 5, 6]

The zinc layer thicknesses on the two sheet sides can be modified precisely in a range between 60 and more than 750 grams per square meter, by adjustments of bath analysis, bath temperatures and dipping time in consequence of changing sheet surface properties and steel grades. The zinc layer thicknesses of the hot galvanized samples utilized in the experiments was uniformly, about 72 grams per square meter.

Experimental equipment. Tests were conducted on the laboratory scale. A precinct containing the sample is placed in the heating furnace (figure 4).
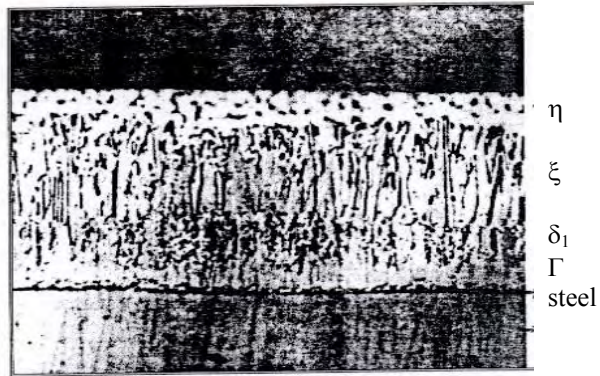
Figure 2. Structural phases in the galvanized layer formed at the bath temperature 460 ^0C
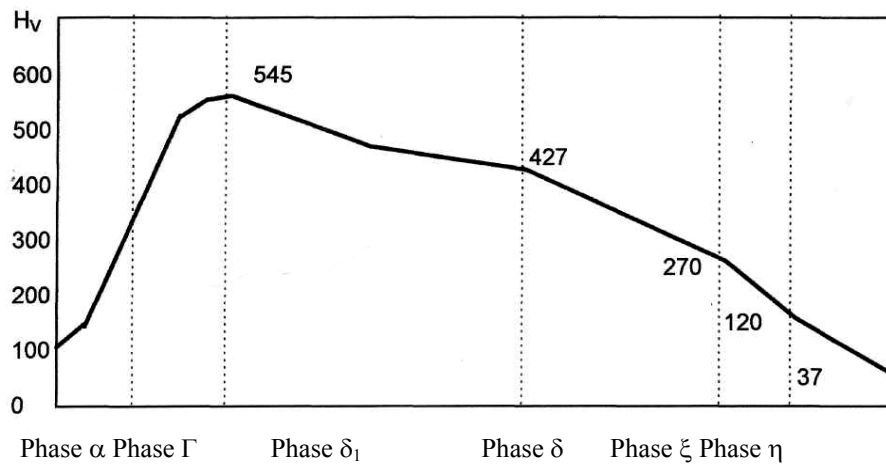
Figure 3. The microhardness on the depth layer on the sheet sides.
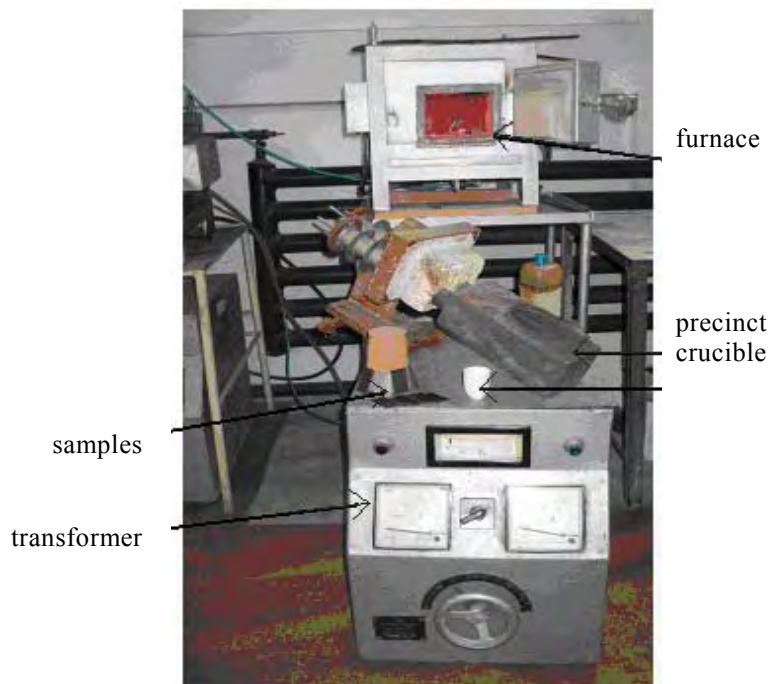
Figure 4. Experimental installation for the galvanized steel treatment.

Experimental conditions. The samples were heating in the air and chlorine mixture. Air and chlorine are readily available, by the chloric acid oxidation. An excess chlorine was using, for the complete chloric acid oxidation, more than the literature ratio air/chlorine. Depending of the zinc content in the sheet layers, chloric acid between 9 and 15 cm^3 is utilized for an experimental precinct with a volume of 0,003 m^3.

The heating is developed at the variable temperatures, from 570 to 860 ^{0}C. Each sample was maintained then minutes to the constant temperature and then was slowly cooled.

4. Results and discussion

During chlorination at the varied heating temperatures, the appearance of the galvanized steel samples is modified. Theirs comparable evolution and remarks are given in table 2

Table 2. *The samples, after chlorination at the varied heating temperatures*

No. sample	The heating temperature, (^{0}C)	The surface of the sample	Remark
1.	before heating		Normal surface of the galvanized steel sheet before chlorination
2.	570		Small areas of the nonconsumed zinc coating (grey areas), and zinc free-zone composed by the ferric oxide (red areas)
3.	630		Punctiform areas of nonconsumed zinc coating (grey areas), and extensive ferric oxide areas (homogeneous red areas)
4.	650		Ferric oxide is present nearby of the all area (homogeneous red areas); the nonuniform surface given the varied colors shades.
5.	680		Ferric oxide is greatly extended of the all area (homogeneous red areas); small oxide areas are detached from the surface sample
6.	710		Ferric oxide areas is present; great oxide areas are detached from the surface sample
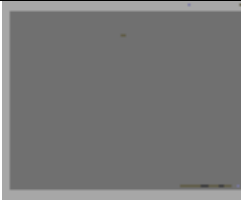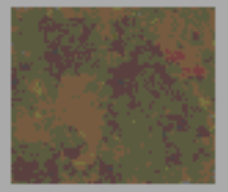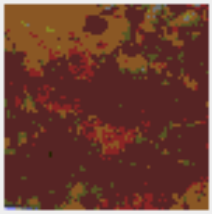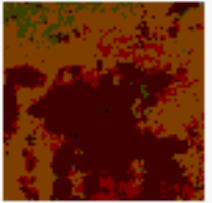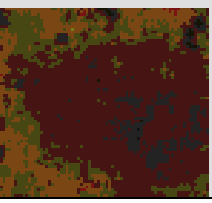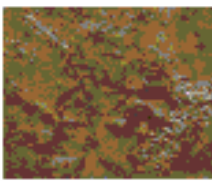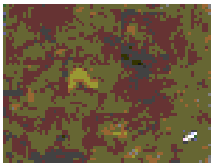
7.	760		Ferric oxide areas; the oxide areas detached from the surface sample is enlarged
8.	790		Ferric oxide areas (red colour) alternated with ferroferric oxide areas (black colour)
9.	820		Ferroferric oxide areas (black colour) and small ferric oxide areas (red colour)
10.	840		Ferroferric oxide areas (black colour) and greatly reduced ferric oxide areas (red colour)
11.	860		Ferroferric oxide areas (black colour) and punctiform ferric oxide areas (red colour)
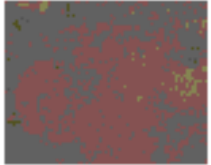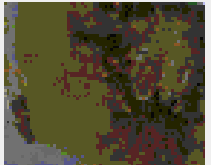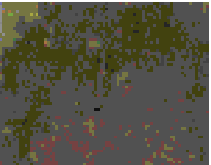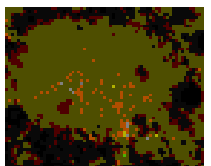
Results from researches show a zinc removal variation with the temperatures. At the temperature increase, the great iron oxide areas early appear: firstly the ferric oxide and then the ferroferric oxide. This iron oxide coating has replaced the zinc coating.

The microstructural analysis cross section of the some samples (No. 2, 4 and 11), heated at 570, 650 and 860 ^{0}C respectively, is presented in figure 5. For the different zones of the same sample, a variable rate of removal is observed. In these cases the nonuniform consistence of the zinc layer is possible to be the cause. For the maximum heating temperature, an acceptable rate of removal was obtained.

The ferric oxide zone and the small nonconsumed zinc marks
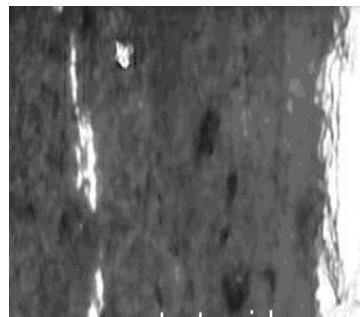
The ferric oxide zone and the extended nonconsumed zinc areas

(a)
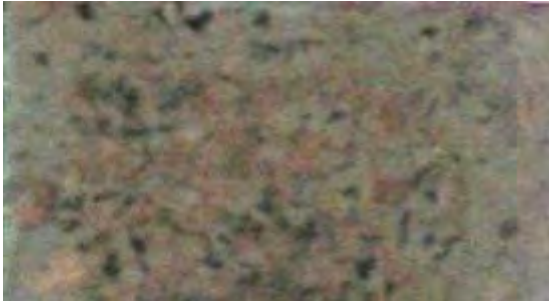
The ferric oxide layer and the intergranular and intragranular oxidation
on the all length sample
(b)
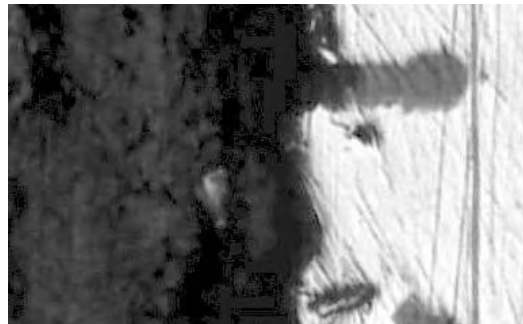
The great iron oxidation is observed; the ferric and ferroferric oxide are formed
(c)

Figure 5. *The microstructural analysis cross section for the different zones of the same sample, heated at 570 (a), 650 (b) and 860 ^0C (c) respectively (500 x).*

In accord with thermodynamically data, the depth of the oxide layer ranges with heating temperature. The correlation between these two parameters is given in figure 6.
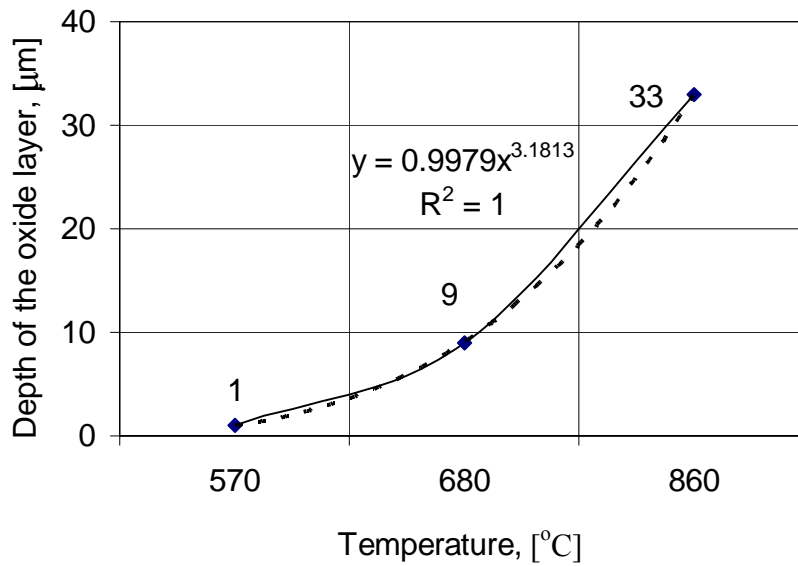
Figure 6. *The variation of the iron oxide layer depth during heating.*

4. Conclusion

This method is technically possible to the cleaning of the galvanized steel scraps before the utilization for new steel making. Also, the recovery of the zinc from volatile chlorides is easy to realize. For an efficient zinc removal rate, the process parameters (heating temperature and time, concentration air/chloride mixture), established in correlation with the nature galvanized scrap (steel grade, properties of the zinc layer and the steel sheet), must be check very accurately.

References

[1]. *** „A few facts about steel – North American's recycled material", http://www.recycle-steel.org/index2.html

[2]. J. K. S. Tee, D.J. Fray, JOM, August, (1999), p.24

[3]. J.K.S. Tee, „Recycling of galvanized steel scrap. A feasibility study" R'99 Congress, 1999

[4]. T. Radu, S. Constantinescu, L. Balint, „Materiale metalice rezistente la coroziune", Editura Fundaţia Metalurgia Română, Bucureşti, (2004)

[5]. T. Radu, S. Constantinescu, „Cercetări privind structura şi proprietăţile acoperirilor cu aliaje zinc-fier pe benzi din oţel", Revista Metalurgia nr. 8, (2004), p.20

[6]. T. Radu, O. Mitoşeriu, L. Balint, „Experimental researches on the zinc-iron coating", Analele Universităţii „Dunărea de Jos" din Galaţi, Fascicola IX, Metalurgie şi Ştiinţa Materialelor, (2004), p.133-136.

ELASTOPLASTIC MODEL FOR THE STEEL BARS
UNDER THERMAL TREATMENTS

Petrică ALEXANDRU, Octavian POTECAŞU, Florentina POTECAŞU

"Dunarea de Jos" University of Galati
palexandru61@yahoo.com

ABSTRACT

In order to understand material behavior, during the stresses action produced by thermal effects of volume, was started from Hooke relations, whereat was added the expressions that take into account these effects. Have been chose the expressions in cylindrical coordinates for the relations simplification reason, but and because cylindrical pieces are frequent in practical thermal treatments

Keywords : Hooke relations, thermal strain, quenching bar.

1. Introduction

The Hooke relations in cylindrical coordinates in the elastic domain:

$$\varepsilon_r = \frac{1}{E}\left[\sigma_r - \nu(\sigma_t + \sigma_z)\right];$$

$$\varepsilon_t = \frac{1}{E}\left[\sigma_t - \nu(\sigma_r + \sigma_z)\right];$$

$$\varepsilon_z = \frac{1}{E}\left[\sigma_z - \nu(\sigma_t + \sigma_r)\right];$$

$$\gamma_{rz} = \frac{2(1+\nu)}{E}\tau_{rz};$$

(1)

where:

- $\varepsilon_r, \varepsilon_t, \varepsilon_z$ -the specific elongations on three directions, radial, tangential direction and respective on the height cylinder;

- E_e -the modulus of longitudinal elasticity;

- $\sigma_r, \sigma_t, \sigma_z$ -the normally stresses on three, one radial, tangential direction and respective on the height cylinder;

- ν -the Poisson coefficient;

- γ_{rz} -tangential strain;

- τ_{rz} -tangential stress.

2. Proposed model

The completion with thermal volume effect presupposes considers as much expansion of pure

thermal how much nature and these produced by transformations of phase, as well as plastic deformation [1]. Through the addition in relations (1) of terms eh comprise these modifications was obtained:

$$\varepsilon_r = \frac{1}{E}\left[\sigma_r - \nu(\sigma_t + \sigma_z)\right] + \varepsilon_r^{pl} + \varepsilon_{vol};$$

$$\varepsilon_t = \frac{1}{E}\left[\sigma_t - \nu(\sigma_r + \sigma_z)\right] + \varepsilon_t^{pl} + \varepsilon_{vol};$$

$$\varepsilon_z = \frac{1}{E}\left[\sigma_z - \nu(\sigma_t + \sigma_r)\right] + \varepsilon_z^{pl} + \varepsilon_{vol};$$

$$\gamma_{rz} = \frac{2(1+\nu)}{E}\tau_{rz} + \gamma_{rz}^{pl};$$

(2)

where:

- $\varepsilon_r^{pl}, \varepsilon_\theta^{pl}, \varepsilon_z^{pl}, \gamma_{rz}^{pl}$ -the plastic deformations on radial, tangential direction, on height and respective, the tangential strain in a plan perpendicular to radius and measured in direction of cylinder height;

- ε_{vol} -the thermal volume effect.

Envisaged as much his dilatation the contraction produced of the temperature variation in the existence domain of a certain how much phase and the volume modifications motivated of the phase transformations must as the volume deformation be write:

$$\varepsilon_{vol} = \varepsilon_0 + \beta\Delta T$$

(3)

Through ε_0 is taken into account variation of volume to crossing abs existing structure to surrounding temperature to proper structure

temperature whereat is found out the supposed Through the substitution in the relations (2) expressions (3) was obtained.

$$\varepsilon_r = \frac{1}{E_e}\left[\sigma_r - \nu(\sigma_\theta + \sigma_z)\right] + \varepsilon_r^{pl} + \varepsilon_0 + \beta\Delta T \; ;$$

$$\varepsilon_\theta = \frac{1}{E_e}\left[\sigma_\theta - \nu(\sigma_r + \sigma_z)\right] + \varepsilon_\theta^{pl} + \varepsilon_0 + \beta\Delta T \; ;$$

$$\varepsilon_z = \frac{1}{E_e}\left[\sigma_z - \nu(\sigma_\theta + \sigma_r)\right] + \varepsilon_z^{pl} + \varepsilon_0 + \beta\Delta T \; ;$$

$$\gamma_{rz} = \frac{2(1+\nu)}{E_e}\tau_{rz} + \gamma_{rz}^{pl} \; ;$$

$$(4)$$

The plastic components of strains caused through analysis at every turn of time state every volume element from angle of behavior to deformation. Was calculated the intensity compliant stresses power hypotheses of plasticity (Mises

$$\sigma^k = \sqrt{(\sigma_r - \sigma_\theta)^2 + (\sigma_\theta - \sigma_z)^2 + (\sigma_{zr} - \sigma_r)^2 + 6\tau_{rz}^2}$$ A

nd if these exceeds the resistance values to proper deformation temperature and material structure

$$\sigma^k \geq R_d^k, \; R_d^k = \sqrt{2}R_e \; ,$$

Re represents the tension for which material pass through stage plastic to the draft unidirectional solicitation), the element into analyses was considered

element of volume according as the figure 1 present. in elasto-plastic domain of deformation. Calculated the plastic deformations was considered that elastic cumulated energy after touch critical state is changed to in mechanical energy of plastic deformation. When the mechanical energy of shape variation exceeds the critical value any growth of total energy be changed into mechanical energy of plastic deformation.

If noted the time whereat consisted the touched critical stage with t_f, and with $t_s = t_f - \Delta t$, the time whereat was did previous analysis of behavior to deformation, have been presupposed a linear variation of tensions intensity σ^k, unitary efforts, σ_r, σ_θ, σ_z, τ_{rz} and temperature of which depending the mechanical characteristics of material σ_r, σ_θ, σ_z, τ_{rz}, in the very short interval $\Delta t = t_f - t_s$ represents as a matter of fact a step of time. How on this moment t_s, the volume element is still in the elastic domain of deformation with $\sigma^k < R_d^k$, and on the passed moment t_f in one elasto-plastic, characterized through $\sigma^k > R_d^k$, was considered the moment of time whereat is produced the equality $\sigma^k = R_d^k$, is in middle time interval,

$$t_k = t_s + \frac{t_f - t_s}{2} = t_s + \frac{\Delta t}{2} \; .$$

Accordingly, result
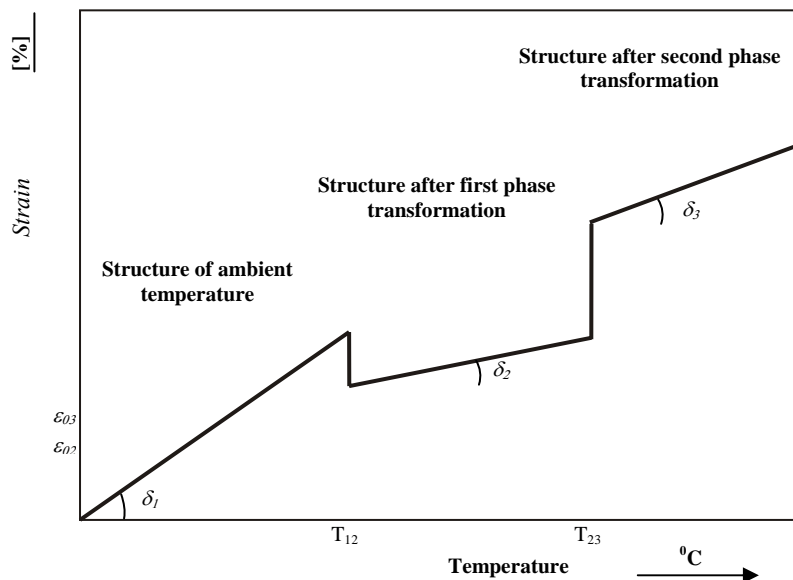
Fig. 1. *Thermal strain variation in a case of material with multiple phase transformations.*
-T12, T23-The critical temperatures of phase transformations;
-ε_{01}, ε_{02} -The strains variation from critical temperatures T12, T23;
-$\beta_1 = tg\delta_1$, $\beta_2 = tg\delta_2$, $\beta_3 = tg\delta_3$, The dilation coefficients of three structures.

$$\sigma_r^k = \frac{\sigma_r^s + \sigma_r^f}{2} \; ;$$

$$\sigma_\theta^k = \frac{\sigma_\theta^s + \sigma_\theta^f}{2} \; ;$$

$$\sigma_z^k = \frac{\sigma_z^s + \sigma_z^f}{2} \; ;$$

$$\tau_{rz}^k = \frac{\tau_{rz}^s + \tau_{rz}^f}{2} \; ;$$

$$(5)$$

$$\varepsilon_r^k = \frac{1}{E_e}\left[\sigma_r^k - \nu\left(\sigma_\theta^k + \sigma_z^k\right)\right] + \varepsilon_r^{pl} + \varepsilon_0 + \beta\Delta T \; ;$$

$$\varepsilon_\theta^k = \frac{1}{E_e}\left[\sigma_\theta^k - \nu\left(\sigma_r^k + \sigma_z^k\right)\right] + \varepsilon_\theta^{pl} + \varepsilon_0 + \beta\Delta T \; ;$$

$$\varepsilon_z^k = \frac{1}{E_e}\left[\sigma_z^k - \nu\left(\sigma_r^k + \sigma_\theta^k\right)\right] + \varepsilon_z^{pl} + \varepsilon_0 + \beta\Delta T \; ;$$

$$\gamma_{rz}^k = \frac{2(1+\nu)}{E_e}\tau_{rz}^k + \gamma_{rz}^{pl} \; ;$$

$$(6)$$

Theses estimates are convenient in the case of bodies division in a big number of elements. In figure 2 is presented the variation of stress σ_r depending on strain over a time step in which is produced the crossing in the elasto-plastic domain of deformation.
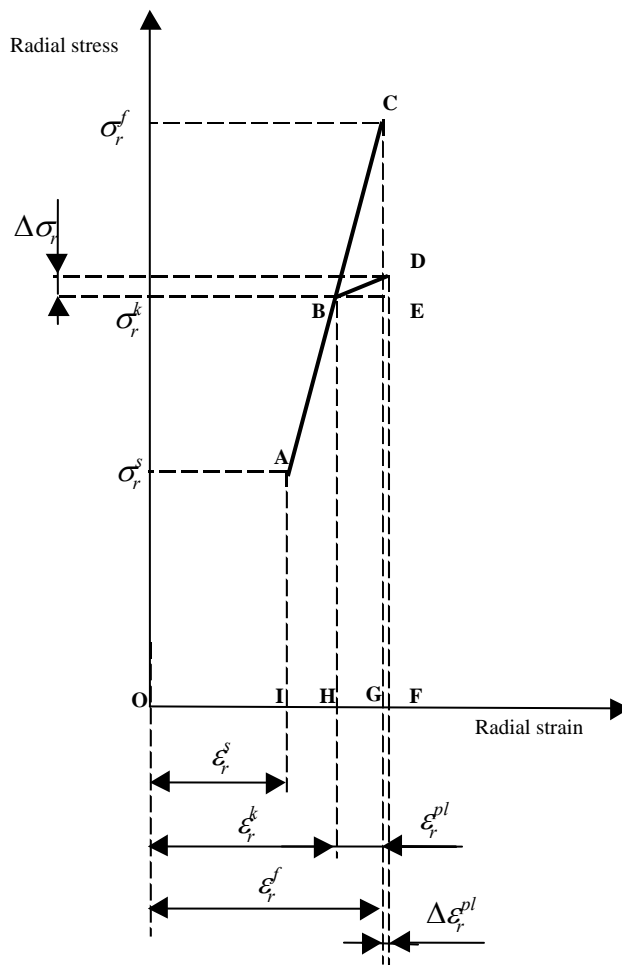
Fig. 2. *Approximation calculation of plastic radial strain into elementary volume.*

σ_r^s, σ_r^k, σ_r^f -*The radial stress in elastic domain from the beginning, middle and end of time step;*

ε_{re}^s, ε_{re}^k, ε_{re}^f -*The radial strains in elastic domain from the beginning, middle and end of time step;*

$\varepsilon_r^{pl\Delta t}$ - *The radial strains in plastic domain from the end of time step;*

$\Delta\sigma_r$, $\Delta\varepsilon_r$ -*The approximation error of calculation of radial strain and stress in plastic domain.*

$$L_r = \frac{1}{2}\left(\sigma_r^f + \sigma_r^k\right)\left(\varepsilon_r^f - \varepsilon_r^k\right),$$

where represents the mechanical energy of elastic deformation stores in material after touch critical state. The trapeziums area HBCG can be divided in the triangle BCE and the rectangle HBEG. If these two areas are shared

$$\frac{S_{BCE}}{S_{HBEG}} = \frac{\frac{1}{2}\left(\sigma_r^f - \sigma_r^k\right)\left(\varepsilon_r^f - \varepsilon_r^k\right)}{\sigma_r^k\left(\varepsilon_r^f - \varepsilon_r^k\right)} = \frac{\sigma_r^f - \sigma_r^k}{\sigma_r^k} \approx 0 .$$

Because, $\left(\sigma_r^f - \sigma_r^k\right) << \sigma_r^k$ (the variation tension is very small beside the own value) what permits the approximation calculus

$$L_r = \sigma_r^k\left(\varepsilon_r^f - \varepsilon_r^k\right),$$

this will be consumed through a plastic deformation production

$$L_r = \sigma_r^k\left(\varepsilon_r^f - \varepsilon_r^k\right) = \sigma_r^k \varepsilon_r^{pl\Delta t} ,$$

where through $\varepsilon_r^{pl\Delta t}$, was noted the plastic deformation produced in the element of volume on the analyzed time Δt, who confer for this, a value of the difference between the radial deformation appropriate of a the exhausted The deformation can be calculated without took count of the cold working (considering on duration of time step is very small in order to do not influence the deformation resistance of material) with a simple relation

$$\varepsilon_r^{pl\Delta t} = \varepsilon_r^f - \varepsilon_r^k$$

step of time and one appropriate the of critical attained domain. The other plastic strains was write likewise:

$$\varepsilon_\theta^{pl\Delta t} = \varepsilon_\theta^f - \varepsilon_\theta^k ,$$

$$\varepsilon_z^{pl\Delta t} = \varepsilon_z^f - \varepsilon_z^k ,$$
$$\gamma_{rz}^{pl\Delta t} = \gamma_{rz}^f - \gamma_{rz}^k .$$

These are added with the sums of plastic deformations already produced in previous interval Δt in the considers element.

For the stresses depending on deformations then next set of equation resulted:

$$\sigma_r = \frac{E_e}{(1+\nu)(1-2\nu)}\left[(1-\nu)\varepsilon_r + \nu(\varepsilon_\theta + \varepsilon_z) - (1+\nu)\beta\Delta T - (1-2\nu)\varepsilon_r^{pl} - (1+\nu)\varepsilon_0\right]$$

$$\sigma_\theta = \frac{E_e}{(1+\nu)(1-2\nu)}\left[(1-\nu)\varepsilon_\theta + \nu(\varepsilon_r + \varepsilon_z) - (1+\nu)\beta\Delta T - (1-2\nu)\varepsilon_\theta^{pl} - (1+\nu)\varepsilon_0\right]$$

$$\sigma_z = \frac{E_e}{(1+\nu)(1-2\nu)}\left[(1-\nu)\varepsilon_z + \nu(\varepsilon_\theta + \varepsilon_r) - (1+\nu)\beta\Delta T - (1-2\nu)\varepsilon_z^{pl} - (1+\nu)\varepsilon_0\right]$$

$$\tau_{rz} = \frac{E_e}{2(1+\nu)}\left(\gamma_{rz} - \gamma_{rz}^{pl}\right).$$

4. Simulation to water quenching of steel bar

As with most heat-treatment processes, the quenching conditions continue to be established empirically by trial-and-error procedures. A good prediction of microstructure and hardness distribution, as well as distortion and residual stresses, after quenching, clearly is desirable from the standpoint of both cost savings and enhanced product quality.

In the present paper a mathematical model, based on the finite-difference method, has been developed to predict the interaction among temperature, stress, water quenching process [4]. Internal stresses are induced by density changes resulting from cooling and phase transformations during quenching; but in same time the evolution of the microstructure depends on the thermal history as well as stress development in the part. The block diagram for the proposed mathematical model is shown in figure 3[1,2].
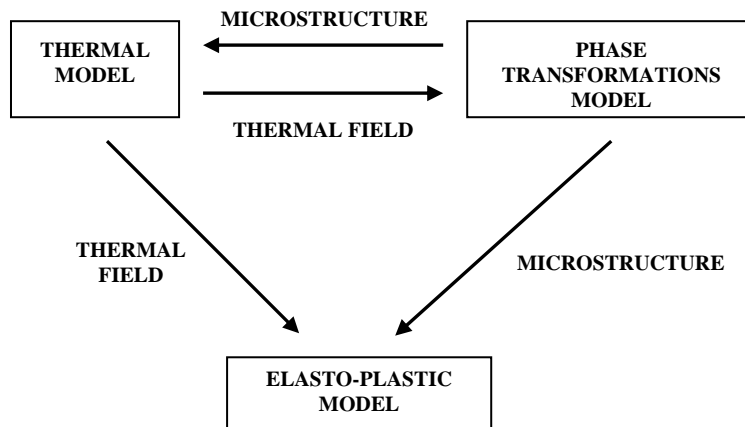
Fig.3 *General configuration of the mathematical model for the quenching steel bars.*

The stress influence at the phase transformations have been neglected in internal stress models of quenching. The applicability of

completion with the other terms depending on the specifies case.

The model can be used to optimize process
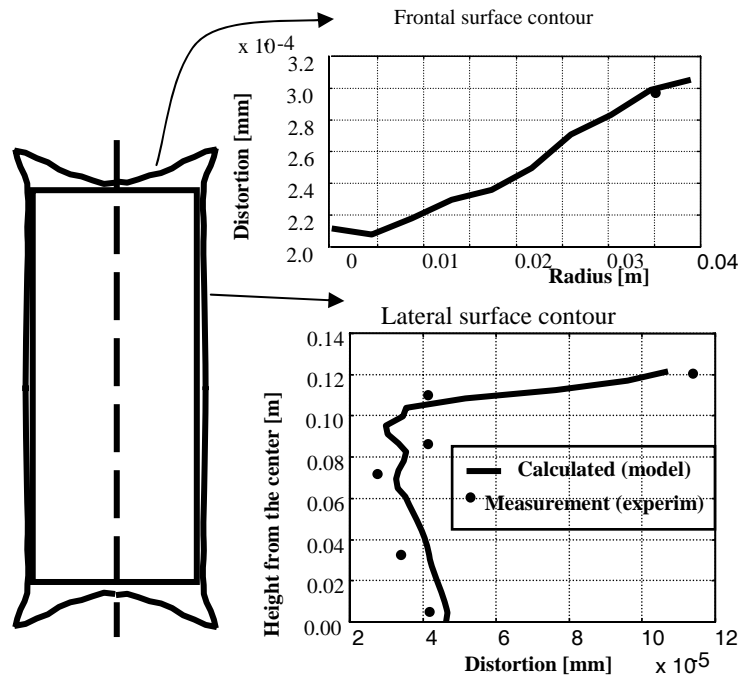
Fig. 4. *Model prediction for the distortion at the middle length surface and the frontal surface contour of the quenched bar (φ 80x240 mm, 1C45)*

this model for the simulation in the water quenching of a round steel bars *φ80x240 mm, 1C45 plain carbon grade was* compared with of the experimental measured and determined results. Figure 4 shows predicted frontal and lateral surface profiles after quenching as well as a comparison to experimental distortions after quenching. Good agreement can be observed.

5. Conclusions

The use of precedent equations (7) is indicated for the thermal treatments modeling by numerical method, such us the finite elements method or finite differences method, but in

parameters, at least in a comparative manner. Their use is limited currently by the large material database required as input.

References

[1]. Y. Nagasaka, J.K Brimacombe, E. B. Hawbolt, I.V. Samarasekera, B. Hernandez-Morales and S. E. Chidiac: *Metall. Trans*. 1993, vol 24A, p. 795-808.
[2]. P. Alexandru: Ph. D. Thesis, The University of Dunarea de Jos, Galati, 2002.
[3]. H. Y. Yu, A New Model for the Volume Fraction of Martensitic Transformations, *Metall. Mater. Transactions*, vol 28-A, 12, 1997
[4]. K. Inoue, K., Haraguchi, S., Kimura, *Trans ISIJ*, 1978, vol 18(1), p. 11-15

MANUSCRISELE, CĂRŢILE ŞI REVISTELE PENTRU SCHIMB, PRECUM ŞI ORICE CORESPONDENŢE SE VOR TRIMITE PE ADRESA:

MANUSCRIPTS, REVIEWS AND BOOKS FOR EXCHANGE COOPERATION, AS WELL AS ANY CORRESPONDANCE WILL BE MAILED TO:

LES MANUSCRIPTS, LES REVUES ET LES LIVRES POUR L'ECHANGE, TOUT AUSSI QUE LA CORRESPONDANCE SERONT ENVOYES A L'ADRESSE:

MANUSCKRIPTEN, ZIETSCHRITFTEN UND BUCHER FUR AUSTAUCH SOWIE DIE KORRESPONDENZ SID AN FOLGENDE ANSCHRIFT ZU SEDEN:

UNIVERSITATEA "DUNĂREA DE JOS" DIN GALAŢI
REDACŢIA ANALELOR
Str. Domnească nr. 47 – 800036 Galaţi, ROMÂNIA
E-mail: marian.bordei@ugal.ro